

UNCLASSIFIED

AD 402 625

*Reproduced
by the*

DEFENSE DOCUMENTATION CENTER

FOR

SCIENTIFIC AND TECHNICAL INFORMATION

CAMERON STATION, ALEXANDRIA, VIRGINIA



UNCLASSIFIED

NOTICE: When government or other drawings, specifications or other data are used for any purpose other than in connection with a definitely related government procurement operation, the U. S. Government thereby incurs no responsibility, nor any obligation whatsoever; and the fact that the Government may have formulated, furnished, or in any way supplied the said drawings, specifications, or other data is not to be regarded by implication or otherwise as in any manner licensing the holder or any other person or corporation, or conveying any rights or permission to manufacture, use or sell any patented invention that may in any way be related thereto.

Avco

CORPORATION

research and advanced development division

201 Lowell Street • Wilmington, Mass.

4 June 1963

TELEPHONE AREA 617
EXCHANGE 668-8911

AD 402 625

DISTRIBUTION

Subject: RADC TDR-63-112
Contract AF 30(602)-2809

Gentlemen:

Be advised that when subject report was distributed it did not contain a notice page as required by Rome Air Development Center.

In order that the report may be given Air Force approval, it is requested that the enclosed sheets be pasted on the inside of the front cover of the report.

Very truly yours,

AVCO CORPORATION
Research and Advanced Development Division

R. D. Fountain
R. D. Fountain
Contract Administrator

RDF/b
enc.

402 625

PATENT NOTICE

When Government drawings, specifications, or other data are used for any purpose other than in connection with a definitely related Government procurement operation, the United States Government thereby incurs no responsibility nor any obligation whatsoever and the fact that the Government may have formulated, furnished, or in any way supplied the said drawings, specifications or other data is not to be regarded by implication or otherwise as in any manner licensing the holder or any other person or corporation, or conveying any rights or permission to manufacture, use, or sell any patented invention that may in any way be related thereto.

ASTIA NOTICE

Qualified requestors may obtain copies of this report from the ASTIA Document Service Center, Dayton 2, Ohio. ASTIA Services for the Department of Defense contractors are available through the "Field of Interest Register" on a "need-to-know" certified by the cognizant military agency of their project or contract.

RADC-TDR-63-112
AD-

63-33

22

402625

AD NUMBER 402625

AD NO. _____

**NATURAL COMMUNICATIONS STUDY
PHASE I**

**FEASIBILITY STUDY ON A RELIABLE
POLAR HF COMMUNICATIONS SYSTEM**

Prepared by

Geoffrey E. Hill
Sidney M. Bennett
Claude J. Mazzola

RESEARCH AND ADVANCED DEVELOPMENT DIVISION
AVCO CORPORATION
Wilmington, Massachusetts

RAD-TR-63-13
Technical Note No. 1
Contract AF30(602)-2809

Prepared for

ROME AIR DEVELOPMENT CENTER
RESEARCH AND TECHNOLOGY DIVISION
AIR FORCE SYSTEMS COMMAND
GRIFFISS AIR FORCE BASE
New York

RADC-TDR-63-112
AD-

This document consists of 142 pages,
89 copies, Series A

NATURAL COMMUNICATIONS STUDY
PHASE I

FEASIBILITY STUDY ON A RELIABLE
POLAR HF COMMUNICATIONS SYSTEM

Prepared by

Geoffrey E. Hill
Sidney M. Bennett
Claude J. Mazzola

RESEARCH AND ADVANCED DEVELOPMENT DIVISION
AVCO CORPORATION
Wilmington, Massachusetts

RAD-TR-63-13
Technical Note No. 1
Contract AF30(602)-2809
Project No. 4519
Task No. 451902

22 April 1963


S. C. Corcitti

Manager, Space Sciences Department

Prepared for

ROME AIR DEVELOPMENT CENTER
RESEARCH AND TECHNOLOGY DIVISION
AIR FORCE SYSTEMS COMMAND
GRIFFISS AIR FORCE BASE
New York

FOREWORD

The authors express their gratitude to Dr. Jack Warga who contributed the programming theory given in section V. A. , and to Miss Margaret Shea who developed a computer program using the equations given in section II. B. and C. We thank Miss Pamela Drane and Miss Jacqueline Beyer for their assistance in carrying out the numerous calculations and preparation of diagrams and figures. Appreciation is expressed to Mrs. Gladys Seifred and Miss Jane Einos for typing the drafts of the manuscript.

ABSTRACT

In this report, the feasibility of obtaining reliable HF communications within and outside of polar regions, especially during disturbed conditions, is investigated. To establish methods by which propagation modes and field strength losses can be found, a number of formulations are developed. These are evaluated using vertical-incidence radio measurements. Also, some experimental data on a test propagation path is analyzed. The observed values are in excellent agreement with the expected ones.

To understand the behavior of the ionosphere during both quiet and disturbed conditions, analysis is made of several ionospheric parameters. Analyses for a large number of disturbances in absorption, sporadic E, and F2-layer critical frequencies are given. Following these analyses, data on HF equipment and systems is presented, so that a basis for selection of equipment parameters is available. A computer program is then developed to determine the optimum routing of traffic after the traffic load and available channels have been found. Some examples are given.

Finally, a completed system is presented for which the maximum possible reliability is found in an example situation. A traffic load is assigned to a hypothetical network during the height of a polar cap absorption event. The results show that communication can be maintained during the event, but at a reduced level.

CONTENTS

I.	Introduction	1
	A. Statement of Problem	1
	B. Scope and Limits of this Report	1
II.	General Theory	2
	A. Radio Wave Propagation Modes	2
	B. Nondeviative Absorption	13
	C. Reflection Coefficient for Sporadic E	24
	D. Transmitters, Receivers, and Antennas	31
	E. Radio Noise	37
	F. Calculation of Received Signal Strength	41
	G. Experimental Data	42
III.	Ionospheric Patterns	47
	A. Undisturbed Patterns	47
	B. Disturbed Patterns	59
	C. Related Solar-Geophysical Data	86
IV.	HF Equipment and Systems	93
	A. Equipment	93
	B. HF Systems	93
V.	Available Channels - Maximum Utilization	101
	A. Computer Program	101
	B. Examples	103
VI.	Completed System	107
VII.	References	120

ILLUSTRATIONS

Figure 1	Ionospheric Layers	3
2	Angle of Incidence versus Reflection Height and Great Circle Path Length	8
3	Transmission Angle versus Reflection Height and Great Circle Path Length	9
4	Graphical Computation of Maximum Usable Frequency	10
5	Idealized Ionogram (Ordinary Component)	12
6	Absorption Coefficient versus Height	15
7	Frequency versus Heights of Reflection in the D Region	16
8	Electron Density Profiles	18
9	Observed Absorption and Computed Absorption for Various Values of b, January 1958	20
10	Observed Absorption and Computed Absorption for Various Values of b, March - April 1958	20
11	Observed Absorption and Computed Absorption for Various Values of b, July 1958	21
12	Observed Absorption and Computed Absorption for Various Values of b, December 1958	21
13	Observed Absorption and Computed Absorption for Various Values of b, August - September 1958	22
14	Month of the Year (1958) versus b	22
15	Electron Density Profiles - Observed and Computed, b = 0.24	25
16	Electron Density Profiles - Observed and Computed, b = 0.35	26
17	Electron Density Profiles - Observed and Computed, b = 0.29	27

ILLUSTRATIONS (Cont'd)

Figure 18	Reflection Loss versus Λ and μ_{N_m}	29
19	Reflection Loss, C, and μ_{N_m}	30
20	Observed Values of Signal Strength and Noise Level	43
21a	Fort Monmouth f-Plot for 11 January 1963	44
21b	Fort Monmouth f-Plot for 12 January 1963	45
22	foE versus Solar Zenith Angle and SSSN	49
23	Number of Occurrences of foEs \geq 5 Mc	52
24a	Receiver Gain versus foEs, Churchill, 11 January 1958	56
24b	Percentage foEs \geq 5 Mc versus Receiver Gain, 11 January 1958, Churchill, Medium Gain 100%	56
25	Storm-time Behavior of foF2	60
26	foF2 Anomalies in the Polar Cap	63
27	foF2 Anomalies in the Polar Cap	64
28	foF2 Anomalies in the Polar Cap	65
29	foF2 Anomalies in the Polar Cap	66
30	Maps for Sudden Ionospheric Disturbance	70
31	Maps for Sudden Ionospheric Disturbance	71
32	Maps for Polar Cap Absorption Events	72
33	Maps for Polar Cap Absorption Events	75
34	Maps for Auroral Zone Absorption	78
35a	Zone Definition for Sporadic-E Analysis	80
35b	Classification of Sporadic E Zones	80

ILLUSTRATIONS (Concl'd)

Figure 36	Observed and Predicted Patterns of Sporadic E during a Geomagnetic Storm	87
37	Observed and Predicted Patterns of Sporadic E during a Geomagnetic Storm	88
38	Observed and Predicted Patterns of Sporadic E during a Geomagnetic Storm	89
39	USCG North Atlantic Weather Patrol HF Communication System	95
40	Norlant - 1958 HF Communication System	96
41	Norlant - 1961 HF Communication System	97
42	Links for the Example Network	105
43	Routing of Messages - Sample Results	105
44	Hypothetical Network	108
45	Ionospheric Maps for 1500 UT, 11 April 1958	112

TABLES

Table	I	Types of Propagation Modes	7
	II	Required Signal-to-Noise Ratios	35
	III	foF2 Anomalies in the Polar Cap.....	68
	IV	Period Studied (Sporadic E).....	82
	V	Tabular Representation of Es Intensity During a Storm	83
	VI	Prediction Table for Disturbed Sporadic E Conditions	84
	VII	Storm-Time Changes in the Prediction Scheme for Sporadic E.....	85
	VIII	HF Narrow-Band System Information	94
	IX	Norlant HF Circuit Information - 1961	99
	X	Addresses and Messages - Example 1	104
	XI	Addresses and Messages - Examples 2 and 3.....	106
	XII	System Parameters of a Hypothetical Communications Network	109
	XIII	Radiated Field Strength and Minimum Signal Levels ...	109
	XIV	Allowable Absorption	110
	XV	Assigned Frequencies	114
	XVI	Frequency Range Available without Propagation Losses	114
	XVII	Computed Values of Received Field Strength	115
	XVIII	Usable Frequencies	116
	XIX	Link Capacities	118
	XX	Message Loads	119

I. INTRODUCTION

A. STATEMENT OF THE PROBLEM

It is the aim of this study to determine the possible ways by which communication to and within polar regions may be maintained throughout ionospherically disturbed conditions. At present, high frequency, 1 to 30 Mc, radio communication between middle and high latitude transmitting and receiving stations is rendered ineffective during ionospheric storms produced by intense solar disturbances. The partial and, at many times, complete blackout of communication links is caused by increased ionization produced by the greatly enhanced solar X-ray and corpuscular radiation which is absorbed in the D region.

In most instances of present-day communication, there is little or no attempt to avoid absorbing regions or to utilize anomalous reflecting regions in any systematic or knowledgable way. It is tacitly assumed that all communication links are simultaneously affected in more or less the same manner. However, analysis of ionospheric data has shown that the spatial locations of the absorbing and reflecting layers vary in a coherent, but complex pattern throughout the lifetime of a storm. Furthermore, the analysis suggests that the patterns occur in a predictable manner.

The problem then is to determine practical ways by which the communication difficulties associated with ionospheric storms can be overcome. Another way to treat the problem is to determine the optimum way in which the disturbed ionosphere should be used for a given system of transmitters and receivers. Viewed in this way the possibilities for improvement of the system itself may be found. It may be that in order to achieve a specified reliability certain alterations of the system may have to be made before the optimum operating procedures can give the desired results.

B. SCOPE AND LIMITS OF THIS REPORT

This study will include factors needed to solve problems related to HF communications, and especially, those problems found during ionospheric storms. At this time, the studies undertaken are in progress so that only preliminary results can be given. However, attempts will be made to show the overall system in as complete a form as possible. It is not intended under this contract to go into the details of transmitting, receiving, or data-processing equipment characteristics, but only the general system parameters are considered.

It is intended that in the next report prepared under this contract, revisions will be made to include improved and additional results. The authors would appreciate helpful suggestions and criticisms of the report.

II. GENERAL THEORY

A. RADIO WAVE PROPAGATION MODES

HF communication between two distant stations on the Earth is possible only if the wave is reflected from the ionosphere. This region is located between about 90 and 500 km above the Earth and is a weakly ionized gas. It is divided into layers designated D, E, F1, and F2 in order of increasing height as shown in figure 1.

When a wave passes through the ionosphere the electrons are set into forced oscillation. The positive ions, because of their large inertia are practically unaffected. The coupling of the wave with the electron motion, affects the phase and group velocity of the wave, and is described in terms of the refractive index. If collisional damping and the Earth's magnetic field are neglected, the index of refraction is given by

$$\mu = \left(1 - \frac{N_e^2}{k m \omega^2}\right)^{1/2} \quad (1)$$

where the phase and group velocities are given by

$$V_p = \frac{c}{\mu} \quad \text{and} \quad V_g = \mu c$$

where c = velocity of light in free space.

Reflection of a vertically incident wave takes place when the refractive index approaches zero, i. e., the group velocity approaches zero. Thus, if the maximum electron density of an ionospheric layer is N_{max} , then the highest frequency which can be reflected is given directly by equation (2).

$$f_o = \sqrt{\frac{N_e^2}{k m 4\pi^2}} \quad (2)$$

In ionospheric terminology this is known as the critical frequency of the layer.

These equations are useful in solving propagation problems even though they are not theoretically satisfying since two important properties of the ionosphere have been omitted in the derivation, namely, the Earth's magnetic field, and collisional damping. These problems are treated in the magneto-ionic theory.

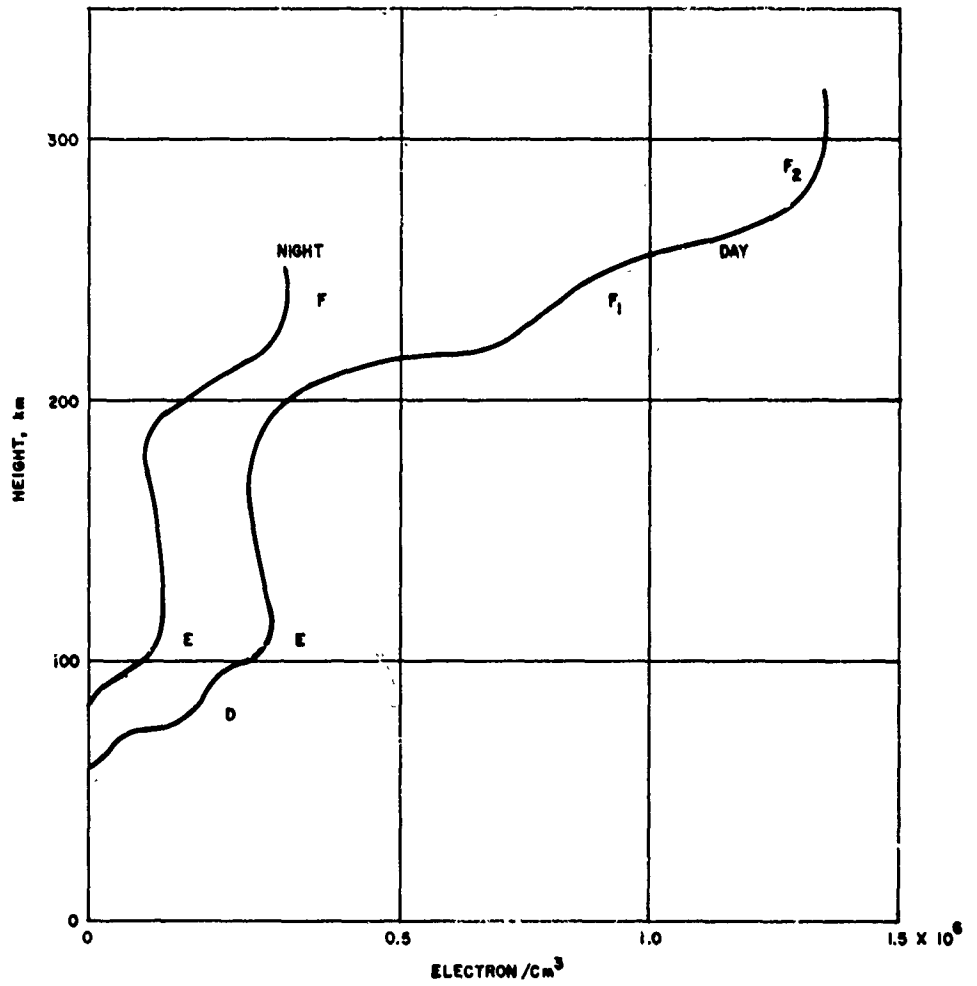


Figure 1 IONOSPHERIC LAYERS
63-3600

Simply stated the magneto-ionic theory is a solution of the wave equation in the presence of a static magnetic field which introduces anisotropy into the index of refraction somewhat analagous to a birefringent crystal. As a result the incident wave emerges as two waves elliptically polarized, one clockwise the other counterclockwise. As in physical optics they are termed extraordinary waves (f_x) and ordinary waves (f_o) respectively. The difference in their critical frequency is given approximately by

$$f_x - f_o = f_H/2 \quad (3)$$

Other results of the magneto-ionic theory will be introduced when necessary. The reader is referred to Budden (1961) or Ratcliffe (1959) for a definitive treatment of the problem.

To determine the behavior of a wave obliquely incident on the ionosphere, Snell's Law of geometrical optics is applied. This law states that at the interface of two homogeneous layers a wave passing through will be refracted according to the relation

$$\frac{\mu_1}{\mu_2} = \frac{\sin \phi_2}{\sin \phi_1} \quad (4)$$

where μ is the refractive index, ϕ is the angle of incidence at the interface, and the subscripts indicate layers 1 and 2. If we consider the ionosphere to be many horizontally stratified layers then we may write

$$\frac{\mu_1}{\mu_2} = \frac{\sin \phi_2}{\sin \phi_1}, \quad \frac{\mu_{i-1}}{\mu_i} = \frac{\sin \phi_i}{\sin \phi_{i-1}}$$

where i refers to the i th layer.

By successive substitution

$$\frac{\mu_1}{\mu_n} = \prod_{i=2}^{i=n} \frac{\sin \phi_i}{\sin \phi_{i-1}} \quad (5)$$

In the case of the ionosphere, n is taken as infinity so that equation (5) refers to a continuously varying media.

If ϕ_1 is the angle of incidence at the ionosphere, then $\mu_1 = 1$. So

$$\mu_\infty = \frac{\sin \phi_1}{\sin \phi_\infty} \quad (6)$$

where μ_∞ corresponds to the index of refraction at the top of the wave path, it will be denoted as μ . Also at the level where the wave has reached maximum height (travelling horizontally), $\phi_\infty = 90^\circ$ and

$$\phi_1 = \sin \phi_i .$$

In other words the refractive index at the point of reflection is given by the sine of the angle of incidence at the ionosphere.

Combining this equation with equation (1)

$$\left(1 - \frac{f_r^2}{f^2}\right)^{1/2} = \sin \phi = (1 - \cos^2 \phi)^{1/2}$$

so

$$\frac{f_r^2}{f^2} = \cos^2 \phi \tag{7}$$

$$f = f_r \sec \phi$$

where f is the frequency of propagation and f_r is the plasma frequency.

$$\left(f_r^2 = \frac{N_e^2}{km 4\pi^2}\right). \text{ Equation (8) is called the secant law for oblique transmission.}$$

The angle of incidence in equation (7) for propagation over a curved Earth, can be found from simple geometric considerations and is expressed

$$\phi = \sin^{-1} \left[\frac{R \cos \theta}{R + h_r} \right] \tag{8}$$

where

R = radius of the Earth

h_r = virtual height of reflection

θ = angle of transmission

The angle of transmission (sometimes called the "take-off angle") written in terms of the height of reflection and the great circle distance d from transmitter to receiver is

$$\theta = \tan^{-1} \frac{\left[h_r - R \left(1 - \cos \frac{d}{2R} \right) \right]}{R \sin \frac{d}{2R}} - \frac{d}{2R} \quad (9)$$

A graph showing the angle of incidence as a function of distance and height of reflection is given in figure 2. Similarly, the transmission angle is given in figure 3. These formulas and graphs are considered standard and can be found in a number of textbooks dealing with HF propagation.

In terms of the maximum range of observed critical frequencies, and reflection heights of the various layers of the ionosphere, table I has been prepared indicating possible reflection modes over a curved Earth. Not all of these possible modes apply to any one frequency, location, or time, but they serve to indicate the ionospheric propagation modes which may be responsible for a signal at a given distance from the transmitter. For example, at nighttime there is no regular E layer or F1 layer. Therefore the only regular mode of propagation is via the F2 layer.

For oblique incidence the maximum usable frequency (muf) is found in the following way. With the aid of equations (4) and (9) the secant law is written as

$$f_t = \frac{f \left(h_r + 2R \sin^2 \frac{d}{2R} \right)}{\left[h_r^2 + 4R(R+h_r) \sin^2 \frac{d}{2R} \right]^{1/2}} \quad (10)$$

where f_t = plasma frequency.

The plasma frequency, which is a function of the height is written

$$f_t = g(h_r) \quad (11)$$

and is given directly on an ionogram. (An ionogram, discussed later in this section, is a record of a vertical-incidence sweep-frequency sounding of the ionosphere.)

The problem is to determine the maximum value of f in equation (11) such that equations (10) and (11) are satisfied simultaneously. To do this, plot f_t versus h_r for different values of f ($f = f_1, f_2, f_3$) as shown in figure 4. Next an ionogram trace is superimposed on figure 4. Obviously, the points at which the curves cross satisfy both equations. The maximum value of f will be found by the curve which is just tangent to the ionogram trace. In this particular case the maximum f corresponds to $f = f_3$.

TABLE I

TYPES OF PROPAGATION MODES

	Mode	0 to 1999	2000 to 2999	3000 to 3999	4000 to 4999	5000 to 5999
1	E	X				
2	F1	X	X			
3	F2	X	X	X		
4	EE	X	X	X		
5	M (F2 F2)			X	X	X
6	F1 F1	X	X	X	X	X
7	F2 F2	X	X	X	X	X
8	EEE		X	X	X	X
9	F2 F2 F2			X	X	X
10	E F2				X	X
11	F2 E				X	X
12	EEEE				X	X
13	EE F2				X	X
14	E F2 E				X	X
15	F2 EE				X	X
16	M (F2 F2 F2)				X	X
17	E F2 F2					X
18	F2 F2 E					X
19	F2 E F2					X

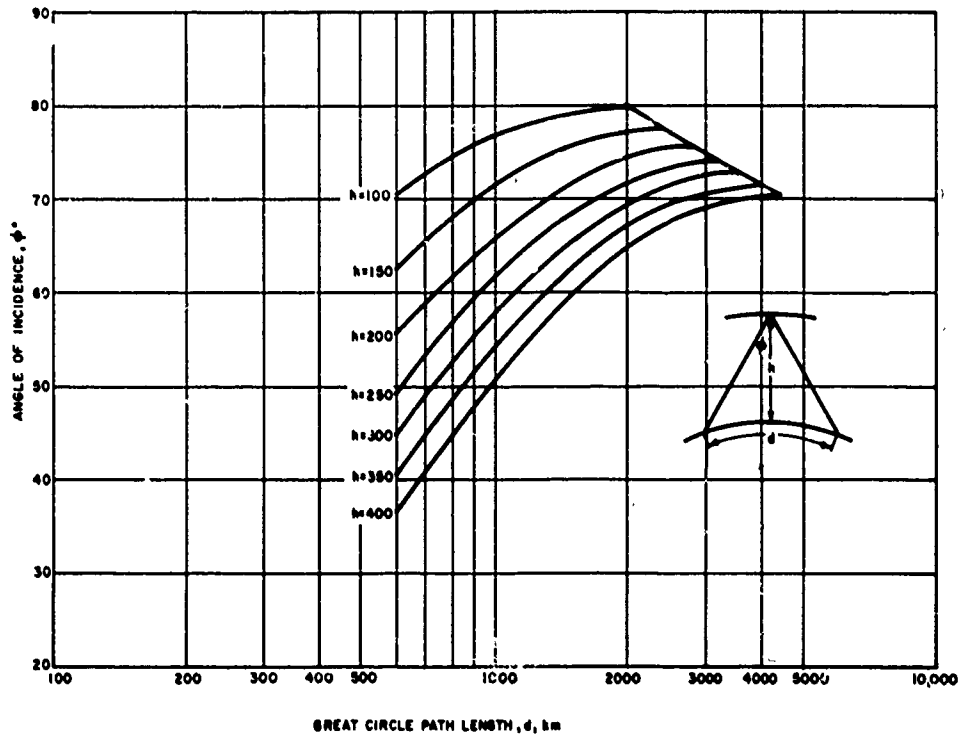


Figure 2 ANGLE OF INCIDENCE VERSUS REFLECTION HEIGHT AND GREAT CIRCLE PATH LENGTH
63-3599

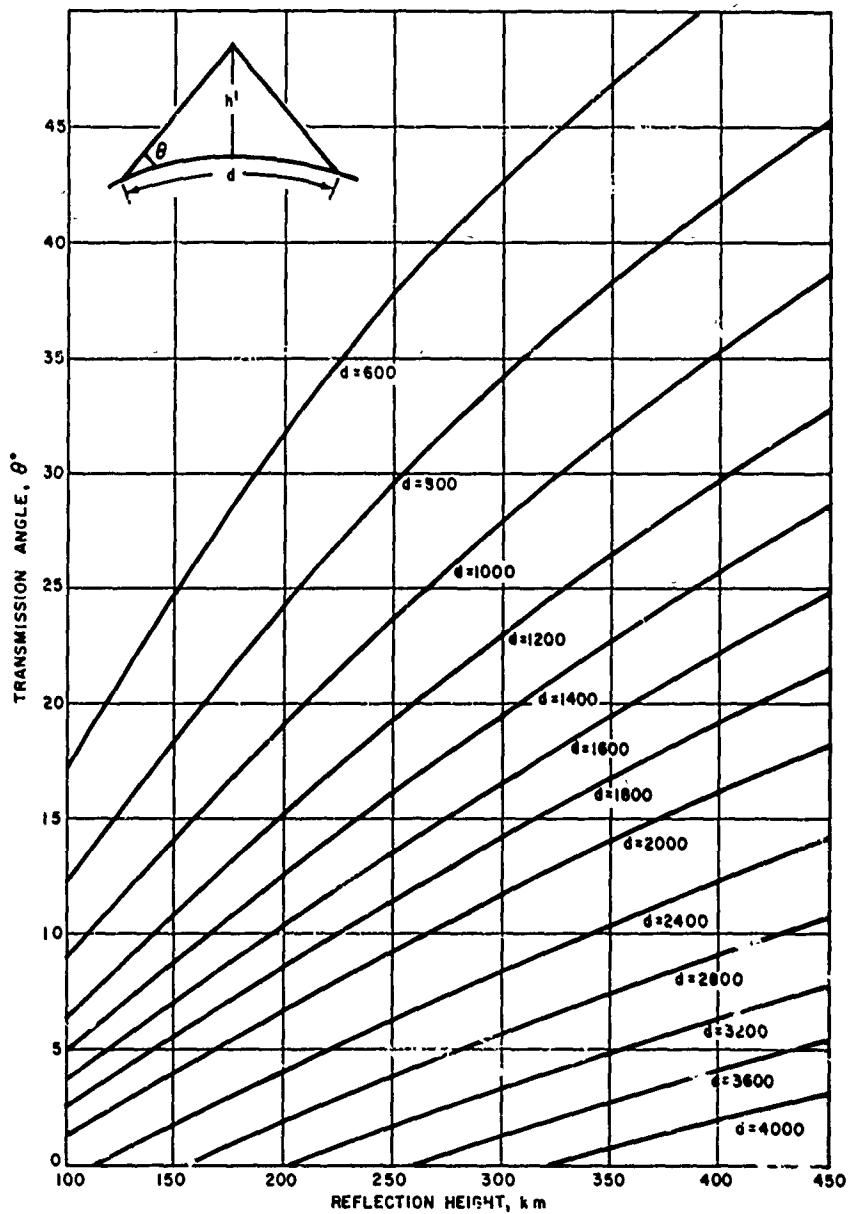


Figure 3 TRANSMISSION ANGLE VERSUS REFLECTION HEIGHT AND GREAT CIRCLE PATH LENGTH
63-3598

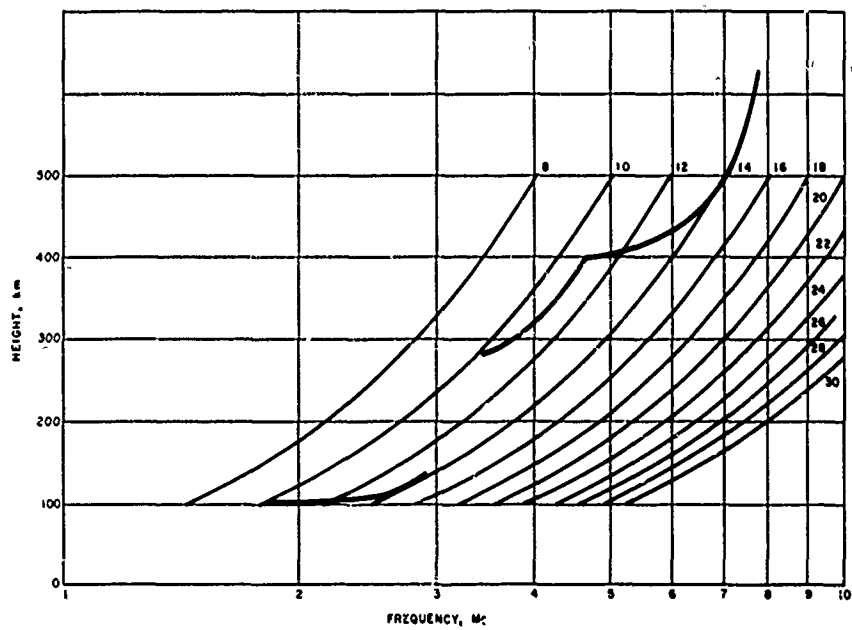


Figure 4 GRAPHICAL COMPUTATION OF MAXIMUM USABLE FREQUENCY
63-3597

1. Ionospheric Data

The electrical characteristics of the ionosphere are determined on a regular basis (every 15 minutes) by over 100 stations in the Northern Hemisphere and by a smaller number in the Southern Hemisphere, each using vertical incidence sounders. Measurements are normally made automatically over a frequency range between about 1 and 25 Mc, the interval being covered continuously on most equipment. The power output, receiver sensitivity, sweep time, and antenna efficiency vary considerably, especially between equipment of different national groups. Results obtained are rather uniform for regular layers, but there are some exceptions as with sporadic E.

Fundamentally, the ionosonde method consists of sending a short pulse of energy toward the ionosphere at a given frequency, and recording its return. Elapsed time is measured, and the (virtual) height of reflection is determined assuming that the radio wave travels with the speed of light. Since this is not strictly true near the height of reflection, the indicated (virtual) height is not the true height. In certain instances the signal may not be returned. There are two causes: (1) the absence of a reflecting layer for the frequency involved and (2) the strong absorption in the D region. In (1) the waves escape outward through the ionosphere (wave frequency is greater than the critical frequency) and is a measure of the maximum electron density of the layer. Absorption, however, is a reduction in signal strength below the sensitivity of the equipment. The ability to receive an absorbed signal is dependent on the receiver gain, antenna gain, and transmitted power, and these are characteristics of the individual station involved.

2. Ionograms

An idealized, typical ionogram is presented in figure 5. The ionospheric parameters which may be determined easily from an ionogram are

- a. E region maximum electron density (f_oE)
- b. F1 region maximum electron density (f_oF1)
- c. F2 region maximum electron density (f_oF2).

Using certain assumptions one can also determine from from the integrated attenuation occurring in the ionosphere up to the reflection height. It is possible to compute the true height of reflection from the virtual height, but this is not normally done, and requires laborious calculation unless a digital machine is used. At present, the only electron density versus true height profiles available on a routine daily basis are Puerto Rico in the CRPL-F series reports. Monthly mean (quiet day) electron-density

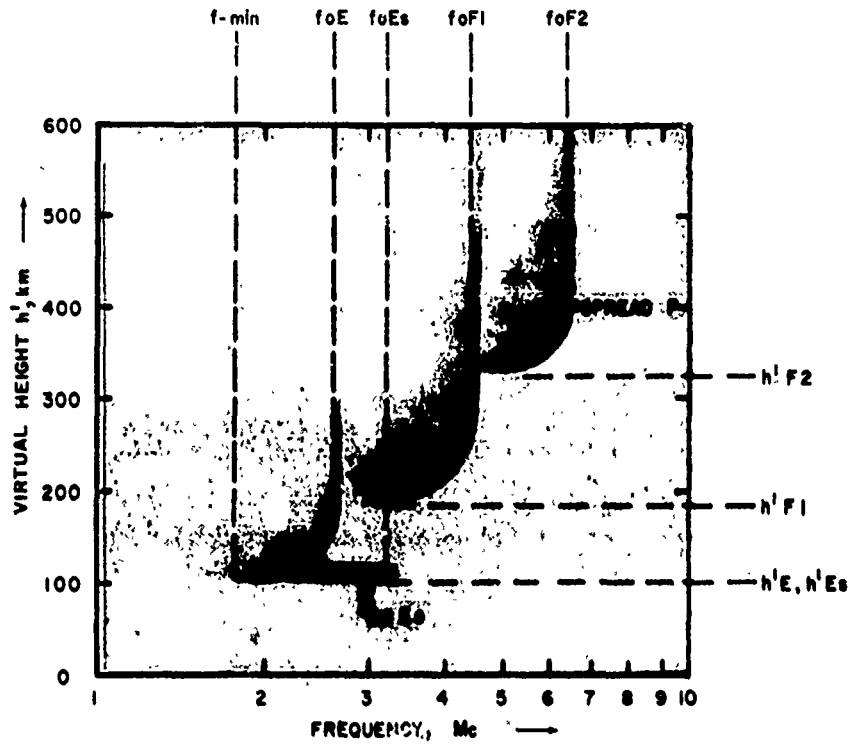


Figure 5 IDEALIZED IONOGRAM (ORDINARY COMPONENT)
63-3596

profiles have been determined for a number of Western Hemisphere stations and ionospheric true-height maps constructed (Wright, Wescott, and Brown). Refer to Wright, Knecht, and Davies (1957) for a further description of types; to Spread F, Penndorf (1962); and to the sections on sporadic E in this report. Scaling procedures are described in detail in Wright, Knecht, and Davies (1957) and Piggott and Rawer (1961) and are most useful in interpreting ionograms.

B. NONDEVIATIVE ABSORPTION

To calculate the signal loss in the D and E regions, consider the expression for nondeviative absorption. The signal loss, expressed in decibels, is given by

$$L = 8.7 p \sec \phi \int_0^{h_r} k ds \quad (12)$$

where p = number of penetrations through the D region and ϕ = incidence angle of the radio wave and

$$k = \frac{2\pi e^2}{mc\mu} \left(\frac{N\nu}{\nu^2 + 4\pi^2(f \pm f_H \cos a)} \right) \quad (13)$$

where

h_r = height of reflection

e = charge of an electron

N = electron-number density

ν = electron-collision frequency

m = mass of an electron

c = velocity of light

μ = refractive index (in the nondeviative region $\mu = 1$)

f_H = gyrofrequency

a = angle between the direction of propagation and the magnetic field

f = wave frequency (where the \pm sign in the denominator corresponds to the ordinary and extraordinary components respectively).

Integration of equation (12) using an electron density profile of Houston (1956) and the collision frequency distribution of Nicolet (1953) shows that ν in the denominator can be neglected. With this approximation equation (12) may be written (for the ordinary component)

$$L = \frac{4.35 p e^2 \sec \phi}{mc} \int_0^{h_r} \frac{N \nu}{(f + f_L)^2} ds \quad (14)$$

where $f_L = f_H \cos \alpha$.

If for the time being only the case of one pass at vertical incidence is considered, it will be possible to develop equation (14) into a more useful form. With these restrictions equation (14) is

$$L = \frac{4.35 e^2}{mc (f + f_L)^2} \int_{h(N=0)}^{h_r} N \nu dh \quad (15)$$

When the reflection height is above the absorbing region, the product $N \nu$ may be treated as a constant and

$$L = \frac{A}{(f + f_L)^2} \quad (16)$$

where A is a parameter which may be found from absorption measurements. (Of course for an independent determination of A , the height distribution of both N and ν must be known.)

When the reflection height is within the absorbing region, $N \nu$ cannot be treated as a constant but must be expressed as a function of height. From the analysis of electron density and collision-frequency profiles an approximation $N \nu \approx a (h - h_{(N=0)})$ may be written where a is a constant, and $h_{(N=0)}$ is set equal to 65 (km). (See example in figure 6.) Thus equation (15) may be written

$$L = \frac{4.35 e^2 a}{mc (f + f_L)^2} \int_{65}^{h_r} (h - 65) dh = \frac{A'}{(f + f_L)^2} (h_r - 65)^2 \quad (17)$$

The reflection height in equation (17) is found with the aid of the height distribution of electron density and the relation $N = 1.24 \times 10^4 f^2$. Empirically, it is found that frequency versus heights of reflection is given by a curve of the type shown in figure 7.

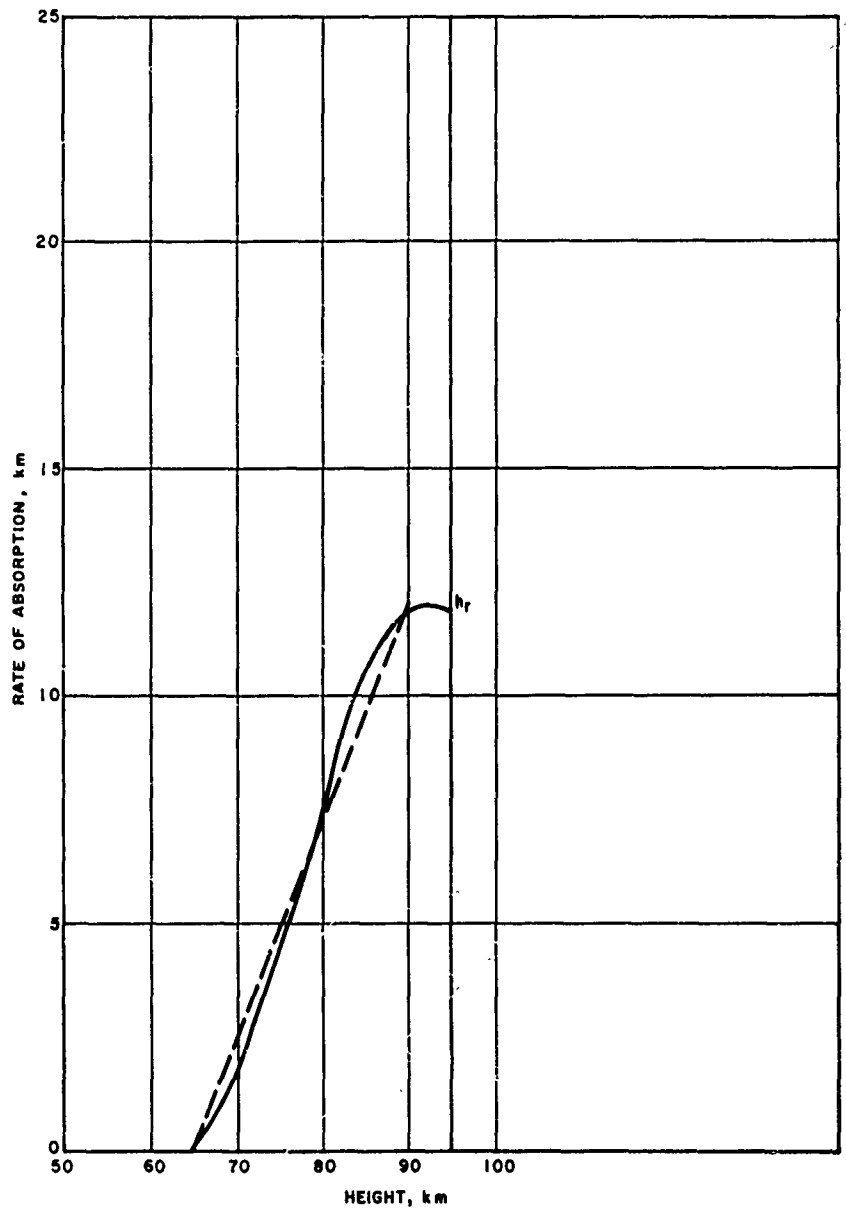


Figure 6 ABSORPTION COEFFICIENT VERSUS HEIGHT
63-3595

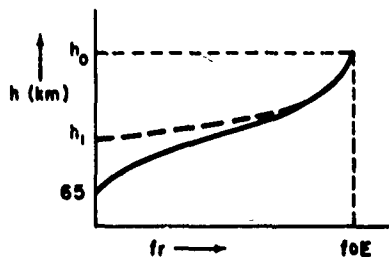


Figure 7 FREQUENCY VERSUS HEIGHTS OF REFLECTION IN THE
D REGION
63-3594

The upper portion of this curve (figure 7) can be thought of as being nearly parabolic whose equation is as follows:

$$(f_r - f_oE) = -b'(h_{ru} - h_o)^2 \quad (18)$$

where

f_r = frequency at reflection

f_oE = E region critical frequency

h_o = height at the critical frequency

h_{ru} = the height indicated by the parabola.

Solving for h_{ru}

$$h_{ru} = h_o \pm \left(\frac{f_oE - f_r}{b'} \right)^{1/2} \quad (19)$$

For reflections below h_o the negative sign is chosen. Evaluating b' for $f_r = 0$ and $h_{ru} = h_1$ and substituting in equation (19)

$$h_{ru} = h_o + (h_1 - h_o) \left(\frac{f_oE - f_r}{f_oE} \right)^{1/2} \quad (20)$$

where h_1 is a constant related to the parabola described by equation (18). This equation represents a curve which cuts the h -axis at h_1 (dotted line in figure 7).

To modify equation (18) so that it agrees with the solid curve, some hyperbolic function must be added, such as

$$h_{rl} = - \left(\frac{foE - f_r}{foE} \right)^2 \frac{c}{f_r + 1} \quad (21)$$

where the first factor on the right guarantees that as the frequency approaches foE, the magnitude of h_r (height contribution of the hyperbolic function) approaches zero which is what is required.

The equation for the complete curve giving the height of reflection h_r can now be written as

$$h_r = h_{ru} + h_{rl}$$

Using the condition, at f = 0, h = 65

$$h_r(f = 0) = h_{ru} + h_{rl} = 65$$

which leads to c = h₁ - 65, and

$$h_{rl} = - \left(\frac{foE - f_r}{foE} \right)^2 \frac{(h_1 - 65)}{f_r + 1} \quad (22)$$

Adding (20) and (22)

$$h_r = h_0 + (h_1 - h_0) E^{1/2} - \frac{h_1 - 65}{f_r + 1} E^2 \quad (23)$$

where

$$E = \left(\frac{foE - f_r}{foE} \right)$$

Substituting (23) into (17) yields

$$L = \frac{\Lambda'}{(f + f_L)^2} \left\{ h_0 - 65 + (h_1 - h_0) E^{1/2} - \frac{h_1 - 65}{f_r + 1} E^2 \right\}^2 \quad (24)$$

Analysis of electron density profiles shown in figure 8 (Kane 1962) indicates that h₀ ≈ 105 km. Inserting this into equation (24), multiplying the left-hand side by (40/40)² and noting that f = f_r at vertical incidence

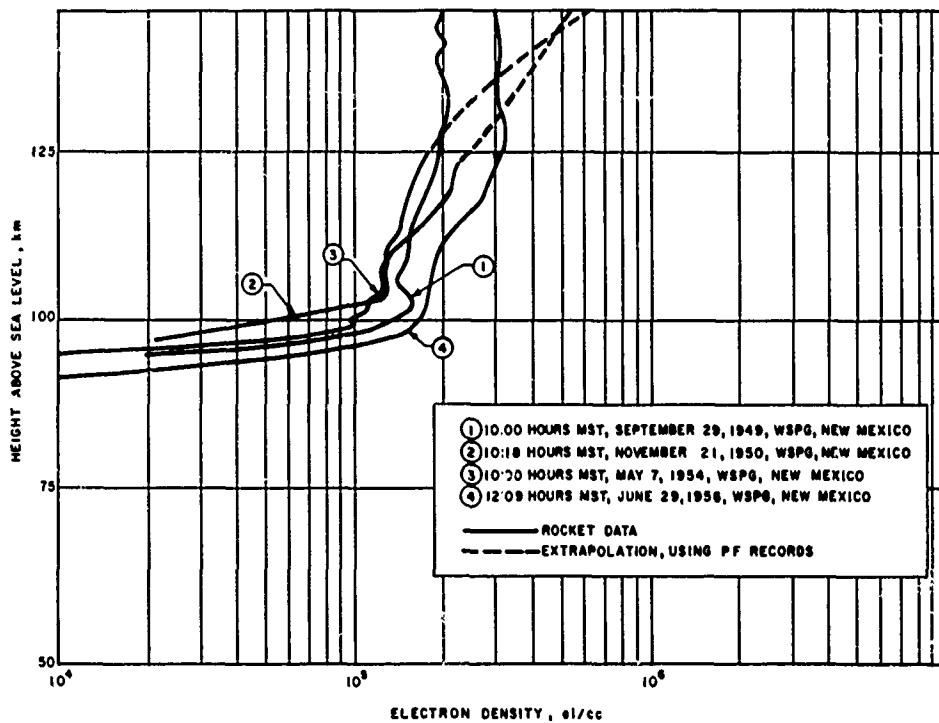


Figure 8 ELECTRON DENSITY PROFILES
 63-2581

$$L = \frac{\Lambda}{(f_r + f_L)^2} \left\{ 1 - bE^{1/2} - \frac{1-b}{f_r + 1} E^2 \right\}^2 \quad (25)$$

where

$$b = \frac{105 - h_1}{40} \quad \text{and} \quad f_r \leq foE .$$

This equation is similar to the inverse-frequency square law for nondeviative absorption except that it is modified by a correction factor (term in the braces). This correction factor is introduced because the height of reflection is not constant with respect to frequency. As a result, for frequencies less than foE it predicts a lower absorption than a simple inverse square law.

The parameters Λ and b in equation (25) are determined with the aid of experimental data. The value of Λ indicates the intensity of ionization in the absorbing region, while the parameter b governs the shape of the electron density profile. The value of Λ may be found by employing frequencies greater than foE and measuring the absorption. In this case the correction term is unity so

$$L = \frac{\Lambda}{(f_r + f_L)^2} \quad (26)$$

if $f_r > foE$.

For low and middle latitudes the monthly medians of absorption can be expressed

$$L_M = \frac{\Lambda'' \cos^{0.5} \chi}{(f_r + f_L)^2} \quad (27)$$

The value of Λ'' is found from measurements of L_M at Freiburg, Germany (Ionosphären-Institut Breisach, 1958) for a sunspot number of around 1b0. Analysis of this data shows that for one pass ($p = 1$) $\Lambda'' = 500$. With $\Lambda = 500 \cos^{0.5} \chi$, equation (25), when applied to monthly median data can be written

$$L = \frac{\Lambda'' \cos^{0.5} \chi}{(f_r + f_L)^2} \left\{ 1 - bE^{1/2} - \frac{1-b}{f_r + 1} E^2 \right\}^2 \quad (28)$$

Having determined Λ the parameter b is found by solving equation (28) for a range of b 's and comparing the results with measured values.

Measurements at Freiburg plotted against $(f_r + f_L)^2$ are shown in figures 9 through 13. Superimposed on these curves are the values of L for various values of b . From these curves the best value of b is taken.

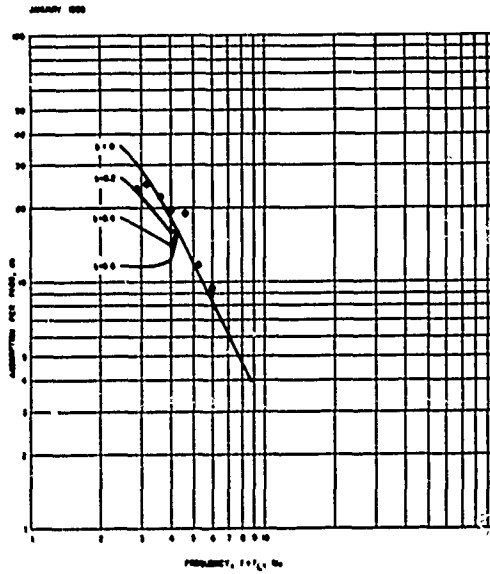


Figure 9 OBSERVED ABSORPTION AND COMPUTED ABSORPTION FOR VARIOUS VALUES OF b , JANUARY 1958
63-3589

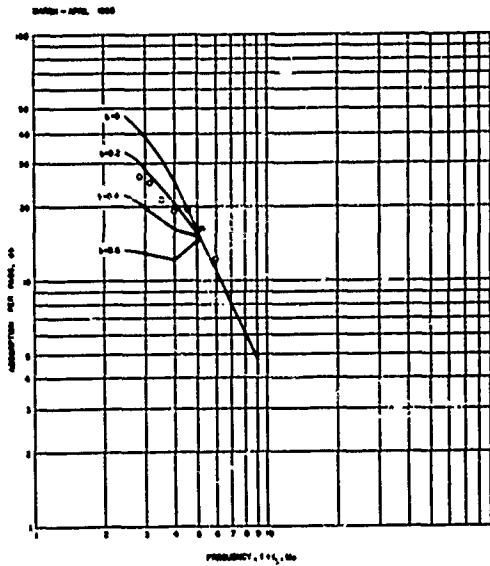


Figure 10 OBSERVED ABSORPTION AND COMPUTED ABSORPTION FOR VARIOUS VALUES OF b , MARCH - APRIL 1958
63-3590

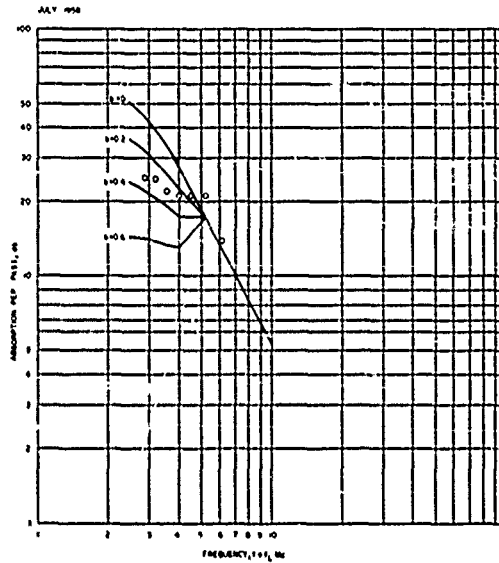


Figure 11 OBSERVED ABSORPTION AND COMPUTED ABSORPTION FOR VARIOUS VALUES OF b , JULY 1958
63-3591

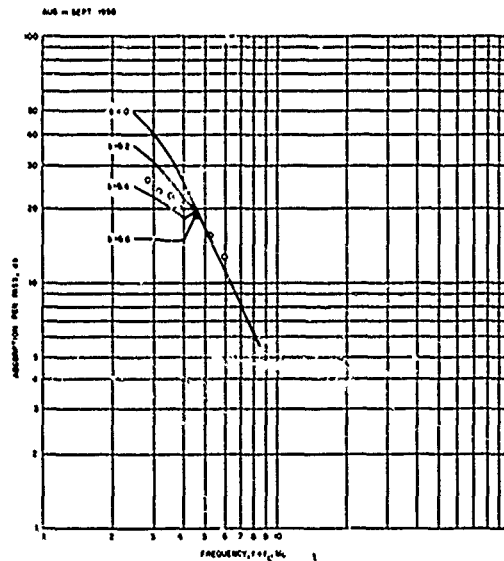


Figure 12 OBSERVED ABSORPTION AND COMPUTED ABSORPTION FOR VARIOUS VALUES OF b , DECEMBER 1958
63-3592

DECEMBER 1958

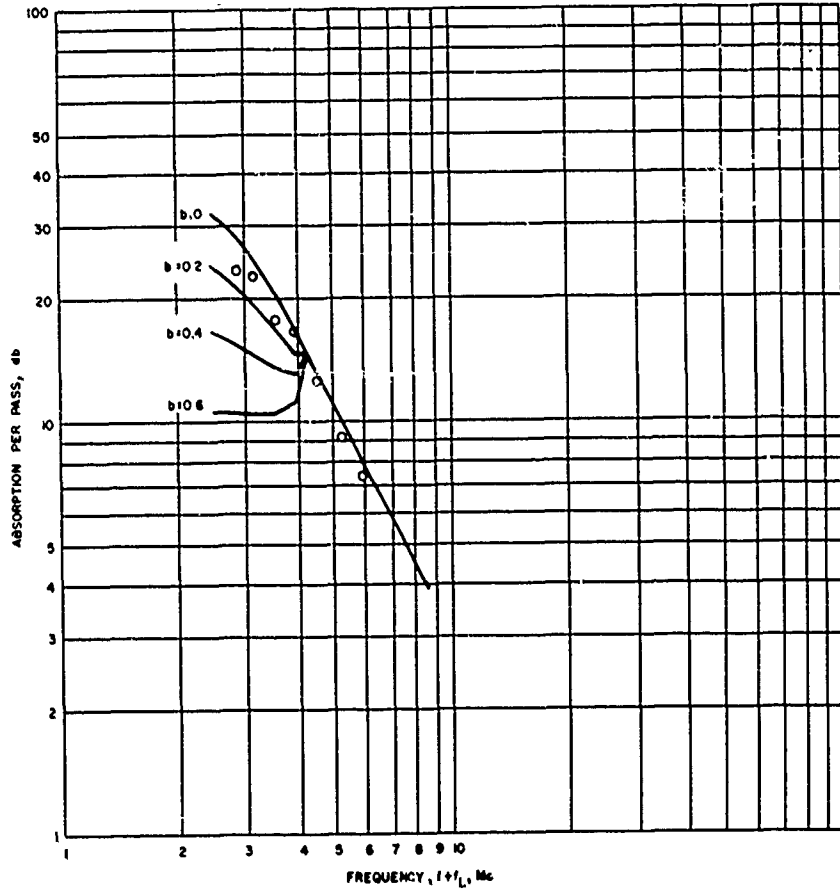


Figure 13 OBSERVED ABSORPTION AND COMPUTED ABSORPTION FOR VARIOUS VALUES OF b , AUGUST - SEPTEMBER 1958
63-3593

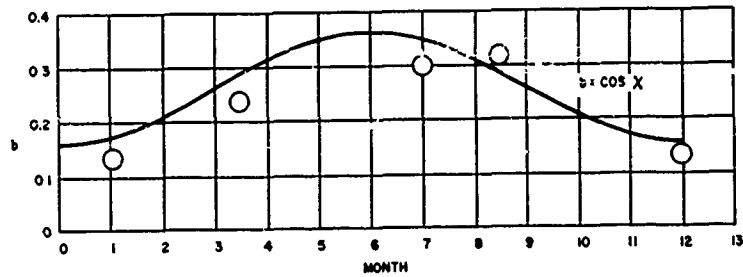


Figure 14 MONTH OF THE YEAR (1958) VERSUS b
63-3358

Seasonal variations of b are apparent, and the estimated variations of b for the year 1958 are plotted in figure 14. Months with a sunspot number greatly different from the yearly average (180) were omitted. It was found that b is related to χ by the expression

$$b = 0.375 \cos \chi \quad (29)$$

In oblique transmission, the distance traversed by the wave in the D region of the ionosphere is increased. This increase in the path length through the absorbing region is proportional to the secant of the angle of incidence. Thus, A in equation (25) is replaced by $A \sec \phi$. The reflection height, on the other hand, is lowered since it is computed on the basis of the secant law,

$$f_r = \frac{f}{\sec \phi}$$

and equation (25) becomes

$$L = \frac{A \sec \phi}{(f + f_L)^2} \left\{ 1 - b E^{1/2} - \left(\frac{1-b}{\frac{f}{\sec \phi} + 1} \right) E^2 \right\}^2 \quad (30)$$

if $f_r \leq foE$.

When f_r is greater than foE equation (26) is modified only by a factor $\sec \phi$ to take into account the longer path length. Thus,

$$L = \frac{A \sec \phi}{(f_r + f_L)^2} \quad (31)$$

if $f_r > foE$.

It should be noted that the value of f_L may be different in oblique propagation from its value in vertical propagation.

The A in both equations (30) and (31) is determined from f_{min} data exactly as described before, with the vertical incidence measurements being made at places where the wave passes through the D region.

These equations for absorption have been verified, so far, only by comparison of computed versus measured values of absorption at vertical incidence; the results of which are shown in figures 9 through 13. It is also desirable to compute electron density profiles by the equation giving the reflection height and compare the results with profiles measured with rocket-borne instruments. By substituting the expression $b = (105 - h_p)/40$ (equation 25) into equation (23), h_r can be written

$$h_r = 40 \left[1 - bE^{1/2} - \frac{i-b}{f_r + 1} E^2 \right] + 65.$$

Replacing the frequencies by the corresponding electron densities using equation (2), the electron density as a function of height is obtained. It is expressed as

$$h_r = 40 \left[1 - bN^{1/2} - \frac{i-b}{f_r + 1} N^2 \right] + 65 \quad (32)$$

where

$$N^* = \frac{N_0^{1/2} - N^{1/2}}{N_0^{1/2}}$$

Equation (32) can be evaluated by finding h_r for various values of N which are less than or equal to N_0 . Such computations are made using values of N_0 (or f_0E) and b appropriate to the time and dates of the measured profiles shown in figure 15 (Heilskila, et al., 1960), figure 16 (Pfister and Ulwich, 1961) and figure 17 (Kane, 1962). As indicated on the figures the computed values give excellent agreement with the measured ones.

G. REFLECTION COEFFICIENT FOR SPORADIC E

Regular ionospheric layers (E,F) are assumed to be totally reflecting below their critical frequency, and transparent above the critical frequency. This is the mathematical result of applying a full-wave solution of Maxwell's equations to a semi-infinite, horizontally stratified, monotonically increasing, slowly varying ionized region with negligible collisions (Ratcliffe, 1959). Below the critical frequency all the power is returned while above it none is reflected. The fact is observationally confirmed in all but a limited number of special situations in which the above referenced solution is not valid. Specifically, this involves the Z trace observed on high latitude ionograms (Rydbeck, 1951). For communications the Z trace is not of practical importance.

In the case of sporadic E, the space gradient of electron density is too high for normal ray theory to be valid; sporadic E is partially transparent below the plasma frequency and partially reflecting above it. The layer is found in the region between 100 to 120 km. Some causes which have been suggested are turbulence, in Whitehead (1962), wind shear in Axford (1962), or ionization due to corpuscular radiation. The latter is likely to be the cause of most high-latitude E_s , while the former two are thought to be operative at lower latitudes. The thickness of the ionized region may be of the order of several wavelengths at HF (Seddon, 1961). An assumption of infinite thickness is not warranted, and rigorous solution of the wave equation must be attempted. The reader is referred to Rydbeck (1943), Epstein (1930), Northover (1962) for several of the solutions. One of these, due to Northover, is selected as offering the most

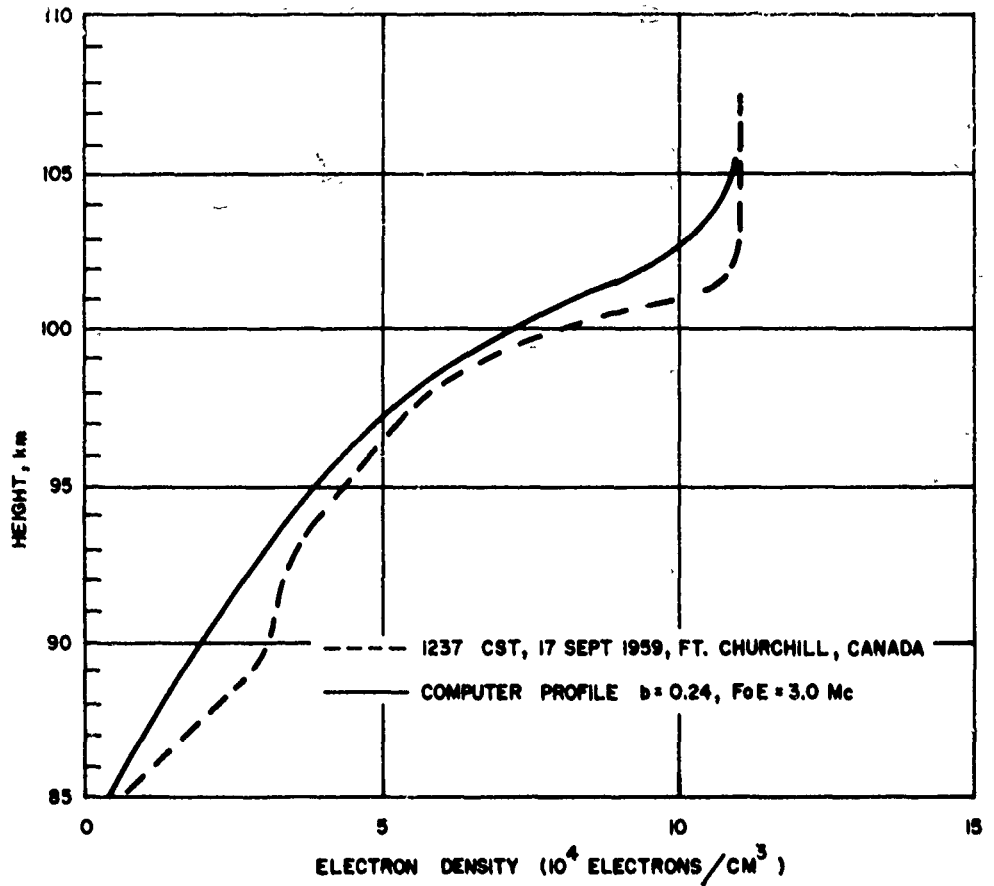


Figure 15 ELECTRON DENSITY PROFILES - OBSERVED AND COMPUTED,
 $b = 0.24$
 63-3587

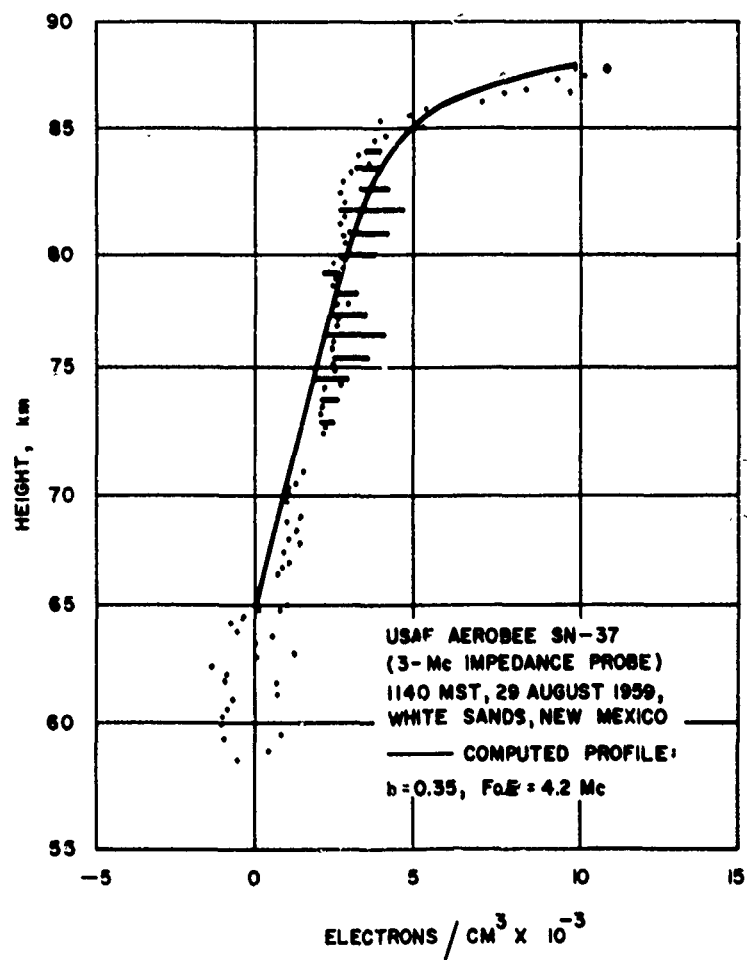


Figure 16 ELECTRON DENSITY PROFILES - OBSERVED AND COMPUTED,
 b = 0.35
 63-3586

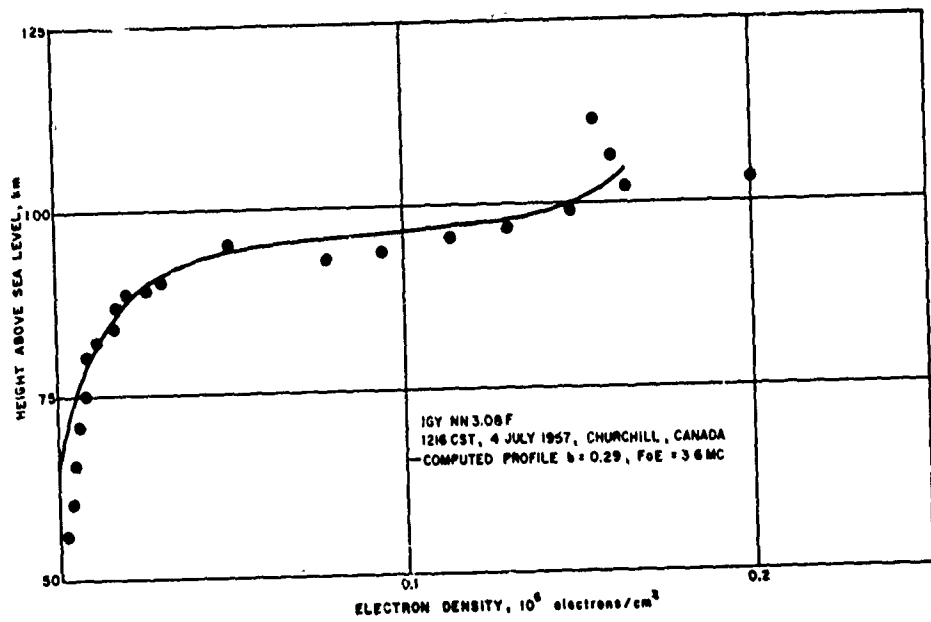


Figure 17 ELECTRON DENSITY PROFILES - OBSERVED AND COMPUTED,
 $h = 0.29$
 63-3585

promise for high-latitude phenomenon. The solution is one which permits the use of the secant law for propagation. It is thus applicable to vertical incidence as well as oblique propagation.

The ionospheric layer is taken to be parabolic in shape with a half thickness r and maximum electron density N_m . Solution of Maxwell's equations yields a reflection coefficient which is graphed in figure 18. These curves are almost indistinguishable from the family of curves which satisfies the equation

$$R = e^{-Af^C} \quad (33)$$

where

R = ratio of incident to reflected voltages.

f = operating frequency in Mc.

A, C are constants characteristic of individual Es layers and may be shown to be (no D-region absorption)

$$C = \frac{\log G_a/L_b}{\log foEs/fbEs} \quad (34a)$$

and

$$\log A = \log \frac{G_a}{20} - \frac{\log \frac{G_a}{L_b}}{1 - \frac{\log fbEs}{\log foEs}} \quad (34b)$$

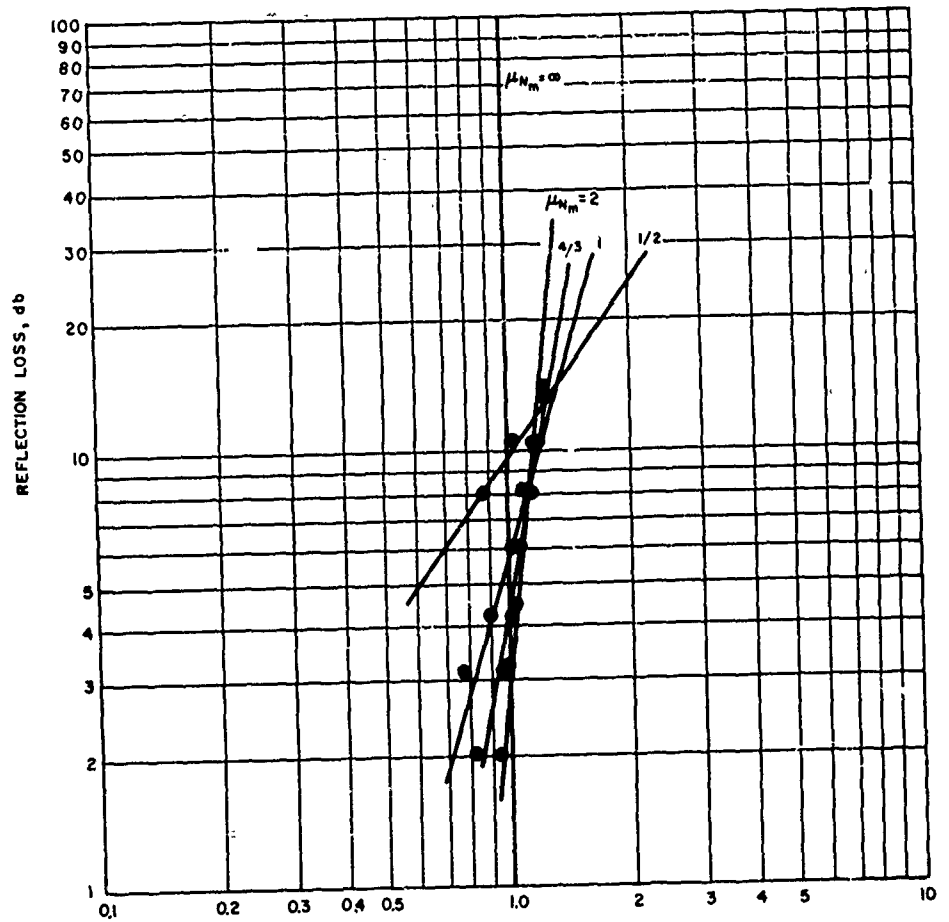
L_b = reflection loss at fbEs ≈ 0.2 db

G_a = ionosonde available gain ≈ 45 db (medium gain).

It is possible using the observed value for C to determine r/N_m the layer thickness parameter, and then from figure 19 read off the reflection loss at the plasma frequency. Using an experimental reflection loss versus frequency graph the plasma frequency is determined. The plasma frequency is not, however, necessary for propagation problems. If the parameters C and A are determined, slant path propagation may be predicted using the secant-law reduced frequency.

$$f_r = \frac{f}{\sec \phi}$$

The reflection coefficient is determined by experimentally using ionosonde film recordings for the hourly gain run. In this section, D-region absorption is neglected: all data is read from twilight or nighttime film. Any change in the foEs of the lowest Es trace or its multiple reflections (if present) must be due to a



$$\lambda = \frac{f}{r_p \sec \theta}$$

Figure 18 REFLECTION LOSS VERSUS λ AND μ_{Nm}
63-3584

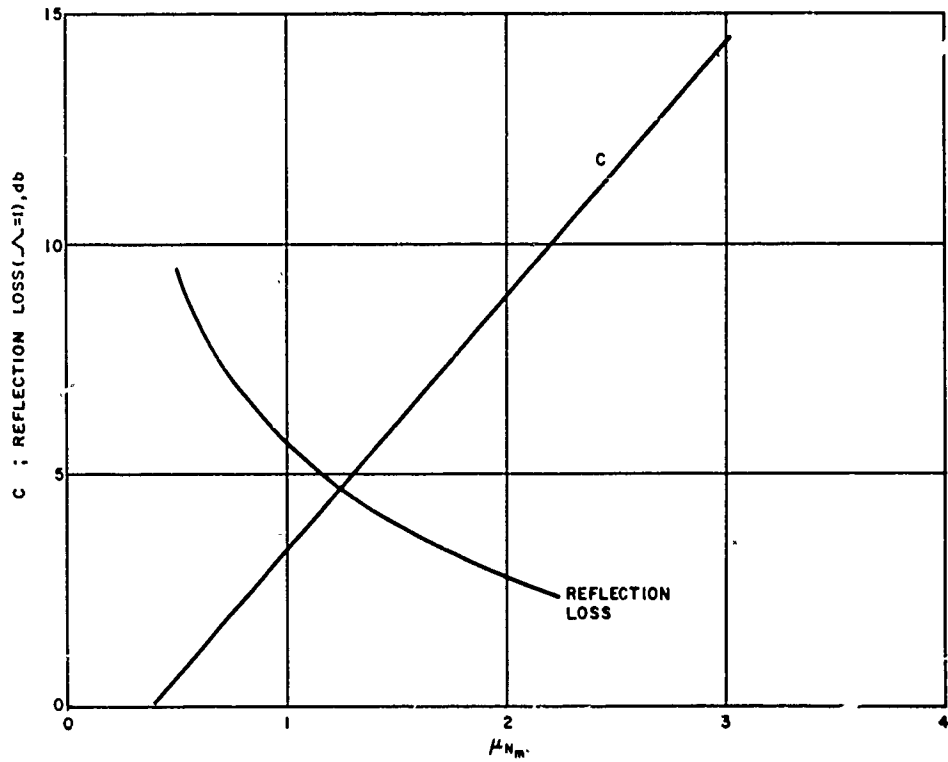


Figure 19 REFLECTION LOSS, C, AND μ_{Nm}
63-3583

partial reflection loss. While the absolute value of ionosonde gain is uncertain, the gain run changes are accurately known and are 20 db/step for the Canadian LG-17 and Cossor Sounders. The gain run steps in the American C-2, -3, and -4 sounders are a function of the receiver medium-gain setting, which is adjusted automatically daily and seasonally; the average change is 10 db/step. When considering the reflection coefficient, the computation is not broken up on a per pass basis. This reflection loss may be expressed in terms of the ionosonde sensitivity, ground reflection loss, D-region absorption, and additional space loss for the multiple reflections.

$$R = (G_a - 20 \log N - G(N-1) - 2NL + \psi)/N \quad (35)$$

where

- G_a = ionosonde gain \pm 40 to 50 db
- N = number of reflections from layer
- G = ground reflection loss \pm 5 db
- L = D-region absorption - per pass
- ψ = ionosonde gain change HI-MED-LO (db).

If the data are taken at night or twilight and f_oE_s for the reflection or its multiple being considered is greater than about 6 Mc, the D-region absorption may be neglected; its effect is most noticeable on multiples $N \geq 5$.

Wright and Gautier (1960) report an approximate verification of the secant law for E_s on a slant path in middle latitudes. Preliminary data from the Washington-Boston path indicate that both the secant law and equation (33) are valid (refer to section II, paragraph G).

D. TRANSMITTERS, RECEIVERS, AND ANTENNAS

Numerical calculations of signal strengths are based on transmitted as well as ionospheric parameters. The factors influencing transmitted signal strength are transmitter output power, and antenna gain, from which the losses in the transmission line and antenna are subtracted. The field-strength voltage E is related to the energy density P by the intrinsic impedance of free space R_0 by

$$E^2/R_0 = P$$

or

$$E = (377 P)^{1/2}, \quad (\text{v/m}) \quad (36)$$

An isotropic radiator in free space transmits power equally in all directions, so that the power is spread over a sphere of area

$$A = 4\pi d^2.$$

d = distance from antenna in km and thus the power density $P(d)$ per unit area is

$$P = \frac{P_t}{4\pi d^2} \text{ watts/km}^2 \quad (37)$$

where P_t is the transmitter power in watts radiated by an isotropic antenna. Combining equations (36) and (37)

$$E = \frac{5.45 \times 10^{-3}}{d} P_t^{1/2}, \text{ v/m} \quad (38)$$

with d in km.

Further, when a transmitting antenna, which has a gain g_t , is used, the voltage in $\mu\text{v/m}$ is given by

$$E = \frac{5.45 \times 10^{-3}}{d} (P_t g_t)^{1/2}, \mu\text{v/m} \quad (38a)$$

and

$$20 \log E = 74.8 + 10 \log P_t g_t - 20 \log d + 10 \log g_t \quad (38b)$$

(db above 1 $\mu\text{v/m}$, with d in km)

In some field-strength calculations, the transmitted power is reduced by 1/3 and called the effective radiated power (NBS Circular 462). This yields a signal strength of $3 \times 10^5 \mu\text{v/m}$ at 1 km for an effective radiated power of 1 kw.

1. Antennas

The characteristics of antennas which are of importance in communications are the gain (relative to either an isotropic antenna, or to a half-wave dipole), the radiation pattern, and the effective area. The latter is useful for receiving antennas, while the former two are employed to describe antennas used for transmitting and receiving systems.

In a receiving system, it is important to know the efficiency with which an antenna can abstract energy from a wave incident upon it. Particularly for a half-wave dipole antenna, the current I through a load in its center induced by a uniform electric intensity $E_o(\text{v/m})$ parallel to the antenna is (Schelkunoff and Friis, 1952),

$$I = \frac{73 E_0 \int_{-\lambda/4}^{+\lambda/4} Y(z) dz}{(Z + 73)}$$

where $Y(z) = \frac{1}{73} \cos \beta z$, $\beta = \frac{2\pi}{\lambda}$, and Z is impedance of load.

$$\text{Thus } I = \frac{\lambda E_0}{\pi(73 + Z)}$$

For maximum signal transfer to the load, $Z = 73 \Omega$, and the voltage developed across the load is

$$\mathcal{E} = \frac{0.707 \times 73 \lambda E_0}{146\pi}, \quad \lambda = \frac{300}{f_{Mc}}$$

$$\text{or } 20 \log \mathcal{E} = 30.6 + 20 \log E_0 - 20 \log f_{Mc} \quad (39)$$

where

\mathcal{E} is in μv

E_0 is in $\mu v/m$.

The space attenuation is given by (38b), and further, equation (39) may be generalized to include the effect of a receiving antenna gain to yield

$$\langle \mathcal{E} \rangle = 20 \log \mathcal{E} = 105.4 + 10 \log P_t G_t - 20 \log d - 20 \log f_{Mc} + G_r + G_t \quad (40)$$

where

$\langle \mathcal{E} \rangle$ = signal in db above one μv at receiver

d = distance in km

f_{Mc} = frequency in Mc

G_r = receiving antenna gain relative to half-wave dipole (db)

G_t = transmitting antenna gain relative to half-wave dipole (db).

2. Receivers

The characteristics of receivers vary with the manufacturer, but an acceptable HF general-coverage communications receiver has a sensitivity of $0.5 \mu\text{v}$ at the antenna terminals for a signal-to-noise power ratio of 10 decibels in a 6 kc bandwidth. Signal-to-noise ratios necessary for communication with a specified error rate are different for various information coding methods. Certain standard signal-to-noise ratios have been established experimentally by Watt et al. (1958) and are given in table II.

The noise power available at the antenna from atmospheric, cosmic, and man-made noise is combined with the antenna thermal noise, and an effective noise figure f_a is defined so that

$$P_n = f_a ktb \quad (41)$$

where

P_n = external noise power

f_a = effective noise figure at antenna terminals

k = Boltzman's constant = 1.38×10^{-23} Joules/deg K

t = temperature in degrees K

b = Effective bandwidth in cps.

Losses occurring in the transmission line and antenna are expressed as equivalent noise figure f_t and f_c while the receiver noise is f_r . The effective noise figure referred to the receiver terminals is

$$f = f_a - 1 + f_t f_c f_r \quad (42)$$

if the temperature is the same in all networks, Friis (1944), and Critchlow et al. (1955). If P_m is the minimum signal power required to maintain satisfactory service when the signal-to-noise power ratio is r , then

$$P_m = r f k t b \quad (43)$$

or in decibels

$$P_m = R + F + B - 204 \quad (44)$$

TABLE II
REQUIRED SIGNAL-TO-NOISE RATIOS*

System	wpm	Noise Dynamic Range		Carrier	C/N 1 kc rms carrier to rms noise in a 1-kc band db		
		Type	db**		10%	1%	0.1%
A CW good operator	15	T†	21	S	- 1	1	(4)
B CW good operator	12	A††	68	S	-11.5	- 2	(4)
C CW fair operator	12	A	68	S	- 3	-	--
D CW good operator	12	A	69	S	-10	(-2)***	--
E CW good operator	16	A	69	S	- 8	(0)	--
F CW good operator	20	A	69	S	- 6	(1)	--
G FSK ± 17 cps	40	T	21	S	- 2.3	0	1.6
H FSK ± 50 cps	60	T	21	S	0	2	3
I FSK ± 25 cps	60	A	68	S	0	10	17
J FSK ± 50 cps	60	A	69	S	3	11	15
K FSK ± 425 cps	60	A	50	S	10	18	21
L FSK ± 425 cps	60	A	40	ionospheric fading	12	23	34
M FM-FSK 576 TTY channels	60/ch	T	21	tropospheric fading	43	48	53
N FM- 36 voice channels	100/ch	T	21	tropospheric fading	49	80	

* As measured by Watt et al. (1958)
 ** 0.001 to 90 percent in a 1-kc band
 *** Numbers in parentheses are extrapolated or based upon extrapolated data
 † thermal noise
 †† atmospheric noise

where

$$P_m = 10 \log P_m$$

$$R = 10 \log r$$

$$F = 10 \log f$$

$$B = 10 \log b.$$

and $10 \log kt = -204$, if $t = 288.48^\circ K$.

In HF communications systems, certain approximations may be made. The losses associated with the antenna circuit and transmission line are small in the HF band, and the limiting factor on signal detectability is external noise of man-made, cosmic, or atmospheric origin. The receiver noise figure f_r is less than that due to external noise at all frequencies below 50 Mc.

In equation (44) we may then replace F by

$$F_a = 10 \log f_a$$

with no loss in accuracy and equation (44) becomes

$$P_m = R + F_a + B - 204 \quad (44a)$$

We may use equation (44a) to calculate the necessary antenna gains and transmitter power necessary for a given signal-to-noise ratio, or using a particular system, determine what information transmission modes will give the lowest error rate.

That is

$$P_t = L_T - G_t - G_r + F_a + R + B - 204 \quad (45)$$

where P_t is the radiated power in watts, $L_T =$ space, reflection, and absorption losses.

E. RADIO NOISE

1. Atmospheric Radio Noise

Probably the greatest limitation to the useful sensitivity is the presence of atmospheric radio noise. The source of this noise is from lightning discharges, but it can be propagated thousands of km as with ordinary transmitted signals. The level of atmospheric radio noise is usually determined by the strength of the several world thunderstorm centers. However, when electrical storms are in the immediate vicinity of a receiver, the local source will predominate and will sometimes greatly exceed the normal level. In middle latitudes the occurrence of thunderstorms is limited to about 1 day in 10, and in high latitudes, about 1 day in a 100. Furthermore, the duration of these thunderstorms is only about 2 hours. So, most of the time, the dominating sources are the equatorial ones, e.g., Southeast Asia, Africa and South America. For this reason the monthly medians of measured noise levels indicate the effects of the major thunderstorm centers, rather than local ones.

An attempt to compute the noise expected at middle or high latitude stations requires a consideration of many factors. The important ones are listed in the following:

- a. Radiated power from lightning discharges
- b. Rate of lightning occurrence
- c. Size of thunderstorm area
- d. Distance from source to receiver
- e. Loss of power from absorption
- f. Loss of power from ground scatter
- g. Frequencies which can be propagated by ionospheric reflection.

In the calculation of the power output P of the thunderstorm center, several approximations are made. One is that the average number of lightning strokes per 1-hour thunderstorm is taken to be 200 (Handbook of Geophysics, 1960). The time duration of a single stroke is about 30 μ sec (Pierce, 1966), so the fraction of time $\delta t/T$ of noise output per thunderstorm is $\delta t/T = 200 \times 30 \times 10^{-6}/3600 = 1.67 \times 10^{-6}$.

The average power output in watts of a single lightning stroke for a 1-kc bandwidth is given by $P_E = 1.6 f^{-4}$ where f is in Mc (Handbook of Geophysics

1960). So the power output per thunderstorm is $P_E \delta t$ or $1.67 \times 10^{-6} \times 1.6 \times f^{-4} = 2.67 \times 10^{-6} f^{-4}$. The total power output per thunderstorm region is $P = n P_E \delta t / T$ where n is the number of thunderstorms simultaneously occurring in the region. Thus $P = 2.67 \times 10^{-6} n f^{-4}$. The value of n depends upon the region considered, the season, and local time of day.

The ionospheric propagation modes are now considered in order to ascertain the contribution of each thunderstorm area to the noise at a particular location. As an initial approximation, the mode with the smallest number of ionospheric and ground reflections will be least attenuated and thus be dominant. This corresponds to the lowest angle of radiation. At distances greater than 3000 km, the approximation is made that the ray path in km, the approximation is made that the ray path in km is equal to the distance along the Earth's surface. Further, the low-angle radiation is focused by reflection between a curved ionosphere and Earth and results in a gain, G_f , of approximately 8 db. Applying these corrections to the expression for the field strength previously developed, we find

$$20 \log E = 74.8 + G_f - 20 \log d' + 10 \log P \quad \mu v/m \quad (d' > 3000 \text{ km}) \quad (46)$$

where

G_f = focusing gain $\hat{=} 8$ db.

d' = distance on surface of the earth in km

P = total thunderstorm power output in watts/kc.

Other important losses are absorption in the D region and ground reflection loss. The signal voltage after N hops have been reflected at the ground $N-1$ times. Thus

$$E = g^{N-1} E_0 \quad (47)$$

where g is the ground reflection coefficient

$$20 \log E = 20(N-1) \log g + 20 \log E_0 \quad (47a)$$

A typical value of g is 0.63.

In the calculation of L , the absorption is found for each hop, so that

$$L = \sum_1^N L_N \quad (48)$$

where N is the number of hops, and using the results of the previous section.

$$L_N = \frac{rA \sec \phi_D}{(f + f_L)^2} \quad (49)$$

where rA is dependent upon the state of the D region, and ϕ_D refers to the angle of incidence to the D region. For long distance propagation by the E layer, $\sec \phi_D = 5$, and by the F2 layer, $\sec \phi_D = 3$, rA may be found with the aid of f_{min} data just as with normal transmissions.

Combining these loss and production-equations

$$20 \log E = 105.4 + G_f - 20 \log d' + 10 \log P \\ + 20(N-1) \log g - \frac{rA \sec \phi_D}{(f + f_L)^2} - 20 \log f \quad (50)$$

The resultant is the rms noise voltage in τ , 1-kc bandwidth at the antenna terminals of a half-wave dipole. Computation of the atmospheric noise figure at the antenna can be accomplished using equations (41) and (50). Expected values of median radio noise levels may be found in C.C.I.R. Report No. 65, (1957).

2. Cosmic Noise

Cosmic noise is made up from essentially randomly polarized waves of galactic origin. The sources are not uniform, but are located in several major centers in the celestial sphere. The noise level away from these centers is somewhat reduced. Cosmic noise reaches the Earth's surface at frequencies greater than the F2-layer critical frequency multiplied by the secant of the incidence angle. This noise may arrive at a receiver either directly from outer space or indirectly by first arriving at the Earth's surface and then propagating by the usual ionospheric modes.

Above about 25 Mc the major contribution to radio noise is caused by cosmic sources, while below this transition frequency, man-made and atmospheric noise predominates. However, in polar regions where both the f_oF_2 and atmospheric noise may be low, cosmic noise may be the limiting factor at frequencies as low as 5 Mc.

3. Man-made Noise

When atmospheric noise is low, radio noise generated by electrical apparatus such as ignition systems or electric drills may be the limiting factor in the useful sensitivity of a receiver. Radar noise may originate at any point where there is a sudden change in voltage. This condition is most frequent at electrical switches of any type. Radio noise may also originate where an electrical discharge occurs - as a result of ionization of air surrounding a conductor around which there is an excessive voltage gradient (Merriman, 1954). A list of important radio noise sources is provided below:

Power and distribution lines

High-voltage equipment

Electric railway systems

Wire communication systems

Commutator motors and generators

Thermostats

Fluorescent lights

Sign flashers

Oil burning furnaces

Electrostatic discharge

Small generating plants

Industrial, scientific, and medical apparatus

Arc welding equipment

Elevators

Vehicles.

F. CALCULATION OF RECEIVED SIGNAL STRENGTH

In ordinary HF communication it is desirable to compute the received signal strength from some distant transmitter. Such a calculation is basic to this study and what follows will serve as an example showing how the calculation is made if certain parameters are first specified. These parameters involve the following factors:

1. Equipment characteristics
2. Distance from transmitter - space attenuation
3. Possible modes
4. Absorption
5. Other losses
6. Radio noise.

The basic equipment characteristics required are the effective radiated power along with the antenna gain, and the receiver sensitivity and its antenna gain. Included in the receiver sensitivity is the allowable signal-to-receiver noise ratio for the type of communication service under consideration.

Under normal conditions the receiver noise level is replaced by the external noise level. For example, in the absence of external noise a receiver sensitivity of $1\mu\text{v}$ means that a received signal of $1\mu\text{v}$ would give a signal-to-noise ratio of say 10. However, in the presence of atmospheric noise at a level of one μv the signal-to-noise level would only be one. To maintain a signal-to-noise level of 10, the received signal strength would have to be increased to $3\mu\text{v}$ i.e., 10 db. So it can be seen that the maximum amount of allowable signal loss between the transmitter and the receiver is the difference between the signal strength just after transmission and the minimum allowable signal strength after reception. Of the factors determining the signal-strength loss between the transmitter and receiver, the least variable of these factors is space attenuation. Although this varies slightly with the mode of propagation it is essentially dependent solely upon the distance of propagation.

In determining the maximum frequency of propagation, it is necessary to consider the layer critical frequencies and their height. Also, this is necessary to determine the amount of absorption. In other words, before losses can be determined it is necessary to find the modes possible. When this is done, it is possible to compute the loss from absorption by making use of equations (29) or (30).

Other losses such as ground loss and reflection losses associated with sporadic E also should be taken into account. If the total of the losses for a particular frequency is less than the maximum allowable signal loss, then that frequency may be used successfully.

G. EXPERIMENTAL DATA

Field-strength data is obtained from recordings at Wilmington, Massachusetts of WWV transmission at 2.5, 5, 10, 15, and 20 Mc. Records of these measurements for a period of a day and a half are shown in figure 20. Inspection of these graphs shows several interesting features. These are as follows:

1. Daytime absorption on 2.5 and 5 Mc.
2. Enhanced signal level on all frequencies around 0000 LT, 12 Jan 1963 in connection with sporadic E layer.
3. Large changes in the signal strength of 10 Mc during the daytime over short-time periods.

Explanation of these features is readily understood with the aid of "f-plots," i.e., graphs showing the basic ionospheric parameters from vertical incidence soundings at 15-minute intervals. f-plots for 11 and 12 Jan 1963 taken at Ft. Monmouth, New Jersey are shown in figure 21. The parameters and values appropriate to the features listed above are:

- a. f_{min} at 1200 LT, 11 and 12 Jan 1963 is 2.3 Mc on each day. Using the results of the section on absorption the absorption formula as applied to ionosondes is

$$L_I = \frac{rA}{(f_{min} + f_{L_v})^2} \quad (51)$$

With $L_I = 18$, $r = 0.75$, $f_{L_v} = 1.4$ and $f_{min} = 2.3$ the value resulting for A is 328.

For oblique transmission at 5 Mc the absorption formula is written

$$L = \frac{rA p \sec \phi_D}{(f + f_L)^2}$$

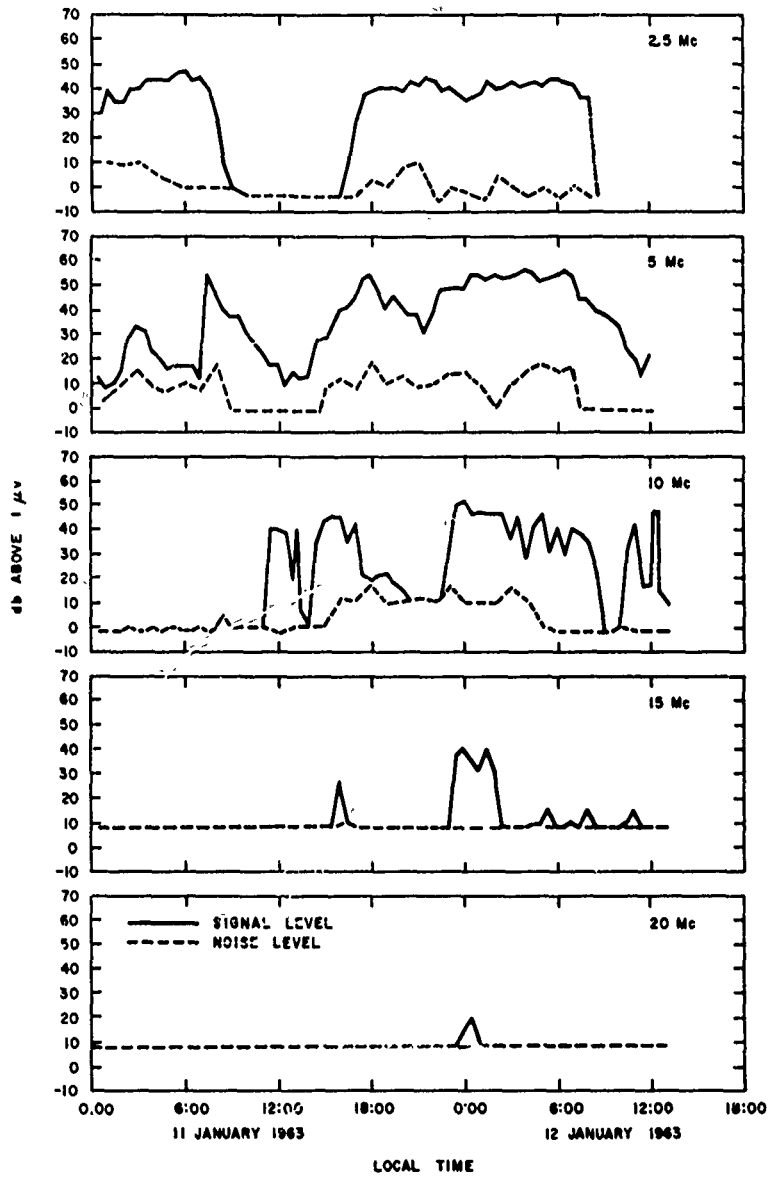


Figure 20 OBSERVED VALUES OF SIGNAL STRENGTH AND NOISE LEVEL
63-3620

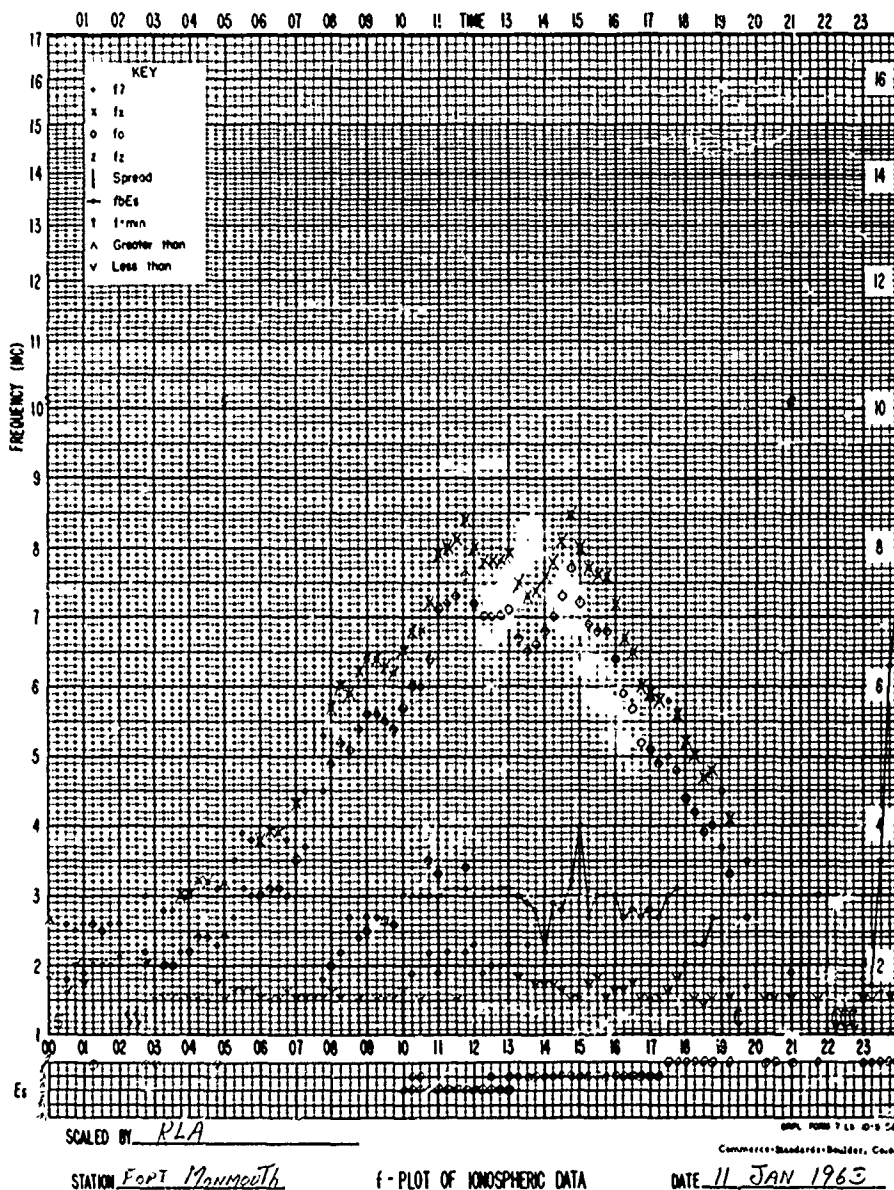
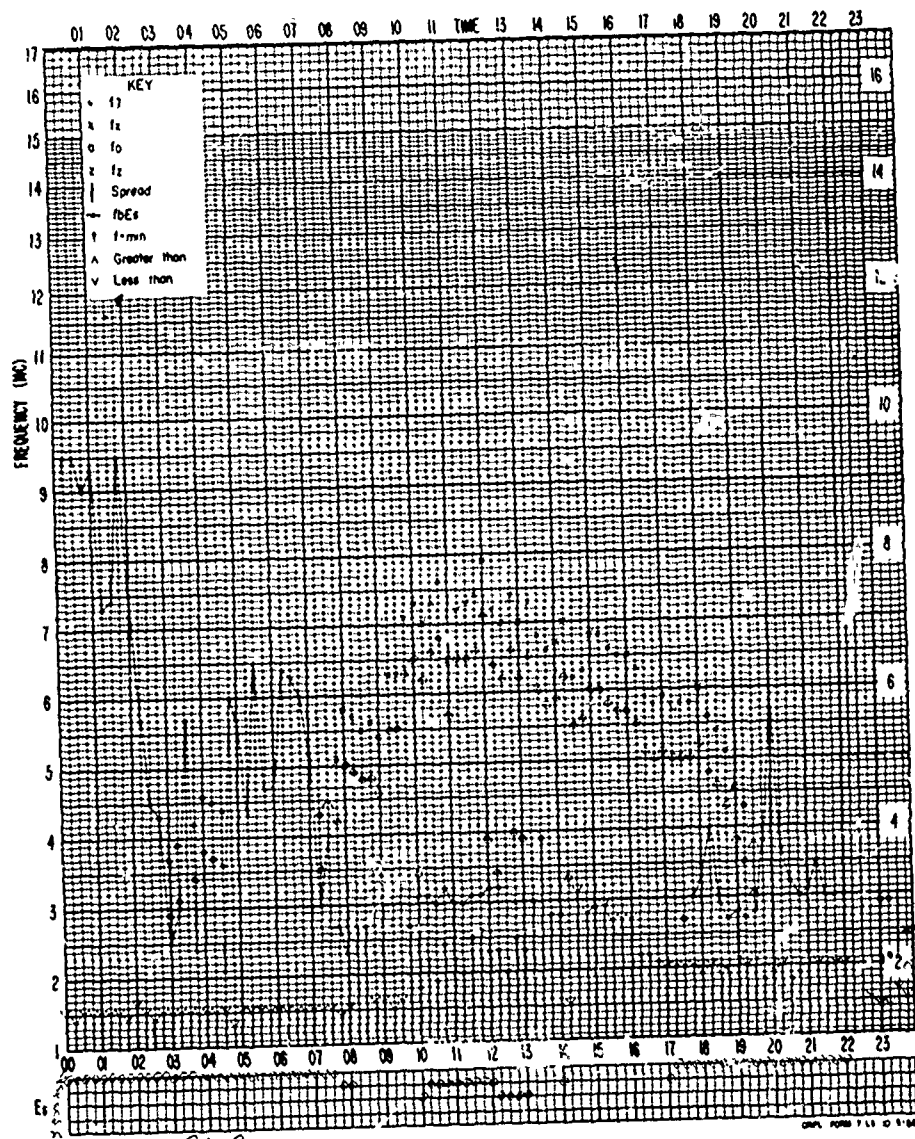


Figure 21a FORT MONMOUTH f-PLOT FOR 11 JANUARY 1963
63-3582



SCALED BY RHA

COMMERCIAL-BRANDING - MILITARY, CIVIL

STATION Ft Mon

f-PLOT OF IONOSPHERIC DATA

DATE 12 Jan 1963

Figure 21b FORT MONMOUTH f-PLOT FOR 12 JANUARY 1963
63-3582

with $r = 0.66$, $p = 2$, $\sec \phi_D = 3.2$, $f_L = 0.6$, $f = 5$, and the calculated value of $A = 328$, absorption at 5 Mc is $L_5 = 44$ db. This is about the same as the difference shown on figure 20 between the day and night level of signal strength at 5 Mc. (If absorption at night is negligible, then this difference is approximately the absorption at noon).

b. When f_oE_s is greater than 6.7 Mc ($\sec \phi_E = 3.0$) reception on 20 Mc is possible. As shown on the f -plot as is the case between 0000 and 0200 LT, 12 Jan 1963 - the same time as the 20-Mc reception of WWV.

c. When f_oF_2 is greater than about 6.7 Mc ($\sec \phi_F = 1.6$) reception of WWV on 10 Mc is high, otherwise it is absent unless sporadic E is present. On the 11 Jan 1963, f_oF_2 is sufficiently high between 1100 and 1545 LT except for a brief period around 1330. On 12 Jan 1963 f_oF_2 is sufficiently high only around 1045 and again at 1200 LT. WWV reception during the daytime as shown on figure 20 corresponds closely to these intervals.

III. IONOSPHERIC PATTERNS

A. UNDISTURBED PATTERNS

1. E layer

The E layer is a regular ionospheric layer in the sense that the critical frequency f_0E is directly related to the solar zenith angle χ . When ionization is caused by photo-ionization, and the only loss mechanism is caused by recombination, the variation of electron density may be stated

$$\frac{dN}{dt} = I - \alpha N^2 \quad (52)$$

where

I = intensity of ionizing radiation

α = recombination coefficient

N = number density of electrons .

Equilibrium conditions are assumed, which yields

$$I = \alpha N^2 \quad (53)$$

$$N = (I/\alpha)^{1/2} \quad (53a)$$

That is, the electron density at a given height, under equilibrium conditions, is proportional to the square root of the ionizing radiation intensity. Consider for a moment, the photon radiation from the sun. The light rays have an intensity I_0 per unit cross section. Projecting into a horizontal plane, the radiation intensity becomes

$$I = I_0 \cos \chi \quad (54)$$

and from (53a)

$$N \sim (\cos \chi)^{1/2} \quad (55)$$

Thus the ordinary wave critical frequency f_oE is, by equations (2) and (55)

$$f_oE = A \cos^{1/4} \chi \quad (56)$$

where A is a function of the sunspot number only, and is the E region critical frequency for $\chi = 0^\circ$ (subsolar point). Equation (54) is based on an assumption that there is no loss in intensity of solar radiation as it passes through the ionosphere above the point described in the E region. This is particularly important near sunrise and sunset and is included in a theory due to Chapman (1931) and yields the same result for f_oE when the density varies in accordance with the barometric equation for an isothermal atmosphere

$$N = N_0 \exp(-z/H) \quad (57)$$

where

N = number of molecules

z = height in km

H = scale height.

Sunlight is not monochromatic nor is the scale height constant. These problems have been treated by Chapman (1939) and Shimazaki (1959) but yield more complicated results.

An empirical expression has been constructed which represents the variation of f_oE . Monthly median data from the CRPL-F series was selected to represent low, medium, and high latitude stations and was sorted according to solar zenith angle and smoothed sun spot (SSSN). A good fit (within ± 3 percent) is obtained with

$$f_oE = E_0 + S \cos \chi \quad \text{for } \chi \leq 90^\circ, \quad (58)$$

where

$$E_0 = 2.65 \text{ Mc}$$

$$S = (0.55 + 0.0066 \text{ SSSN})$$

A graph showing these results is given in figure 22.

2. F1 layer.

The F1 layer is solely a daylight phenomenon; and it is prominent in equatorial latitudes in all seasons, and in all latitudes during the local

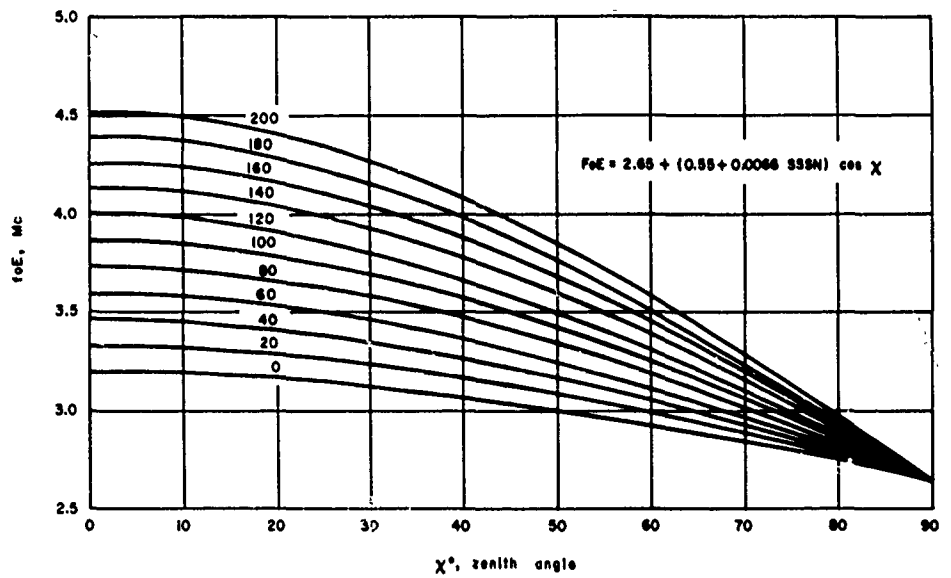


Figure 22 foE VERSUS SOLAR ZENITH ANGLE AND SSSN
63-3580

summer months. On the ionosonde, the frequencies near the critical frequency, suffer group retardation causing a cusp in the ionogram. Rawer (1956) gives a simple formula for foF1,

$$foF1 = K(F1) \cos^{0.2} \chi \quad (59)$$

where

$$K(F1) = (4.3 + 0.011 \bar{R}) Mc .$$

A detailed analysis of CRPL-F noon median values indicates that a seasonal, as well as solar zenith angle dependence exists. Although this complication has no immediate explanation, it is probably related to long-term changes in the F2 region. The formulation to be used is

$$foF1 = 4.25 - 0.007 \chi + \left[0.017 + 0.0015 \cos \left(\frac{N}{12} \frac{2\pi}{360} \right) - 0.001 \cos \left(\frac{N}{6} \frac{2\pi}{360} \right) \right] [1 - 10^{-2} \chi] SSSN \quad (60)$$

where

N = month number (e. g., January = 1)

SSSN = smoothed sunspot number

3. F2 layer.

The behavior of foF2 when undisturbed is more complicated than with foF1. Undisturbed foF2 is the condition present when the F2-layer critical frequency is not greatly different than that indicated by the monthly medians, provided that the individual values of the median show a relatively small standard deviation. Since foF2 is closely correlated to geomagnetic disturbances, it is also possible to define an undisturbed F2-layer condition as that which is found when there is only little or no geomagnetic disturbance present. Undisturbed foF2 can be predicted in a way similar to foF1 or foE. The value of foF2 depends upon local time, solar zenith angle, the geographic coordinates, the season, and sunspot number. The local time dependence is somewhat different than with foE or foF1. At sunrise there is usually a sharp increase in foF2, but at sunset the change is a gradual one. The geographic coordinates must be considered for two reasons. Whereas the geographic dependence of foE and foF1 can be expressed as a simple function of the solar zenith angle, the geographic dependence of foF2 may be quite different from that indicated by a simple solar zenith-angle relationship. Also, geographic coordinates must be taken into

account because f_oF2 values vary partly in accordance with the Earth's magnetic field. These variations are sometimes referred to as a longitude effect. For prediction of f_oF2 monthly medians a method has been worked out by Jones and Gallet (1962). Also, use of monthly median maps is quite suitable to determine normal frequencies of operation.

4. Sporadic E.

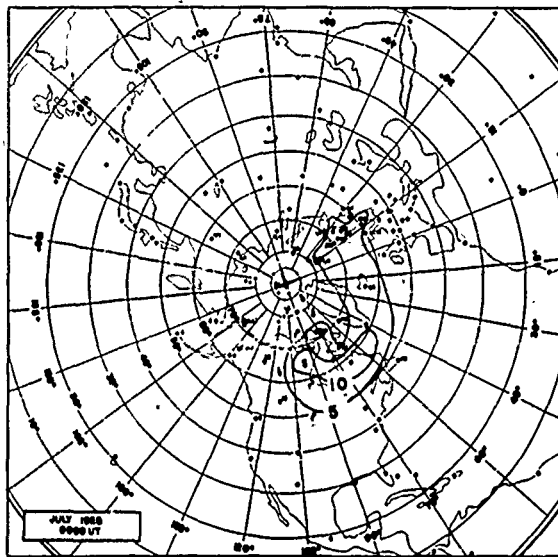
Sporadic E cannot be classified as a regular ionospheric phenomenon. That is, one cannot demonstrate a 1-to-1 correspondence between E_s and some physical cause -- e.g., the solar visual-emission spectrum. This is possible with the D, E, and F layers. In spite of the fact that there are areas where sporadic E is common in high geomagnetic latitudes, it is unusual for E_s to be present more than half of the time at a given hourly measurement (e.g., $f_oE_s \geq 5$ Mc).

The sorting criteria (i. e., $f_oE_s \geq 5$ Mc) is established to eliminate the possibility of the regular E layer obscuring a sporadic E layer embedded in it. Further, it provides a suitable lower bound on the electron density of the layer and permits comparison with the results of other workers, (Smith, 1957).

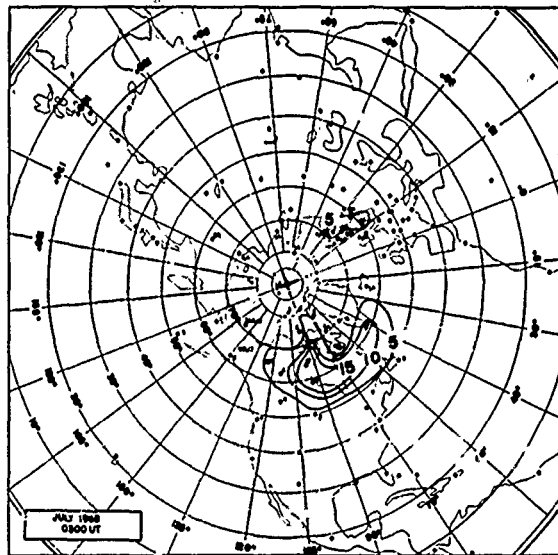
To illustrate the phenomenon, maps for July 1958 have been prepared for stations north of 50 degrees geomagnetic latitude, and are included as figure 23 (a to h). Although the maps are presented every 3 hours, a map was constructed for each hour. The data are not normalized, but qualifying symbols are added to indicate whether blackout or equipment trouble reduced the number of data days.

Various ionosondes placed at an identical geographic location can be expected to report different values of f_oE_s . To ascertain the actual effect of differing equipment sensitivity, an analysis of 1 day of the film on hand from the ionosonde at Churchill, Canada was made. As suggested in the IGY-URSI operating schedule, hourly ionograms were made using three different gain settings. Fortunately, the relative gain change is accurately known. For the LG-17 sounder (in use at Churchill) the difference between successive gain settings is 20 db, making the total variation in gain 40 db. It is unlikely that the nominal gain at other stations differs from that at Churchill by more than ± 10 db.

The raw data from a "typical" daily scaling (figure 24) indicates qualitatively that the ionosonde gain enters into the reported value of f_oE_s , but it does not change the number of occurrences of $f_oE_s \geq 5$ Mc by more than ± 10 percent with respect to the Churchill medium gain as a base. While perhaps altering the shape of the pattern contours slightly, it does not in any way invalidate the general results discussed above.

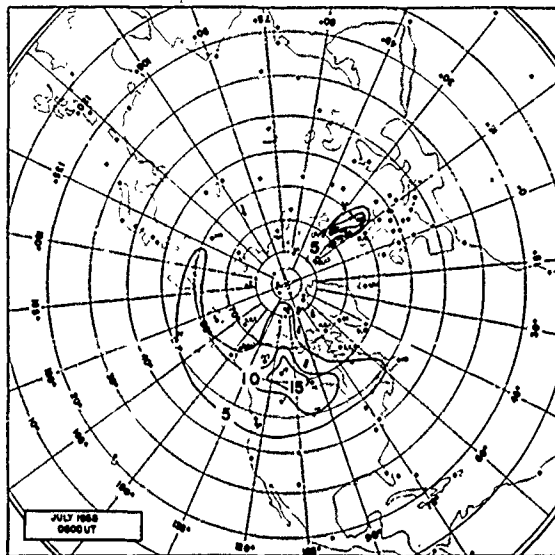


a. 0000 UT

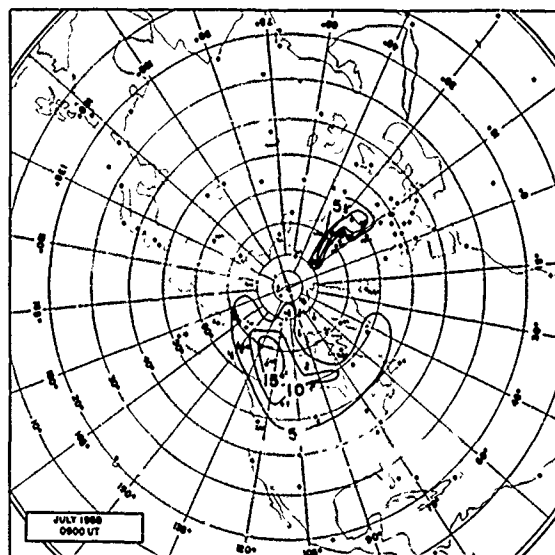


b. 0300 UT

Figure 23 NUMBER OF OCCURENCES OF foEs ≥ 5 Mc
63-3579

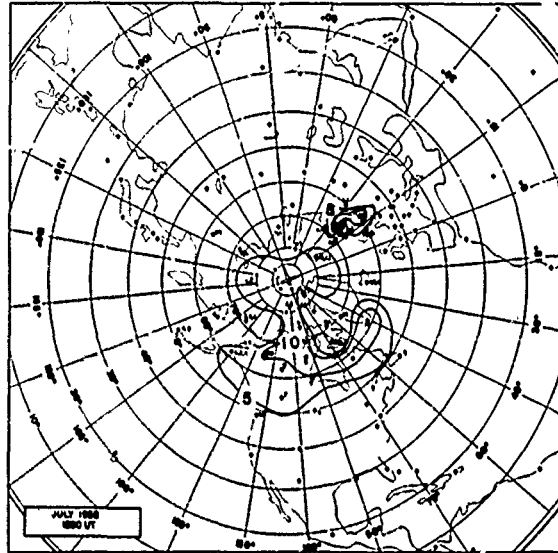


c. 0600 UT

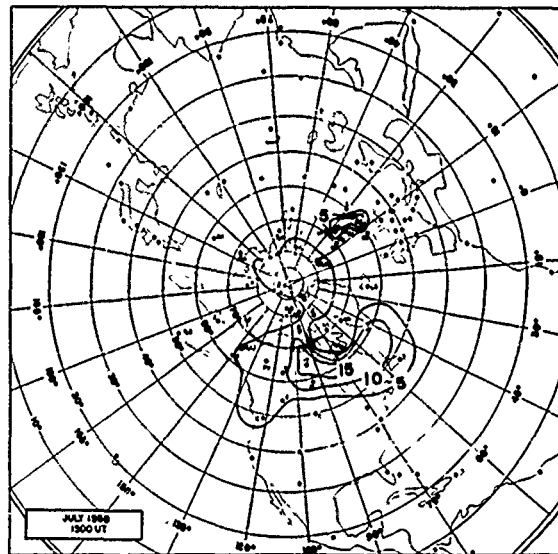


d. 0900 UT

Figure 23 (Cont'd)

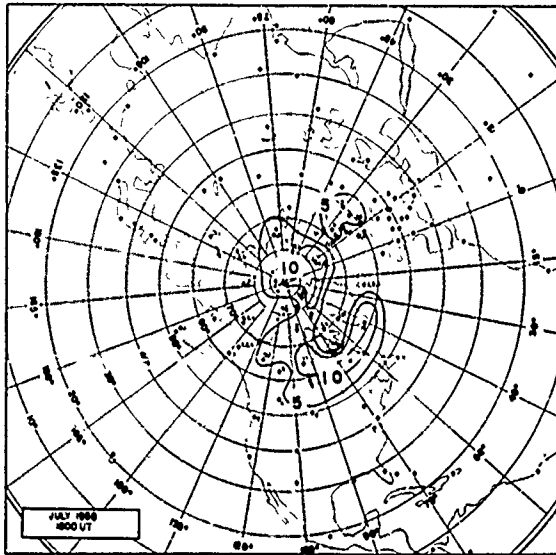


e. 1200 UT

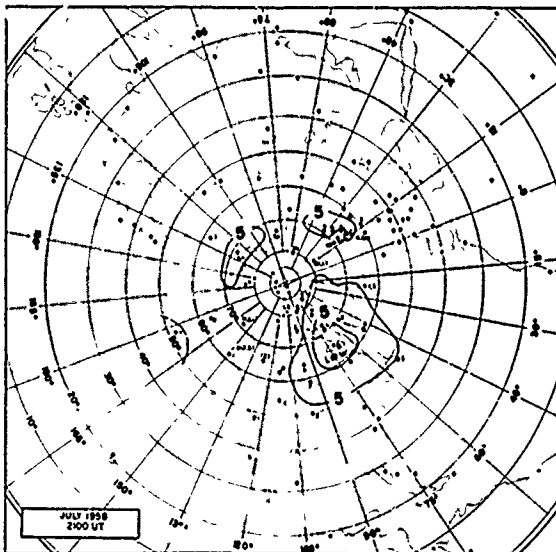


f. 1500 UT

Figure 23 (Cont'd)



g. 1800 UT



h. 2100 UT

Figure 23 (Concl'd)

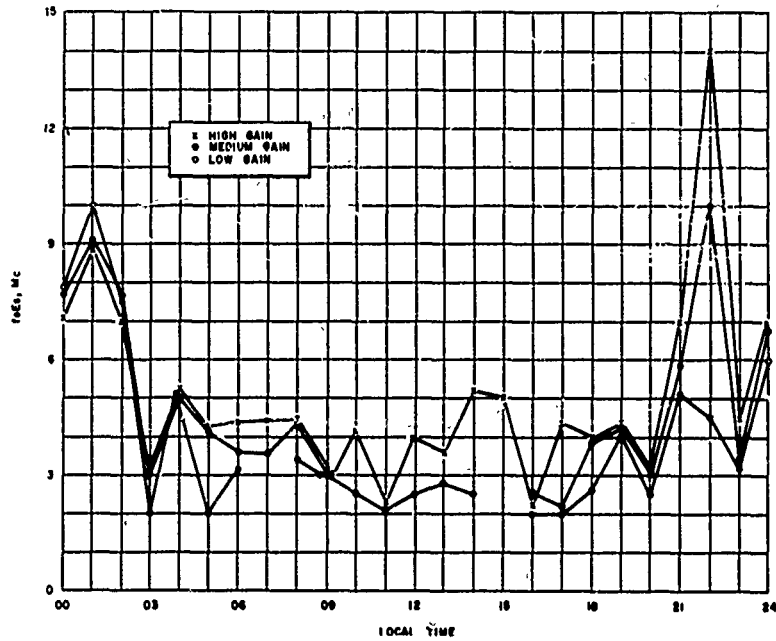


Figure 24a RECEIVER GAIN VERSUS foEs, CHURCHILL, 11 JANUARY 1958
63-3577

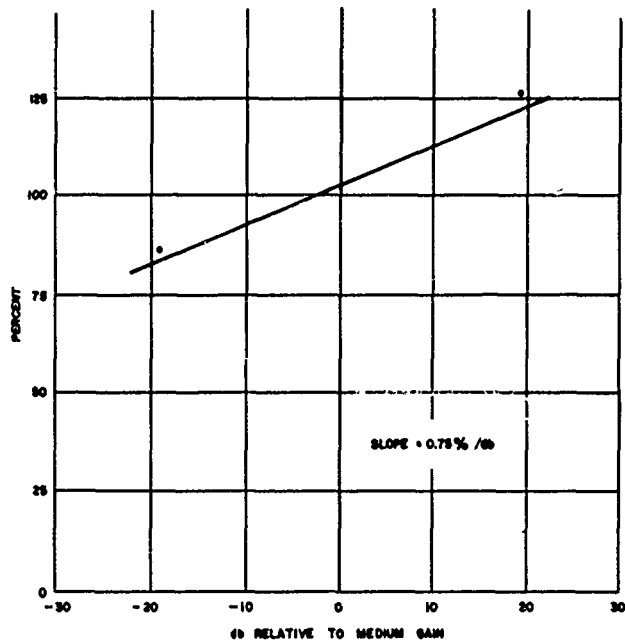


Figure 24b PERCENTAGE foEs ≥ 5 Mc VERSUS RECEIVER GAIN
11 JANUARY 1958, CHURCHILL, MEDIUM GAIN 100%
63-3577

During auroral disturbances, stratified Es may be observed at heights ranging from 115 to 220 km. This consists of one or more layers or sporadic E which are not multiple reflections of the lowest layer. It may be shown that these reflections come from tilted ionospheric layers at about 110 km and are slant-path propagation. The minimum observable frequency, f_{\min} of the several sporadic E layers are related by

$$f_{\min 2} = \left(\frac{h_1'}{h_2'} \right) (f_{\min 1} + f_H) - f_H \left(\frac{h_1'}{h_2'} \right) \quad (61)$$

where

- $f_{\min 1}$ = f_{\min} of lowest layer
- $f_{\min 2}$ = f_{\min} of any other Es layer
- h_1' = virtual height of lowest Es
- h_2' = virtual height of any other Es layer
- f_H = local gyrofrequency (magnetic field assumed vertical).

If the lowest layer is above 120 km, it is probable that it too is a slant reflection.

Analysis of sporadic E data as described in the foregoing shows that on the average, there appear to be several recurrent patterns. The primary one is the propensity of sporadic E in the Canadian auroral zone and in Arctic regions. Secondly, a distinct traveling region is present which encompasses the region extending ± 45 degrees from local midnight. The coincidence of the above described zones produces a nighttime maximum of considerable importance in Canada. A third sporadic E region is found over Scandinavia during the hours 0600 to 1200 UT, and while small is apparently significant (Maehlum, 1961). The Canadian maximum is the only stationary pattern which remains distinctly observable throughout the day. A more precise description of this pattern places the maximum approximately 15 degrees east of the line joining Baker Lake and Churchill. The northern extent is probably not more than 5 degrees north of Baker Lake; it certainly does not reach Resolute Bay. To the south it reaches a position somewhere between Churchill and Winnipeg, and it appears to extend further to the east than the west. Seasonally, the solstice months are more important than the equinoctial; however, this applies with certainty to IGY data only.

The midnight traveling auroral-zone peak is, as its name implies, associated with the commonly defined auroral zone. It appears most intense in the sector 180°E through Canada to 45°E. Certainly this result is somewhat influenced by the density and location of the reporting stations.

Scandinavia appears to be another preferred region for Es, though considerably less extensive than the Canadian maximum, and furthermore not all stations report a definite daytime peak. The temporal maximum lies somewhere between 0600 and 1200 UT. The pattern is not distinctive during the winter months.

A summertime and equinoctial phenomenon known as "Thule type" Es reaches a maximum at about 17 UT over a major part of the polar cap north of 75° geographic latitude, Penndorf and Coroniti (1958). It appears to be a quiet-time phenomenon, but may be present though obscured when absorption events (PCA) are in progress.

5. Layer Height

To compute the various modes of propagation available, it is necessary to know the virtual height of reflection from the E, F1, and F2 layers. Analysis of vertical incidence data in middle latitudes shows that the height of the E-layer base is very close to 100 km. For the F1 layer the base height is about 210 km on the average, while the height corresponding to the maximum usable frequency for hops of 2000 or 3000 km is about 260 km. An overall average height may be taken as 235 km. In the case of the F2 layer the variations in height are greater than those of the F1 layer. The base heights and the heights corresponding to hops of 3000 to 4000 km are given below:

	h'F2 vertical incidence	h'F2 3 to 4000 km
Summer: Day	400	460
Night	285	460
Winter: Day	400	460
Night	285	460

For an overall average, a value of 400 km may be used. There is a certain condition, under which, the height of the F2 layer may be much greater than any of the values listed above. This occurs when the difference between f_oF2 and f_oF1 , denoted by Δf , is small. The increase in virtual height is caused by the increase in group retardation while the wave is passing through

the F1 region near its critical frequency. The empirical relationship between the F2 virtual height and Δf is approximately

$$h'F2 = \frac{555}{\Delta f^{1/3}} \quad (62)$$

if $\Delta f \leq 3 \text{ Mc}$.

B. DISTURBED PATTERNS

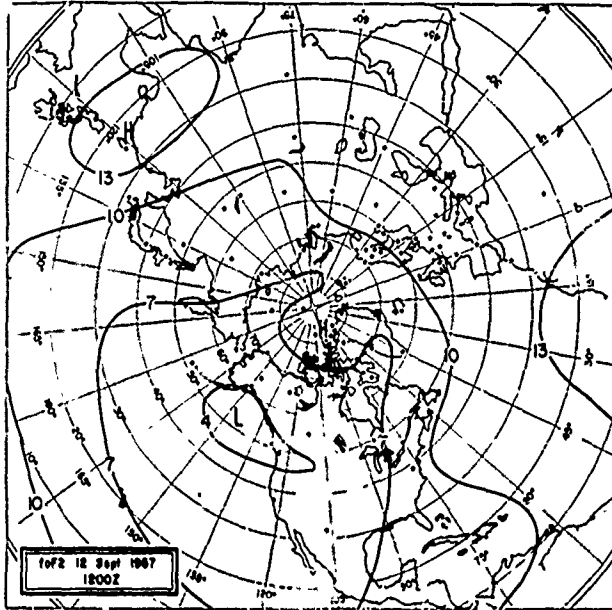
1. F2 Layer

There are a number of types of F2 layer disturbances which are of importance to communications. Probably the most important of these is the world-wide decrease in the F2 layer critical frequency associated with geomagnetic storms. Details of such disturbances have been described by Obayashi (1954). The decrease begins at about the same time the main phase of the geomagnetic storm begins. The specific location and intensity of depressed values depend upon the universal time, the time elapsed from the beginning of the main phase, and the main-phase intensity. Usually, the recovery of f_oF2 to its normal pattern takes a longer time than does the the recovery of the geomagnetic field.

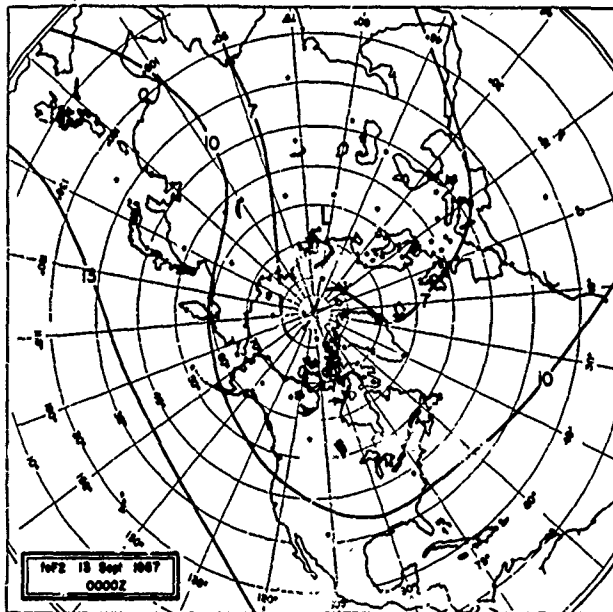
An example of the storm-time behavior of the F2 layer is provided in figure 25 (a to f); see Hill (1960). Isopleths of critical frequencies are shown in intervals of 3 Mc. Departures from the monthly median values are shown by dashed curves, also in intervals of 3 Mc. As shown in figure 25, the departures from f_oF2 monthly medians increase in value and geographical extent even after the maximum of geomagnetic disturbance, i. e., around 1200 UT, 13 Sept 1957. The most depressed f_oF2 values are found sometime around 0000 UT on 14 Sept 1957.

Another type of f_oF2 disturbance occurs in polar regions during equinoctial and winter months. The outstanding feature of this type of disturbance is an anomalous increase in the value of f_oF2 . Such increases have already been reported (Kamiyama, 1962). In the present work anomalous f_oF2 increases are studied with the aid of synoptic maps, so that the geographical extent, the development and movement, and the relationship to the normal pattern may all be found.

Such disturbances are shown in figures 26 through 29. These are typical ones selected out of some 28 separate cases. In these disturbances the high daytime values of f_oF2 extend into polar regions and sometimes well across into the nighttime side of the polar cap. The width of this region of high values is about 2000 km on the average. In just about every case the maximum value in the anomalous region is within 1 Mc or so of the maximum value found in middle latitudes. The duration of these disturbances

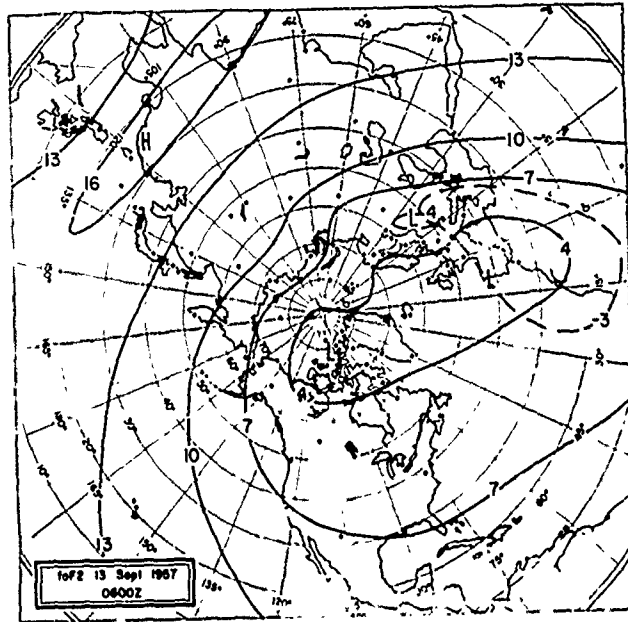


a. 1200Z, 12 Sept 1957

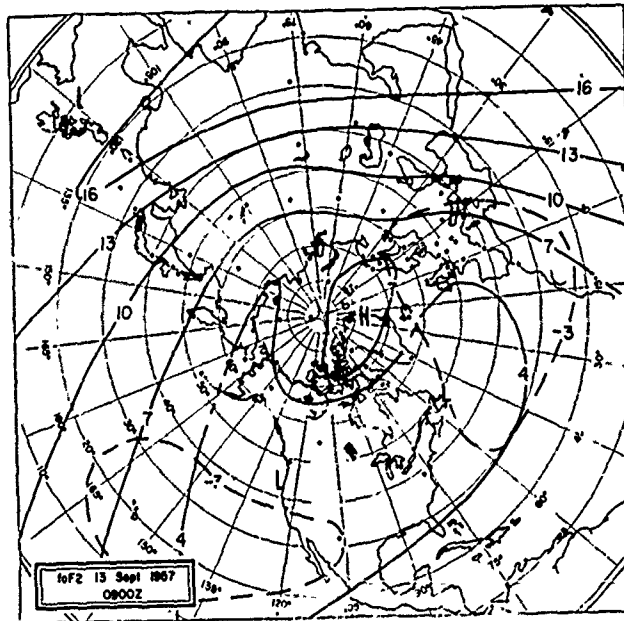


b. 0000Z, 13 Sept 1957

Figure 25 STORM-TIME BEHAVIOR OF foF2

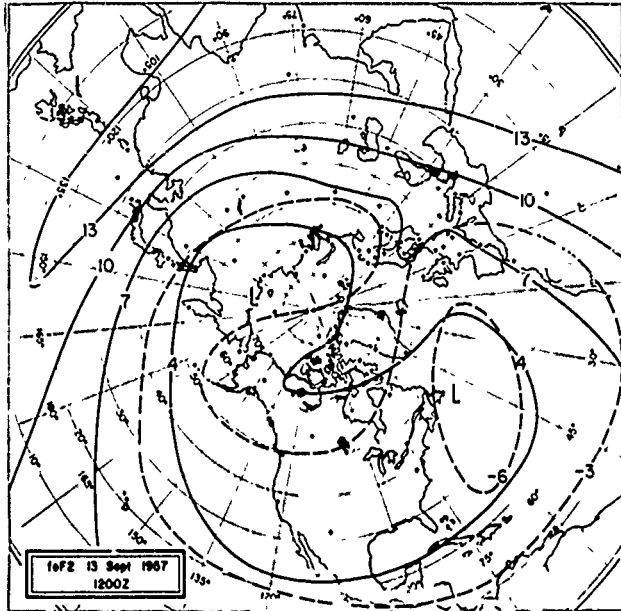


c. 0600Z, 13 Sept 1957

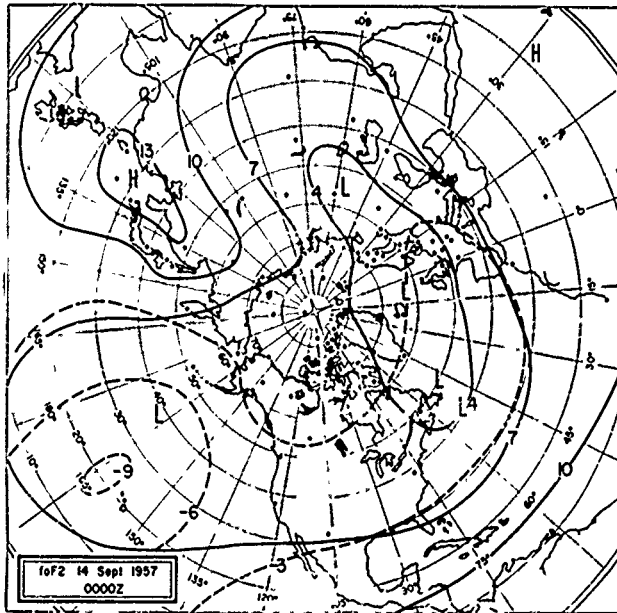


d. 0900Z, 13 Sept 1957

Figure 25 (Cont'd)

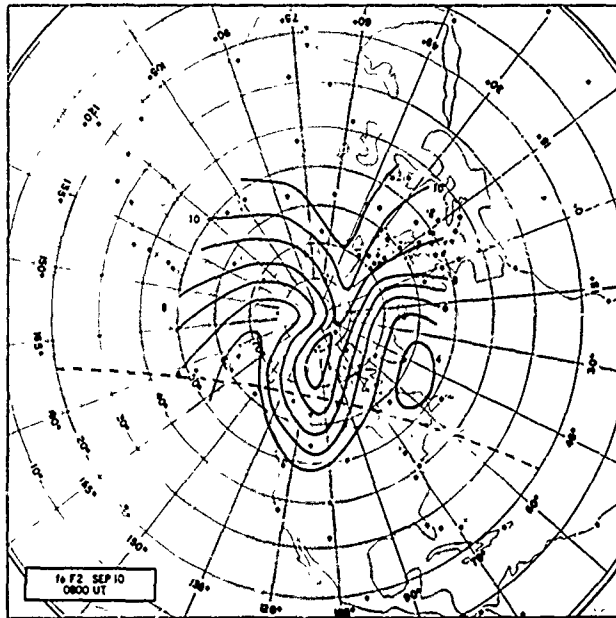


e. 1200Z, 13 Sept 1957

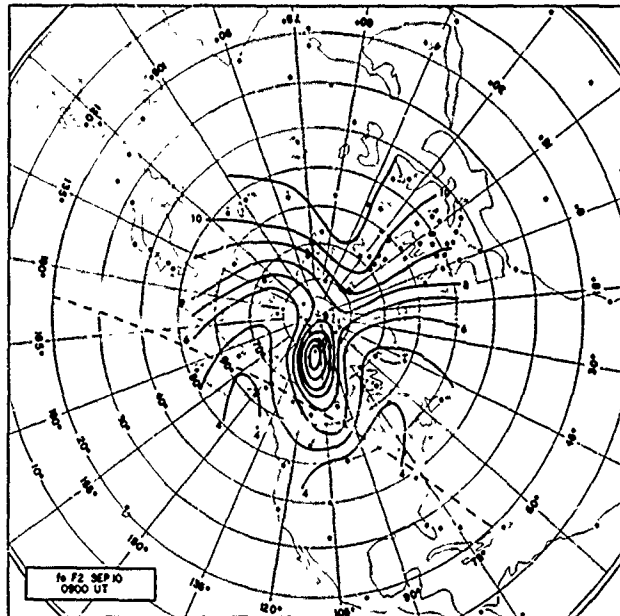


f. 0000Z, 14 Sept 1957

Figure 25 (Concl'd)

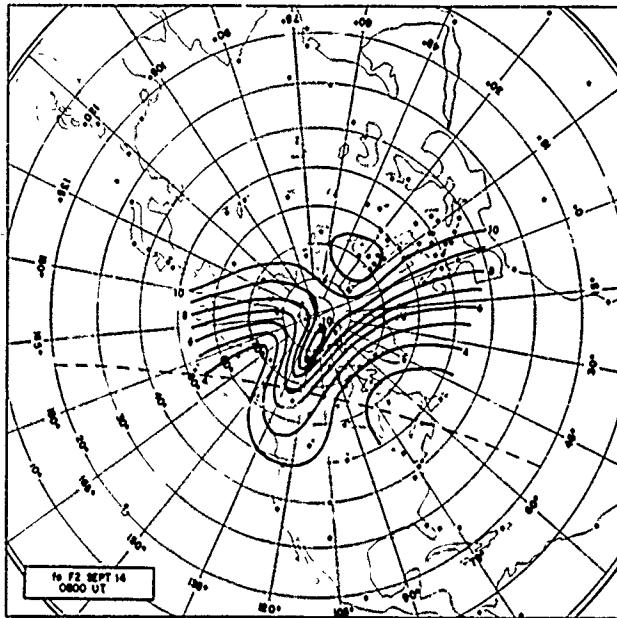


a. 0800 UT, 10 Sept

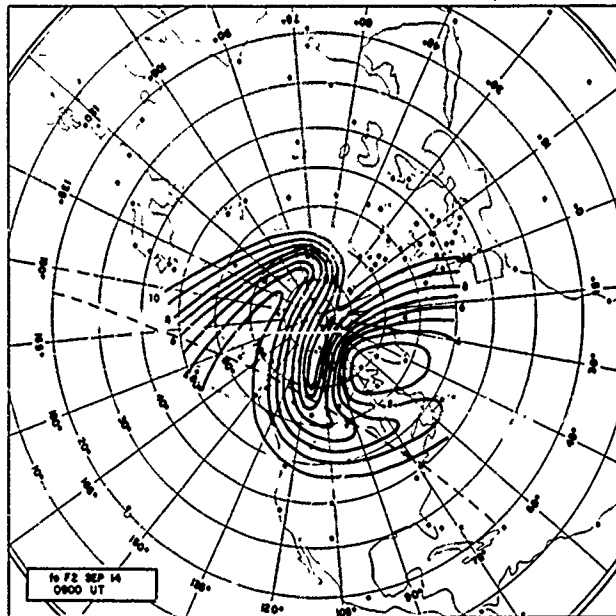


b. 0900 UT, 10 Sept

Figure 26 foF2 ANOMALIES IN THE POLAR CAP

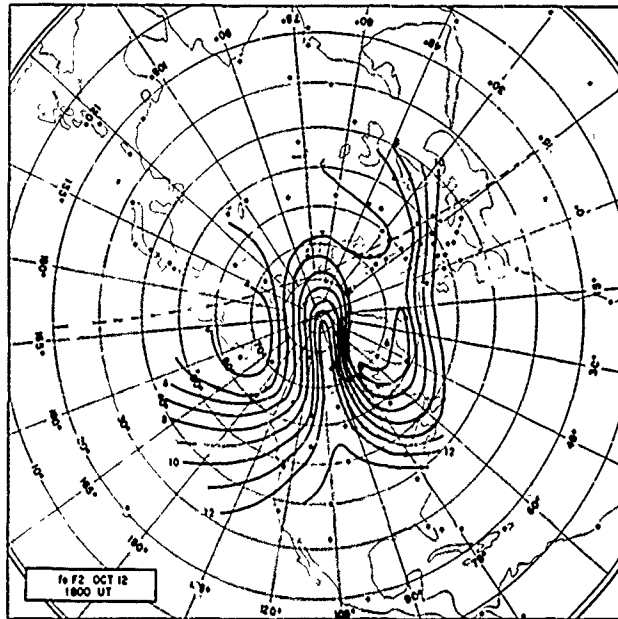


a. 0800 UT, 14 Sept

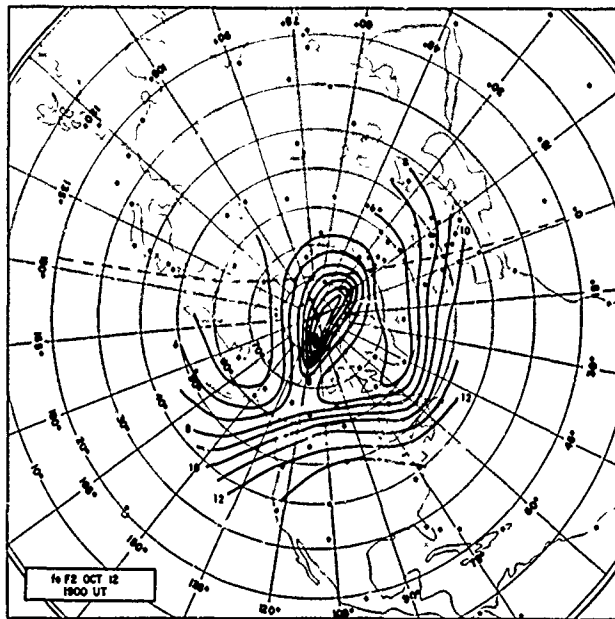


b. 0900 UT, 14 Sept

Figure 27 foF2 ANOMALIES IN THE POLAR CAP

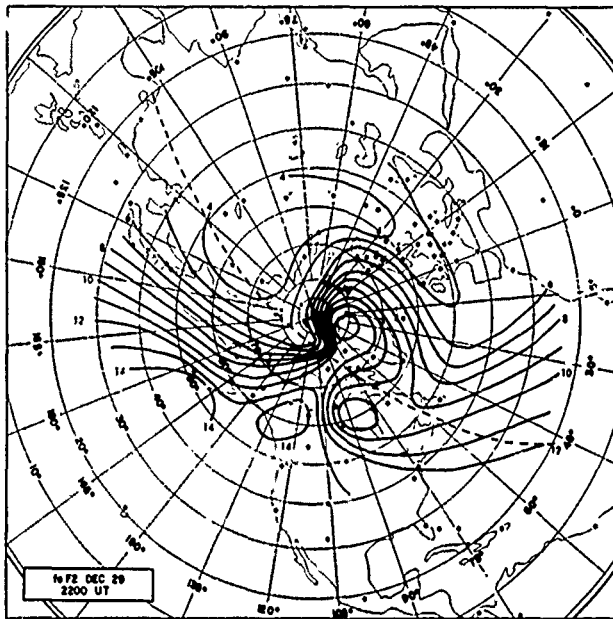


a. 1800 UT, 12 Oct

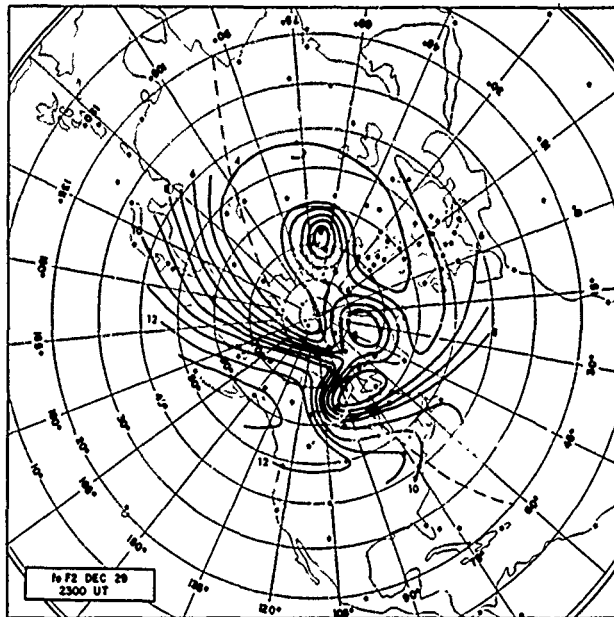


b. 1900 UT, 12 Oct

Figure 28 foF2 ANOMALIES IN THE POLAR CAP

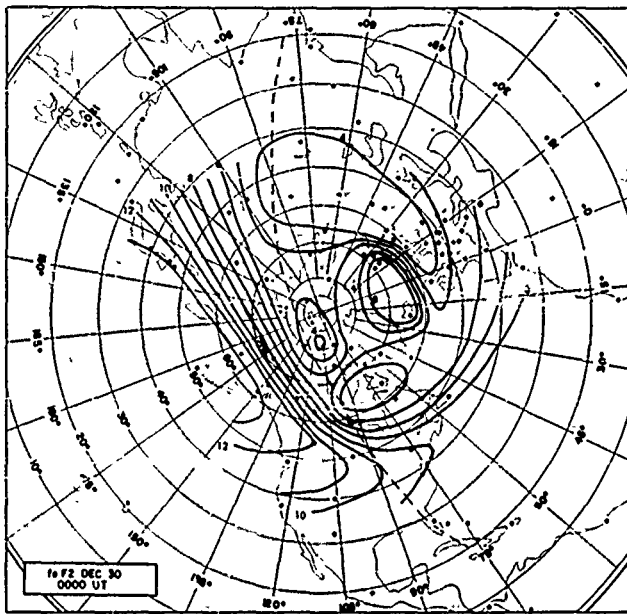


a. 2200 UT, 29 Dec

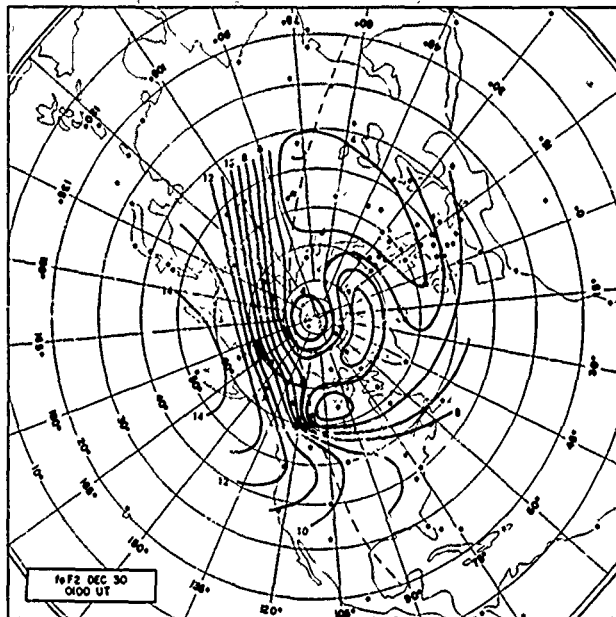


b. 2300 UT, 29 Dec

Figure 29 foF2 ANOMALIES IN THE POLAR CAP



c. 0000 UT, 30 Dec



d. 0100 UT, 30 Dec

Figure 29 (Concl'd)

varies from about 1 hour to a half day, but for the latter, the most intense period is about 2 or 3 hours. The frequency of occurrence of these disturbances may be rather high, but whether or not they occur every day -- between fall and spring -- cannot yet be said. Their occurrence is certainly not restricted to times of geomagnetic storms. A summary of significant information relating to the four disturbances shown in the figures is given in table III. In each of these cases, except the one of 14 Sept 1957 the geomagnetic field was rather quiet. (It may be noted that the maps for this case follow the series of storm maps, described earlier, by 8 hours.)

TABLE III

foF2 ANOMALIES IN THE POLAR CAP

Date (1957)	Time (UT)	Maximum foF2 (Mc)	K _p
10 Sept	0800	9	3
10 Sept	0900	11	3
14 Sept	0800	10	5
14 Sept	0900	10	5
12 Oct	1800	12	3
12 Oct	1900	12	2
29 Dec	2200	13	3
29 Dec	2300	8	3
30 Dec	0000	8	3
30 Dec	0100	7	3

2. Absorption

Three general geographical patterns exist in which anomalous absorption is most often found. These are low- and middle-latitude daytime absorption (associated with solar flare X-ray emissions), polar-cap absorption (associated with solar-flare cosmic rays), and auroral zone absorption (associated with precipitation of charged particles from the outer magnetosphere).

When X-rays or energetic particles reach altitudes of the D region, they produce a large number of electrons and ions. It is, of course, the presence of these electrons together with a high-collision frequency that results in

absorption of radio waves. Besides the production rate there are two other processes governing the density of D-region electrons. These are the recombination rate and the attachment rate. During hours of sunlight the attachment process does not play a role, because the photo-detachment rate is also very high. However, at night, attachment becomes important.

A rather complete review of studies on sudden enhancements in low- and middle-latitude daytime absorption, or SID is given by Warwick (1963). Here, the SID is described only in a general way. A SID begins at about the same time a flare becomes visible. Apparently the solar radiation causing the disturbance occurs only while the flare is in progress. As soon as the flare subsides, so does the absorption. Almost always, the onset of absorption is very rapid, while the decay is somewhat longer. Although not every flare produces a SID, the most intense ones are usually found with large flares, i. e., class 3 or 3+. However, some large flares do not produce very much absorption. On the other hand, small or medium size flares can produce moderate or even intense bursts of X-rays, which lead to corresponding amounts of absorption. The duration of a SID varies over a range of time from a few minutes to 2 or 3 hours. An example of a moderate SID, as represented by the parameter f_{min} , may be found on the chart for 31 Aug 1957, 0600 UT shown in figure 30. An example of a strong one is found on the chart for 18 Sept 1957, 1800 UT shown in figure 31. For communication a SID may cause outage on links which are in daylight. The lowest frequencies on these links would suffer the most absorption. The duration of such outage would last only an hour or two at most.

Polar cap absorption (PCA) is associated with solar flares but in a different way from a SID. Following the occurrence of certain flares, which can be identified by the flare intensity and the associated solar radio noise, protons in the 1-mev to 1-bev energy range arrive near the Earth and are guided into polar regions of both hemispheres by the Earth's magnetic field (Obayashi and Hakura, 1960) and (Hakura and Goh, 1961). The sun-Earth travel time for these protons is about 2 to 6 hours, but in some instances the travel time is well out of this range (Obayashi and Hakura, 1960). The onset of polar-cap absorption falls into two classes, one characterized by a rapid increase in absorption, and the other, a slow increase.

The geographical distribution of polar-cap absorption for typical events is shown in figures 32 and 33. These figures have been taken from a series of synoptic maps of eleven periods of polar-cap absorption (Coroniti, 1963). The solid curves on the maps refer to values of f_{min} in units of Mc. The shaded areas indicate regions where f_{min} exceeds f_oF2 . This condition means that there are no signals returned to the ionosonde in sufficient strength to be recorded. The dashed curve on a map indicates the position of sunrise and sunset at the Earth's surface. Considering the patterns of polar-cap absorption on the basis of where the energetic protons reach the D region, it would be expected that absorption would be greatest near the

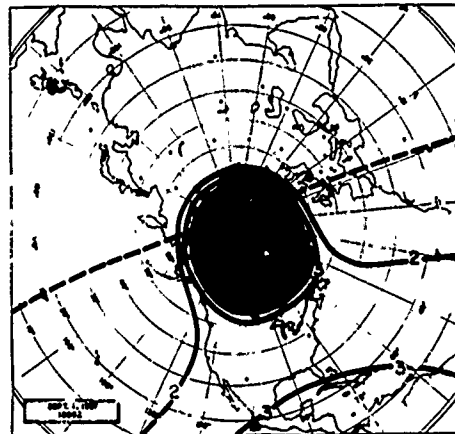
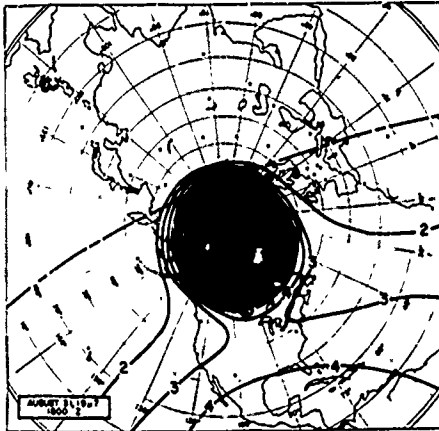
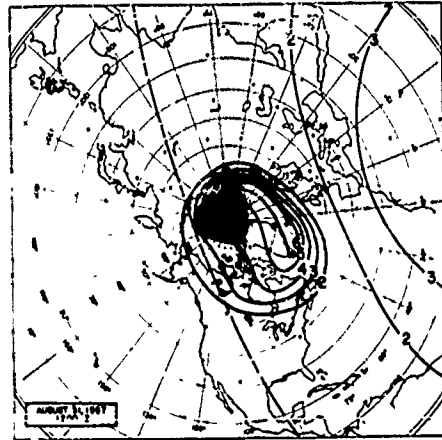
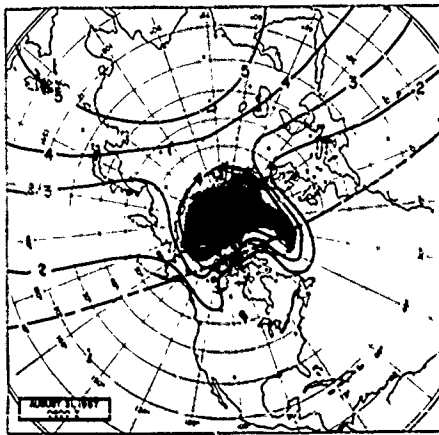


Figure 30 MAPS FOR SUDDEN IONOSPHERIC DISTURBANCE

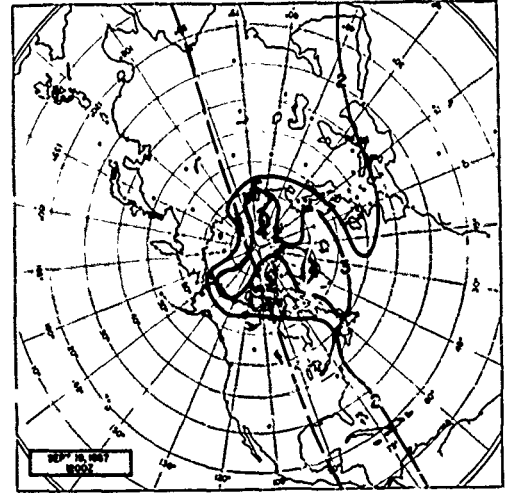
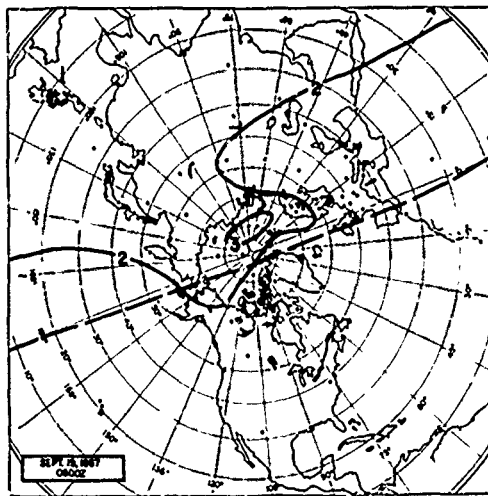
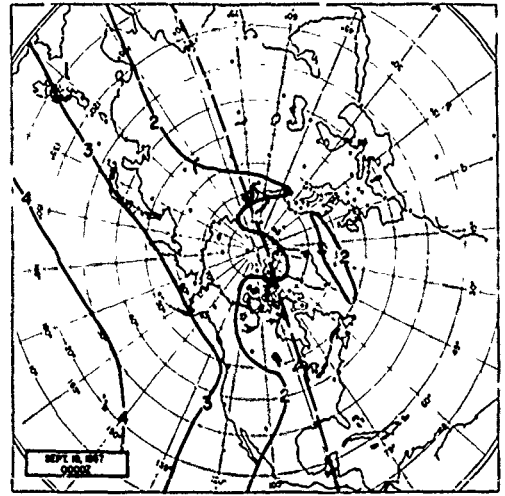
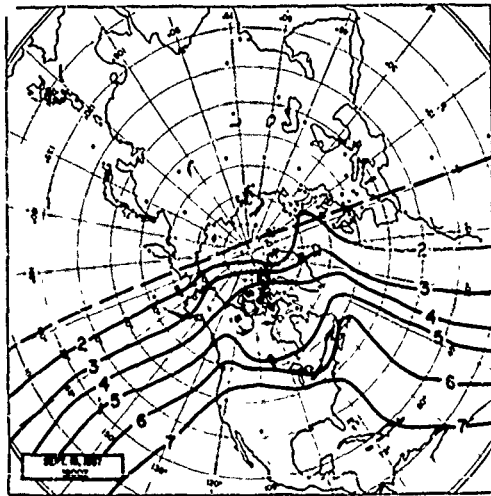


Figure 31 MAPS FOR SUDDEN IONOSPHERIC DISTURBANCE

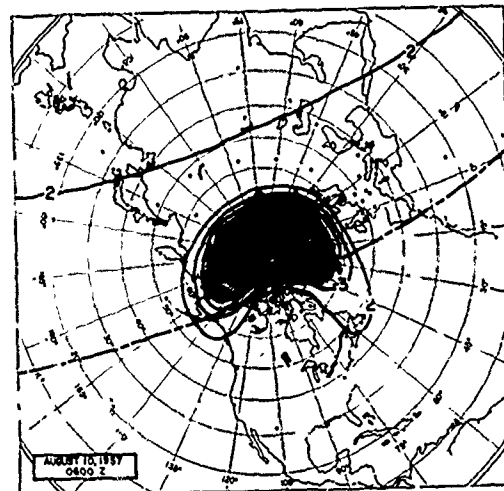
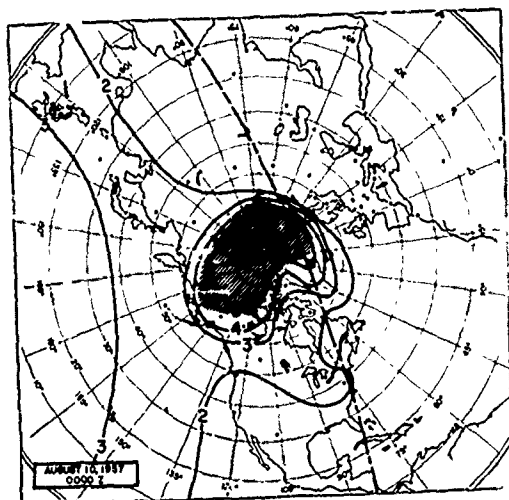
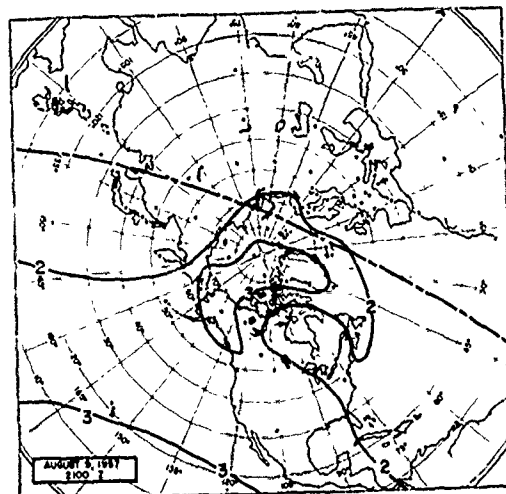
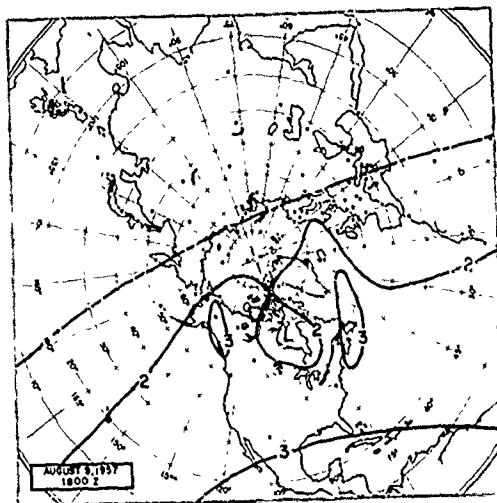


Figure 32 MAPS FOR POLAR CAP ABSORPTION EVENTS

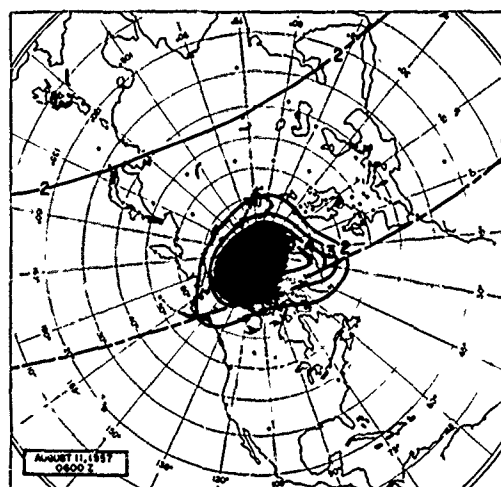
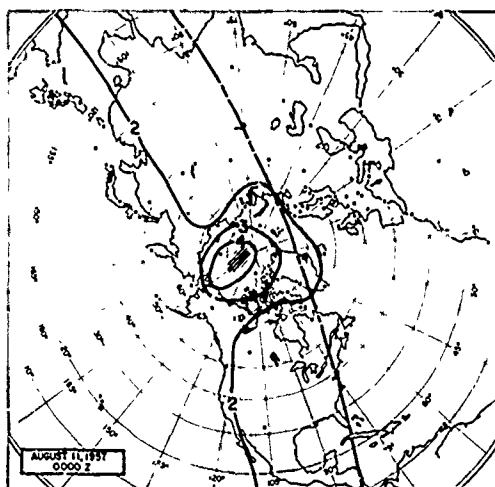
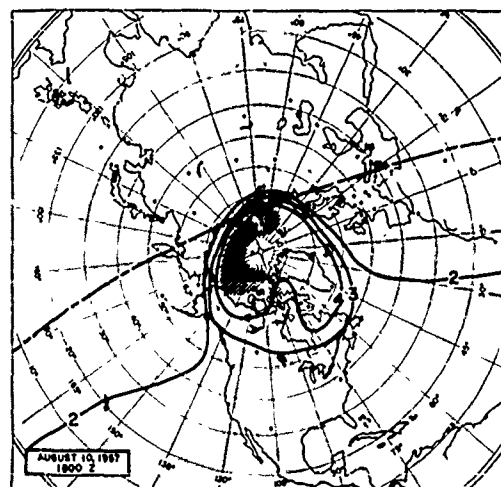
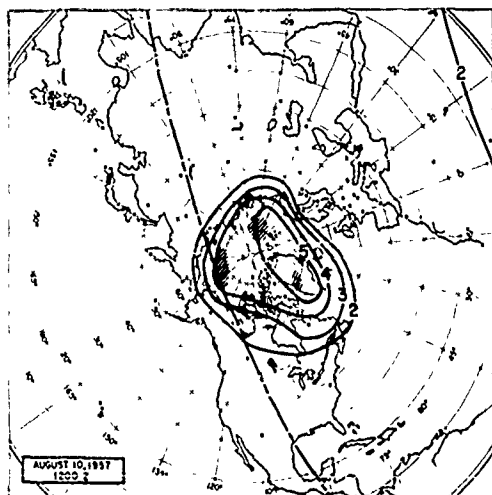


Figure 32 (CONT'D)

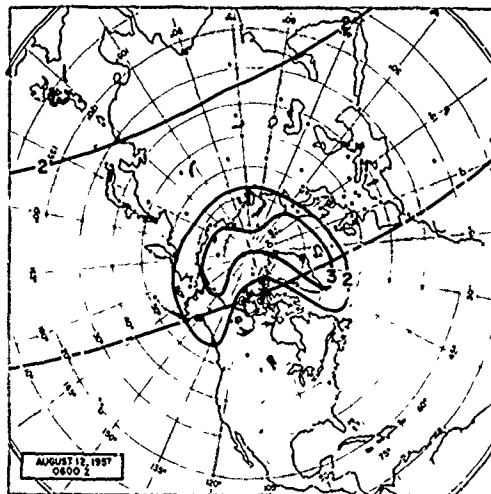
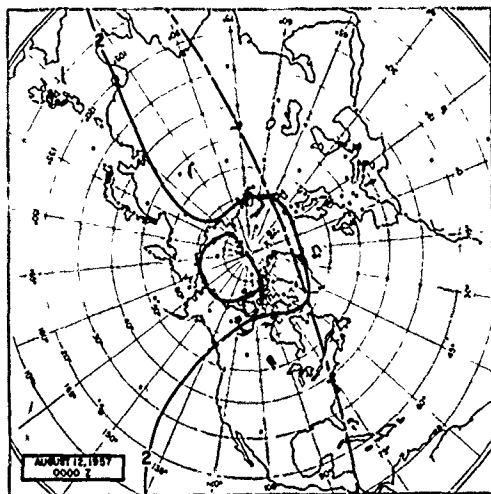
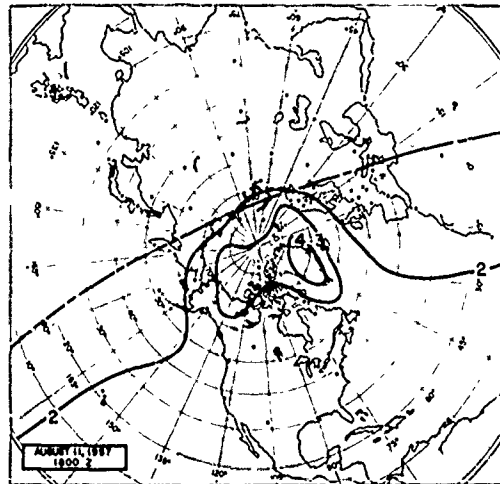
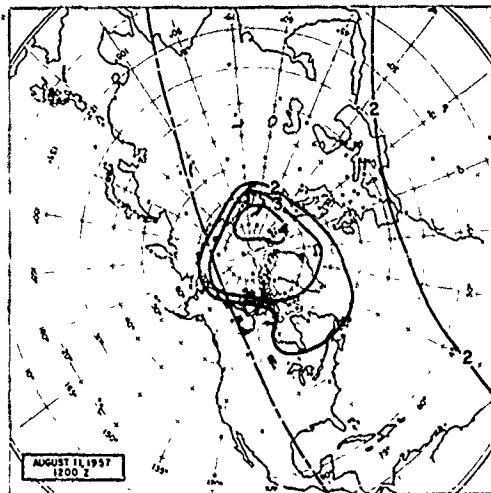


Figure 32 (CONCL'D)

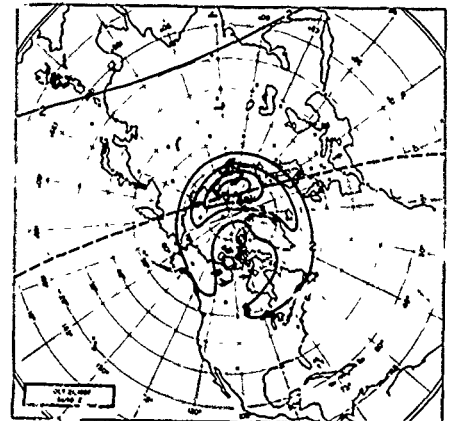
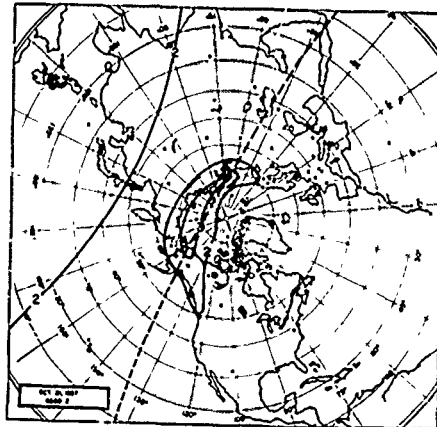
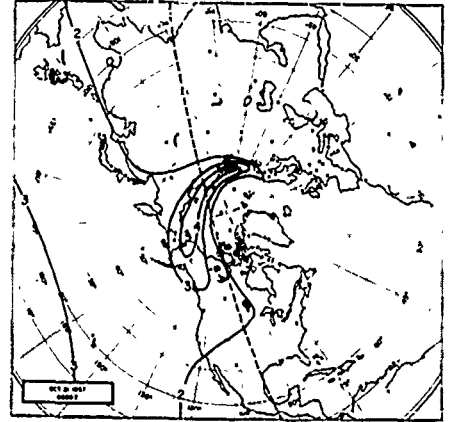
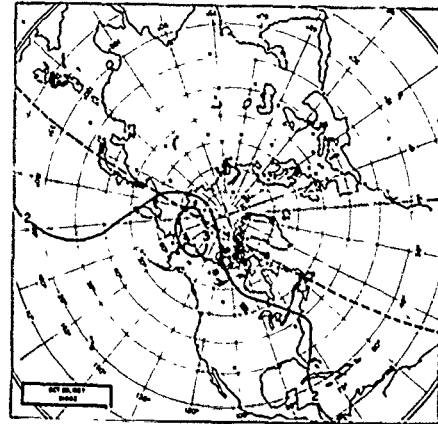


Figure 33 MAPS FOR POLAR CAP ABSORPTION EVENTS

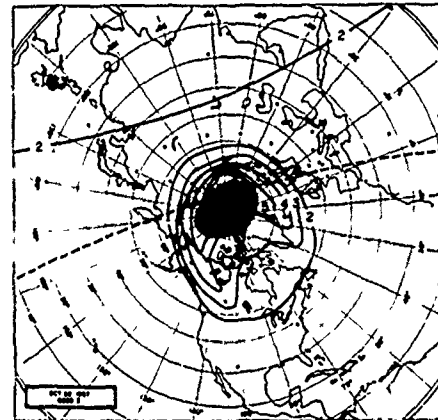
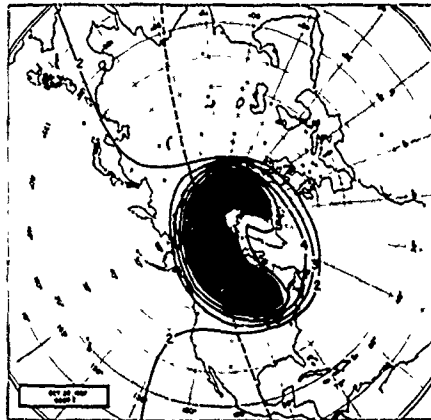
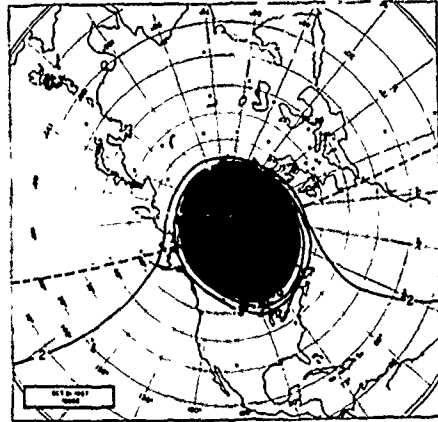
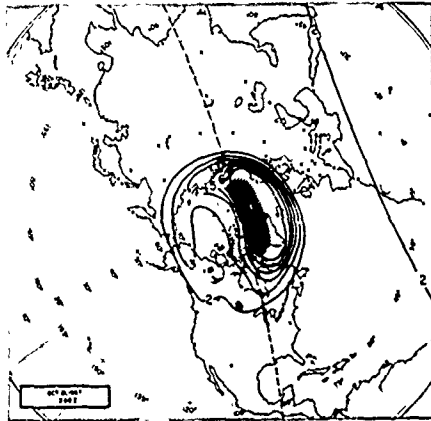


Figure 33 (CONT'D)

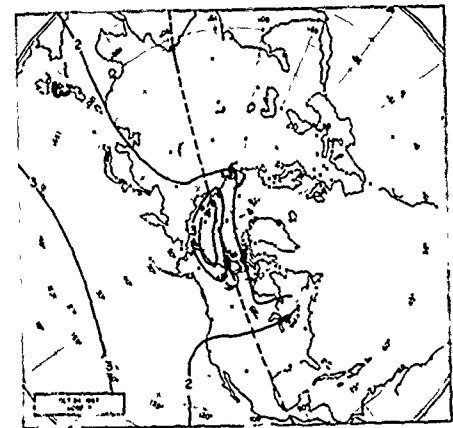
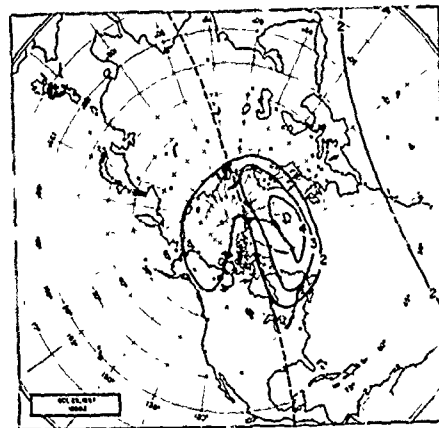
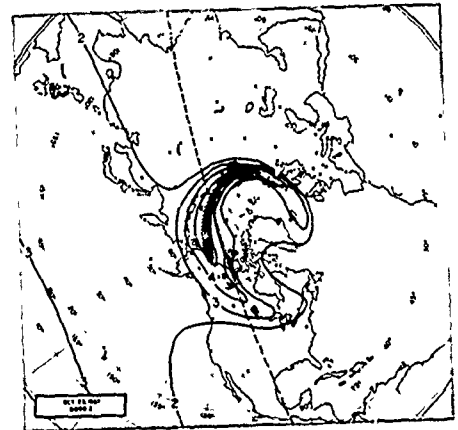
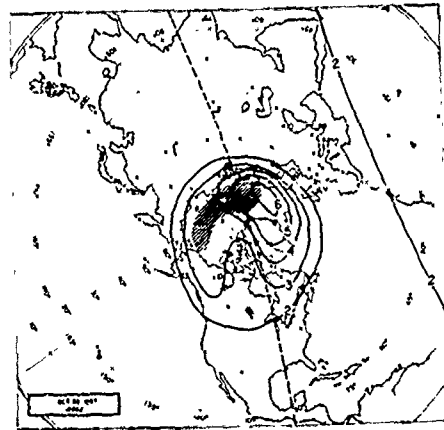


Figure 33 (CONCL'D)

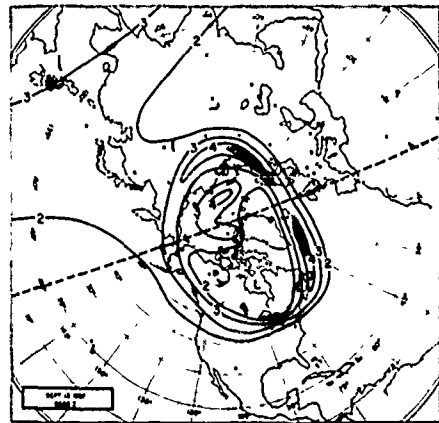
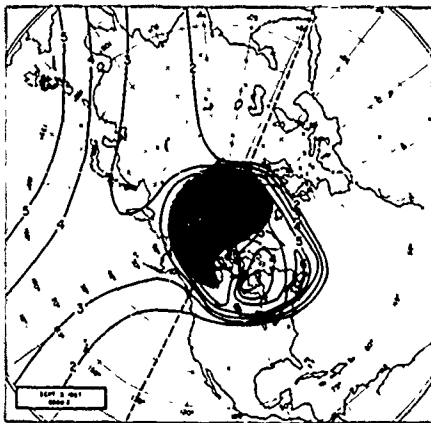


Figure 34 MAPS FOR AURORAL ZONE ABSORPTION

geomagnetic pole and would decrease slowly to a lower geomagnetic latitude (about 65 degrees) and then decrease rapidly further away from the pole. Such a pattern is actually found, but with one important exception, that is, on the darkened portion of the polar cap. Because of a high attachment rate the free-electron density is considerably reduced. Thus, a solar-proton event of a given strength produces, in the summer, a region of absorption covering the whole polar cap, whereas in the winter the region of absorption is confined mainly to the relatively small illuminated portion of the polar cap. Additional information on the extensive work performed in the last few years related to PCA's may be obtained from the summary articles by Hultqvist (1962) and Kahle (1962).

Toward the end or just after a polar-cap absorption event there is usually a geomagnetic storm (Hill, 1961). During this time enhanced absorption is found in the auroral zones. The period of greatest absorption occurs about the same time as the maximum of the main-phase geomagnetic disturbance. The region of absorption in the auroral zone usually progresses a few hundred kilometers in a direction away from the pole (Obayashi, 1959). In severe geomagnetic storms this displacement may be as much as 2000 km (Hakura, 1961). The effects of attachment are not so great as with polar-cap absorption, because the D-region electrons are usually produced at a higher altitude in auroral-zone events than in PCA events. In other words, differences in amounts of day or nighttime absorption will not be as great as with polar cap events. A good example of auroral zone absorption associated with a geomagnetic storm is found on the map for 13 Sept 1957, 0600 UT, shown in figure 34.

Auroral-zone absorption is not limited to periods of geomagnetic storms of a classical type, (preceded by a sudden commencement of geomagnetic activity and a polar-cap absorption event). During periods of minor geomagnetic activity, which occur several times more often than geomagnetic storms, there is usually a portion of the auroral zone where there is increased absorption.

3. Disturbed Es

Observed values of sporadic E critical frequency during geomagnetically disturbed periods (see table IV) have been plotted on polar stereographic maps. The maps are plotted on either a 1 or 3 hour UT basis and isopleths of f_oE_s drawn. Three latitudinal zones are established (U, A, L) roughly 8 degrees wide with the A zone centered in the mean observed auroral zone, and the U and L zones above and below A, respectively, as shown in figure 35. Longitudinally the zones are 30 degrees wide, commencing with a zone centered on the Greenwich meridian. The intensity of the E_s is indicated by a number system:

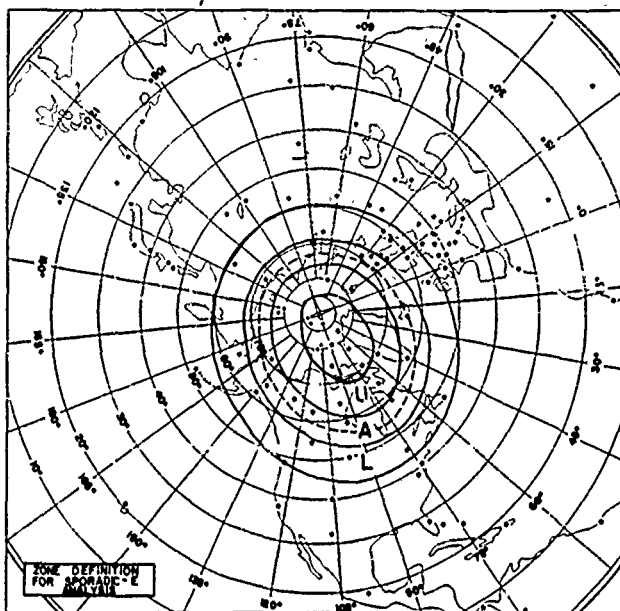


Figure 35a ZONE DEFINITION FOR SPORADIC-E ANALYSIS

SPORADIC E CLASSIFICATION

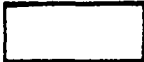
INDEX	RANGE of foEs (Mc/s)	
0	$0 \leq \text{foEs} < 4.0$	
1	$4.0 \leq \text{foEs} < 7.0$	
1½	$4.0 \leq \text{foEs} < 10.0$	
2	$7.0 \leq \text{foEs} < 10.0$	
3	$10.0 \leq \text{foEs}$	

Figure 35b CLASSIFICATION OF SPORADIC E ZONES

<u>Index</u>	<u>Range of foEs (Mc)</u>
0	$0. \leq \text{foEs} \leq 4.0$
1	$4.0 < \text{foEs} < 7.0$
1-1/2*	$4.0 < \text{foEs} < 10.0$
2	$7.0 \leq \text{foEs} < 10.0$
3	$10.0 \leq \text{foEs}$

*The value 1-1/2 occurs in prediction only and results from the addition of the spatial and auroral patterns. In range it encompasses indices 1 and 2, but the maximum probability is at 7 Mc.

From the maps a table is derived which can conveniently represent a series of maps; for example, the map series of 4 and 5 September is represented in table V.

Each map is reduced to a single line in this table. A combination of these indices listed above represents the intensity of Es in the regions of U, A, L, within a given longitudinal zone, e. g., U, A, L equals 1, 0, 3.

A study of disturbed periods (listed in table IV) indicates the presence of an auroral-zone traveling of maximum Es with its center around local midnight. Its latitudinal and longitudinal breadth are similar to the monthly patterns except that during the main phase of "great" geomagnetic storms, the pattern intensifies, moves to the south, and spreads over a greater portion of the night hemisphere. This is also noted in studies of the polar aurora (Akasofu and Chapman 1962; Akasofu 1962). In terms of a spatial pattern, the ionospheric stations at Baker Lake and Churchill report the most persistent sporadic E occurrence. Sporadic E during disturbed periods is related to the average patterns previously described (section III. A. 4.) since the average patterns include both quiet and disturbed intervals.

Using these notions a prediction table is constructed for sporadic E during disturbed conditions (table VI). This prediction table consists of a summation of the spatial pattern and an auroral-zone traveling maximum of Es centered about local midnight. (A predicted value of 0.5 in the total pattern is counted as 0.) This sum in table VI is the basic prediction in universal time. There are also storm-time variations which are dependent on the phase of the storm. Changes in numerical-value assignments for both the spatial and auroral patterns are made to conform with the storm-time changes (table VII).

TABLE IV

STUDY OF DISTURBED PERIODS (SPORADIC E)

	Begin		End		Type of Map
	Date	Time (UT)	Date	Time (UT)	(Interval)
1957	3 Aug	12	4 Aug	15	3
	13 Aug	06	13 Aug	10	1
	3 Sept	00	3 Sept	21	3
	4 Sept	11	5 Sept	12	1
	6 Sept	00	6 Sept	21	3
	13 Sept	00	13 Sept	16	1
	23 Sept	00	24 Sept	06	3
	6 Nov	18	7 Nov	08	1
1958	18 Jan	00	18 Jan	21	3
	11 Feb	00	11 Feb	21	3
	19 Feb	00	19 Feb	21	3
	11 Mar	12	12 Mar	09	3
	15 Mar	00	15 Mar	21	3
	22 Mar	00	22 Mar	21	3
	17 Apr	00	17 Apr	21	3

TABLE V
TABULAR REPRESENTATION OF E_s INTENSITY DURING A STORM

Time UT	0	30 E	60 E	90 E	120 E	150 E	180	150 W	120 W	90 W	60 W	30 W	K _p
4/5 Sept 57													
1100													
1200										100			3-
1300													
1400		021		010	010			010	012	001			
1500		032		010	010	010	002	010					8+
1600		032		010	010	010	001						
1700					010								
1800		003						020					9 ₀
1900		011	001		011			010	011				
2000	021	011							001				
2100	011	011			010					001			8 ₀
2200	011	021								110			
2300		010							010	331	011		
0000		010							001	011	001		8+
0100		020							013	113	111	010	
0200		021							003	002	001	010	
0300	001								002	003	002	001	8+
0400		021							003	302	011	010	
0500	001	020							002	302	021	020	
0600								030	023	011	011		9-
0700	100	032	200	200	200	200	010	021	013	002	120		
0800		010				200		011	012	010			
0900								012	011	101			7-
1000								001	010				
1100	100							001	001				
1200		100	200	200	200	100	190			010			5 ₀

Note: The bar over a value indicates extrapolation.

TABLE VI
PREDICTION TABLE FOR DISTURBED SPORADIC E CONDITIONS

	0	30 E	60 E	90 E	120 E	150 E	180	150 W	120 W	90 W	60 W	30 W
Auroral												
0000	0.5.1.0.0.50.0.1.0.0.5											0.0.1.0.0.5
0200	0.0.1.0.0.3											0.0.1.0.0.50.5.1.0.0.5
0400												0.0.1.0.0.50.5.1.0.0.50.0.1.0.0.5
0600												0.0.1.0.0.50.5.1.0.0.50.0.1.0.0.5
0800												0.0.1.0.0.50.5.1.0.0.50.0.1.0.0.5
1000												0.0.1.0.0.50.5.1.0.0.50.0.1.0.0.5
1200												0.0.1.0.0.50.5.1.0.0.50.0.1.0.0.5
1400												0.0.1.0.0.50.5.1.0.0.50.0.1.0.0.5
1600												0.0.1.0.0.50.5.1.0.0.50.0.1.0.0.5
1800												0.0.1.0.0.50.5.1.0.0.50.0.1.0.0.5
2000												0.0.1.0.0.50.5.1.0.0.50.0.1.0.0.5
2200												0.0.1.0.0.50.5.1.0.0.50.0.1.0.0.5
Plus												
Spatial	0.5.0.5.0.50.5.1.0.0.50.5.0.5.0.0											0.0.1.0.0.50.0.0.5.0.0
Total												
0000	1.0.1.5.1.00.0.1.5.1.0											1.0.1.0.0.0.1.0.1.0.0.0.0.1.5.0.0
0200	0.0.1.5.1.00.0.1.0.0.0											1.0.1.0.0.0.1.0.2.0.1.0.0.1.0.0.0
0400	0.0.1.0.0.0											1.0.2.0.1.0.1.5.2.0.1.0.0.1.5.0.0
0600	0.0.1.0.0.0											0.0.1.5.1.0.0.1.0.2.0.1.0.0.2.0.1.0
0800	0.0.1.0.0.0											0.0.1.5.1.0.0.1.0.1.0.1.0.1.0.0.0
1000	0.0.1.0.0.0											1.0.1.0.0.0.1.0.1.0.0.0.1.0.0.0
1200	0.0.1.0.0.0											1.0.1.0.0.0.1.0.1.0.0.0.1.0.0.0
1400	0.0.1.0.0.0											1.0.1.0.0.0.1.0.1.0.0.0.1.0.0.0
1600	0.0.1.0.0.0											1.0.1.0.0.0.1.0.1.0.0.0.1.0.0.0
1800	0.0.1.0.0.00.0.1.5.0.0											1.0.1.0.0.0.1.0.1.0.0.0.1.0.0.0
2000	0.0.1.5.1.0.0.1.5.0.0											1.0.1.0.0.0.1.0.1.0.0.0.1.0.0.0
2200	0.0.1.5.1.0.1.0.1.5.1.00.0.1.5.0.0											1.0.1.0.0.0.1.0.1.0.0.0.1.0.0.0

TABLE VII

STORM TIME CHANGES IN THE PREDICTION SCHEME FOR Es

Value in table VI*	Storm Type				
	Minor	Moderate		Great	
		Initial Phase	Main Phase	Initial Phase	Main Phase
Spatial					
0.0 0.5 0.0	---**	---	--	---	---
0.5 0.5 0.5	---	---	0.5 0.5 0.0	---	---
0.5 1.0 0.5	---	---	0.5 1.0 0.0	---	0.0 1.0 1.0
0.5 0.5 0.0	---	---	0.5 0.5 0.0	---	---
(0.5 0.5 0.5)	---	---	(0.5 0.5 0.0)	0.0 1.0 0.0	0.0 1.0 1.0
1.0 1.0 0.5	---	---	2.0 1.0 0.5	2.0 1.0 0.5	1.0 1.0 2.0
Auroral					
0.0 1.0 0.5	---	---	---	---	0.0 0 1.0
0.5 1.0 0.5	---	---	---	---	0.0 1.0 1.0

*The values in this column change to the values indicated in the other columns, depending on storm type.

**Dashes indicate no change.

As an example, several hours selected from a moderate sudden-commencement geomagnetic storm on 6 and 7 November 1957 are presented in figures 36 through 38 in map form and compared with the predicted values. The storm began at 1821 UT on 6 November 1957 and had a sudden commencement of the type designated, -SC-. The epoch of maximum main-phase depression of the geomagnetic field occurred at 0100 UT on 7 November with a Dst component of about 100 gammas.

To obtain a preliminary indication of the utility of the prediction scheme, the total is found of the number of times the prediction does not coincide with the observed value. No distinction is made between the indices 1 through 3. There is a total of 36 prediction zones.

Time 6/7 November 1957	Number of Errors	Percent of Error
2100	5	14.0
0000	3	8.3
0300	2	5.6

C. RELATED SOLAR-GEOPHYSICAL DATA

1. Solar Data

The intimate connection between the solar disturbance phenomenon and ionospheric conditions has been introduced in previous sections. Solar sunspots, flares, and associated radio and visual emissions create or influence disturbances of the geomagnetic field and ionosphere. Parameters which characterize the ionosphere electron density have been previously introduced. Some measures of solar and geomagnetic disturbances are now discussed which are used in correlation studies to establish the mechanism of the interaction between the sun and Earth which produces an ionospheric storm.

Logically, the assumed source of the disturbance, the sun would first be described but, in fact, it is beyond the scope of this report to discuss any of the theories of the solar reaction mechanism. Visual and radio observations of the solar disc provide a measure of the solar disturbance. The relative sunspot number is characteristic of the total activity of the sun and is defined as

$$R_s = K(10g + s) \tag{63}$$

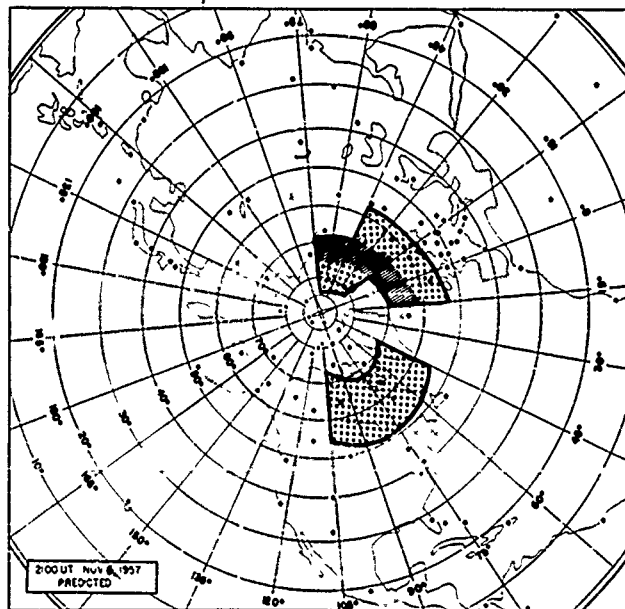
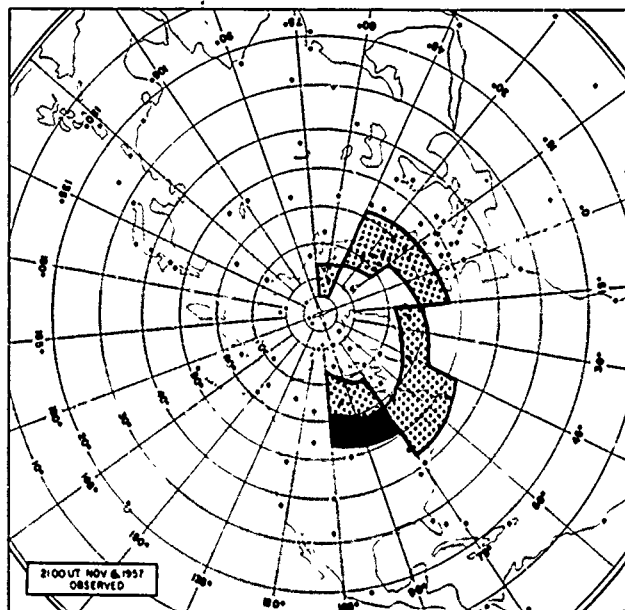


Figure 36 OBSERVED AND PREDICTED PATTERNS OF SPORADIC E DURING A GEOMAGNETIC STORM, 2100 UT

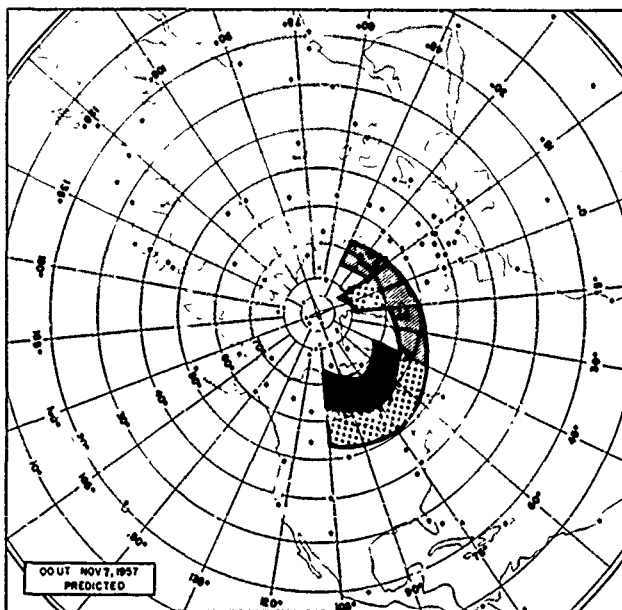
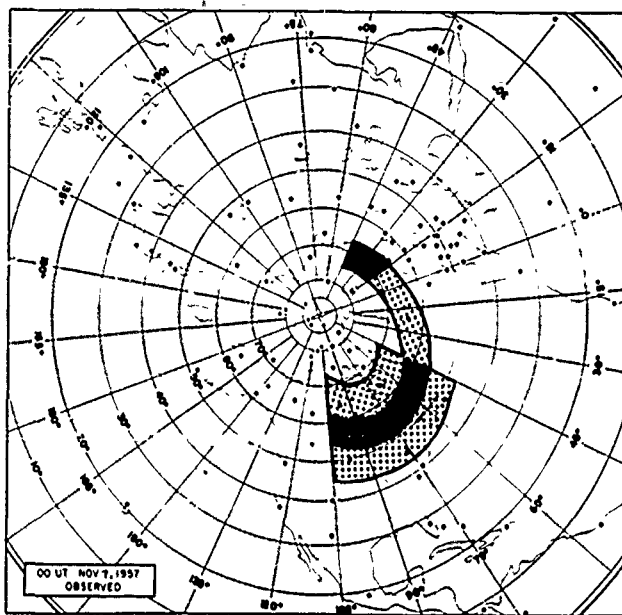


Figure 37 OBSERVED AND PREDICTED PATTERNS OF SPORADIC E:
DURING A GEOMAGNETIC STORM, 0000 UT

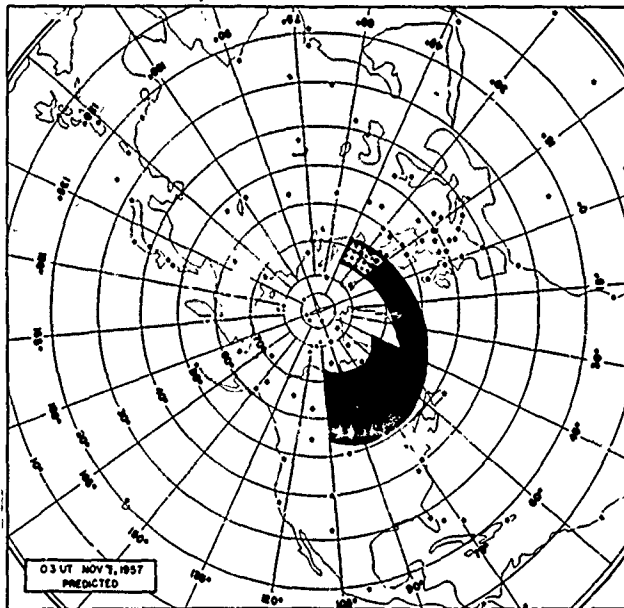
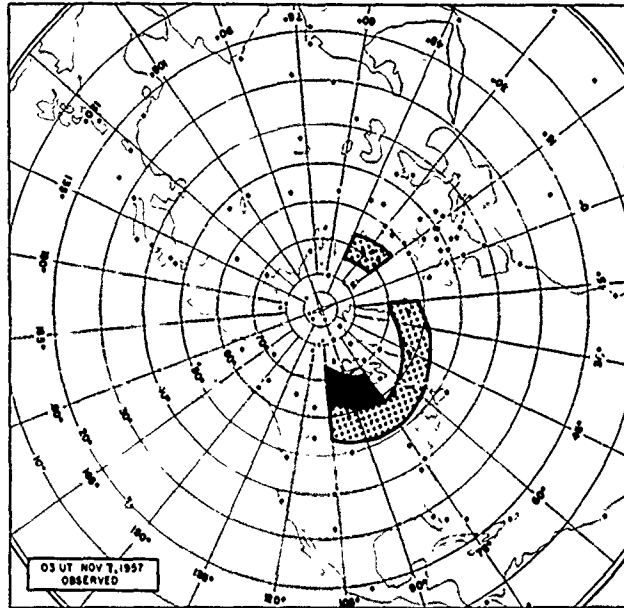


Figure 38 OBSERVED AND PREDICTED PATTERNS OF SPORADIC E DURING A GEOMAGNETIC STORM, 0300 UT

where g = number of sunspot groups

s = total number of distinct spots

K = scale factor depending on observer.

Two different relative numbers are computed, R'_A and R_Z , the American and Zurich relative sunspot numbers. The magnitude of each is different, but the trend is the same. It indicates that the activity of the sun is periodic in about 11 years with a probability that alternate cycles will have the closest amplitude relationship. A 12-month running-mean Zurich smoothed sunspot number is often used for computational purposes and termed the smoothed-observed sunspot number \bar{R} .

At times, small regions of the chromosphere, almost invariably associated with sunspot groups, suddenly intensify their emissions of certain spectral lines, primarily the calcium H and K lines and the hydrogen H_α line. These flares have a lifetime of a few minutes to hours, with the average being about a half hour. The importance of flares is designated: 1-, 1, 2, 3, 3+ primarily upon their visual characteristics. There is a good correlation between solar flares and sudden ionospheric disturbances (SID); so that these ionospheric absorption events can be used to identify a solar flare. Normally, this radiation effect produces abnormally increased HF absorption and is the cause of the sudden short-wave fadeout (S-SWF) and the sudden cosmic-noise absorption (SCNA). Furthermore, the increased ionization in the D-region enhances the ionospheric current systems and produces a discontinuity in the magnetic record called a crochet. These effects last only as long as the flare and are caused by an increase in soft X-ray radiation (Chubb, et al., 1957; Kreplin, 1961).

Another manifestation of solar activity is in the radio spectrum. In addition to the thermal blackbody radiation, nonthermal emissions occur at very irregular intervals with intensities of perhaps 10^5 times as large as thermal. The classification of radio emissions in the band 25 to 10,000 Mc is made in terms of the following spectral types.

Type I -- random bursts of noise which may last for hours or days -- associated with sunspot areas but not particularly with flares.

Type II -- slow-drift burst -- starts at high frequencies, drifts steadily down at about 1 Mc with a duration of several seconds.

Type III -- fast drift burst -- starts at high frequency with a duration of several seconds.

Type IV -- continuum radiation -- strong - long with a duration of several hours.

Type V -- continuum occurring immediately after type III with a duration of several minutes.

2. Riometer Data

Solar cosmic rays (relativistic protons) are generated in significant numbers at the time of large solar flares. They reach the vicinity of the Earth within about a few hours after the beginning of the flare. The trajectories of the incident protons may be described using the theory of Stormer (1955) which treats them as individual particles. Because of the guidance of the magnetic field, solar cosmic rays are confined to the region greater than 60 degrees geomagnetic latitude. Production of ionized particles in the D-region of the ionosphere causes strong absorption of HF signals reflected from the ionosphere. Blackout conditions for HF radio are caused in the polar regions and result in an absence of ionospheric reflections in high-latitude ionosonde recordings. This continues for about 1 day and is termed a polar cap absorption event (PCA or type III absorption).

Ionosonde measurements provide only a qualitative measurement of absorption, especially as the blackout condition is dependent on the F2 critical frequency, and in any event, places only a lower bound on the D-region absorption. A more efficient instrument for measuring absorption has been dubbed a riometer (i. e., relative ionospheric opacity meter). The device is a receiver which continuously records cosmic noise power. In the Arctic, frequencies of about 27 Mc are used while 18 to 20 Mc are usually employed at lower latitudes. At these frequencies terrestrial sources are quite weak, and the cosmic noise sources are paramount. This extraterrestrial noise can penetrate the ionosphere, since the measurement is made above the F-region critical frequency. Under normal conditions, the nighttime D-region absorption is negligible and provides a system of calibration. Daytime photo-ionization of the D region produces absorption and reduces the galactic signal power which penetrates the D region. The noise power which penetrates the D region is a measure of the integrated absorption.

Riometer absorption is usually quoted in decibels per pass at the measuring frequency. The riometer is useful also for identifying other absorption events in the auroral zone (type II absorption). PCA (type III) is smooth and long lasting compared to type II which is associated with visual aurora.

3. Magnetic Data

At the time of optical flares, giant clouds of low-energy gas are emitted from the sun. Moving through the region between the sun and Earth at about 1000 km/sec, these gas clouds reach the Earth 2 days later, on the average (Obayashi, 1961). The average energy of the protons, measured by Explorer X at about 22 earth radii, is of the order of 1 kev (Rossi, 1962).

The interaction of the shock wave associated with the gas cloud, the cloud particles, and the Earth's magnetic field produces a geomagnetic storm. Magnetic records serve to characterize this disturbance: three components are measured, but the horizontal (H) component is most significantly affected. The advancing shock front causes a sudden increase in the H component - the sudden commencement (SC) of the geomagnetic storm. For several hours, the field remains above normal (the initial phase) plunges sharply below normal (main phase) and then returns slowly to its prestorm condition after about 30 hours. The actual magnitude of these effects is individual with each storm but the pattern is similar. Tabulations of sudden commencements and other magnetic disturbances are made, but copies of individual station magnetic records (magnetograms) are difficult to distribute. In order to provide workers with a measure of the disturbance variation, several indices of activity have been devised.

1. The C-figure is an arithmetic mean of the subjective classification by all observatories of each day's magnetic activity on a scale of 0 (quiet) to 2 (storm).
2. K_p is the mean K index from 12 observatories between 47 to 63 degrees geomagnetic latitude. The scale ranges from 0 (very quiet) to 9 (extremely disturbed). It is a measure of the 3-hour range of the most disturbed component of the field. The scale is adjusted to compensate for the latitudinal variation of the disturbance.
3. A_p is a daily index of magnetic activity. It is computed as the mean of 8 values of a 3-hour index a_p which is 1/2 the average gamma range of the most disturbed of the three magnetic components. In practice this is computed from K_p by the schedule:

K_p	0	1	2	3	4	5	6	7	8	9
A_p	0	4	7	15	27	48	60	132	207	400

K_p is the most useful for ionospheric studies.

IV. HF EQUIPMENT AND SYSTEMS

A. EQUIPMENT

While the ionosphere provides a reflecting surface enabling radio signals to be transmitted beyond the horizon and its absence precludes all but scatter propagation, the electronic equipment which generates, transmits, receives, and detects is also essential. Each communication system possesses certain characteristic assets and liabilities and must be matched to the ionospheric conditions, transmission path, and information rate.

Communication ground-to-air is now almost exclusively voice, while ground-to-ground is transmitted in CW, AM, DSB, SSB, and FSK. Several communications systems presently in use are tabulated in table XI.

B. HF SYSTEMS

1. U.S. Coast Guard

In the USCG HF communication system, which is used in connection with the North Atlantic weather patrol, there are 8 stations - ships A through E: Argentia, Newfoundland; Bermuda; and Washington, D. C. These are shown in figure 39. The power output for the ships is 0.5 kw and for shore, 3 and 15 kw. At Washington, a monorhombic antenna is used. Normally, communication from weather-ships is on approximately 4, 6, 8, 12, and 16 Mc. When relays go through Argentia the frequencies used are approximately 0.5, 2, 4, and 7 Mc. Two frequencies are utilized simultaneously to avoid cutoff. During disturbed periods it is the practice to use relays on north-south paths, that is, messages from station A go through C, and messages from B go through Argentia, Newfoundland, or through station D or E. Routing through Bermuda is done only when propagation conditions require it.

2. Norlant - 1958

The HF narrow band system in 1953 served US Air Force installations in the North Atlantic region and in northern parts of North America. Much of the communication in this latter region was in connection with IGY activities. The geographical layout of this system is shown in figure 40. The numbers beside the lines indicate the number of assigned frequencies for that link. Many of these stations are equipped with air-ground and ground-air equipment. Information on this type of equipment may be found in the previous chapter. In connection with networks, only point-to-point equipment need be considered. These equipment parameters are given in table VIII.

TABLE VIII

HF NARROW-BAND SYSTEM INFORMATION

Point-to-Point Systems

Transmitter LD-2

Power output: up to 90 kw peak envelope SSB
Frequencies: 10 preset frequency select any of six
Functional description: transmit four 3 kc channels simultaneously
Antennas: 2 Rhombics, high band and low band, the installation of which is designed for particular paths.

Receiver

- (1) R-390/URR
Sensitivity: $0.5 \mu v$
- (2) Hughes EC-150
Sensitivity: $0.3 \mu v < 10 Mc$
 $0.5 \mu v > 10 Mc$

Functional description: band divided into four 3-kc channels.
Antennas: Rhombics in pairs for high and low bands for space diversity.

- (3) SP-600
Similar to R-390
Approximate sensitivity: $0.5 \mu v$

Ground-Air Systems

Transmitter MW-2 Westinghouse

Power output: SSB (upper or lower)
2.5 kw peak envelope
AM 1.25 kw carrier
Frequency range: 2.0 to 30.0 Mc
Antennas: 5 vertical towers and antennas to cover 5 frequency bands. Towers and antennas are each proportional to wavelength.
Backup: LDT-2
Power output: 4 kw peak

Receiver

Sensitivity: $0.25 \mu v$
Functional Description: 6 channel -- each channel can receive both upper and lower side band separately.
Frequency Range: 4.0 to 30.0 Mc.
Antennas: 4 Granger log-periodic curtain array, vertical polarization, 110-degree beamwidth + 9 db gain over isotropic. For omnidirectional coverage, discone antennas are used.

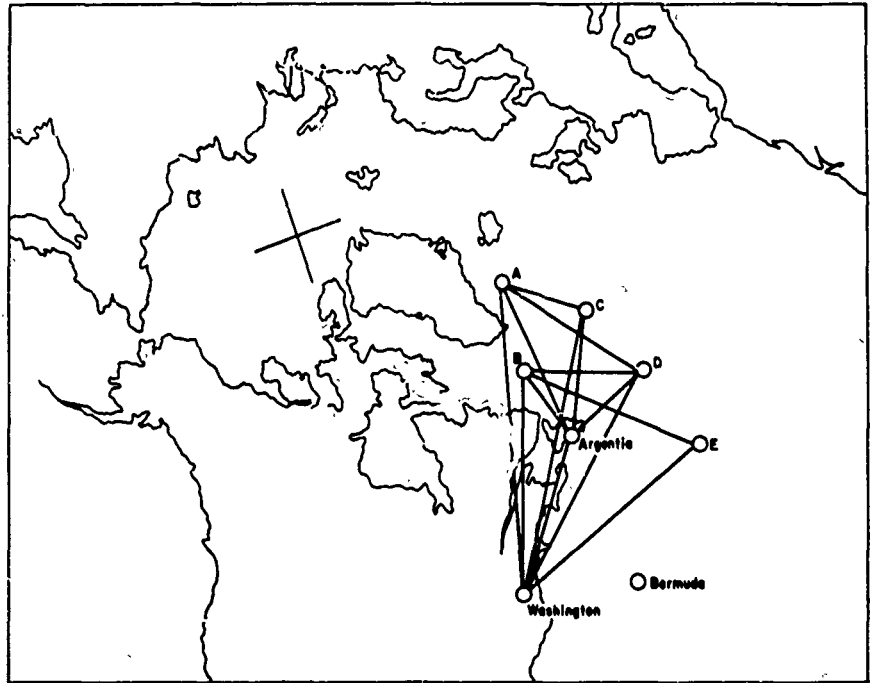


Figure 39 USCG NORTH ATLANTIC WEATHER PATROL HF
COMMUNICATION SYSTEM
63-3576

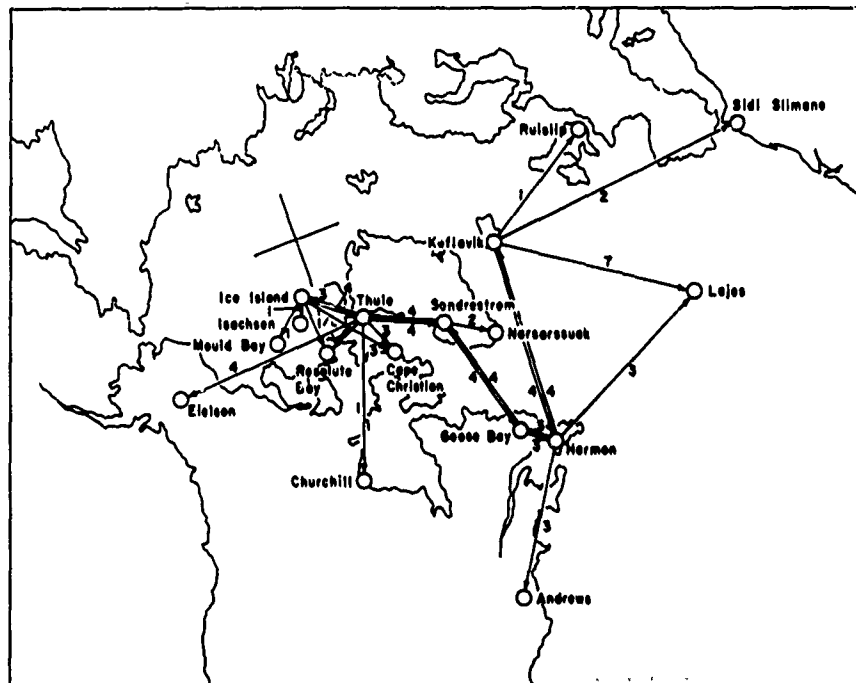


Figure 40 NORLANT - 1958 HF COMMUNICATION SYSTEMS
63-3575

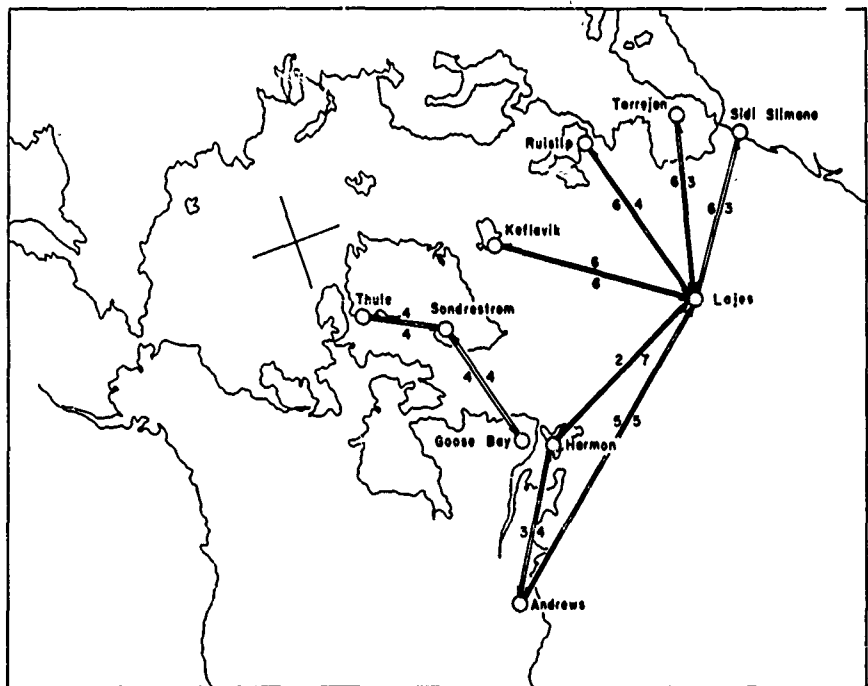


Figure 41 NORLANT - 1961 HF COMMUNICATION SYSTEMS

In practice, this network is used together with others, such as VHF or land-line networks. For this one, only one frequency at a time is used so that the cost of operation can be kept to a minimum. For the major relay station, i. e., Harmon, Goose, and Lajes, relaying is accomplished electronically. If one link is saturated then another is selected.

3. Norlant - 1961

This system is essentially the same as in 1958. The major difference is that the number of stations has been somewhat reduced. This network is shown in figure 41. The equipment installed at these stations is about the same as before. Circuit information, such as the approximate assigned frequencies, bandwidth and power is given in table IX.

Some additional comments on the operation of this network are:

- a. The peak load on common user traffic is from about 1400 to about 2200, local time. Channel utilization is about 50 percent if averaged over the whole day. If a channel is assigned to only one user and his utilization exceeds 50 percent, it is likely that during peak hours a backlog of messages will develop.
- b. The average length of a message is about ten lines, but this varies from one message to another. Messages involving air traffic are usually shorter and have an average length of about two lines.
- c. Relays require less than 1 minute or so handling time. Usually the whole message is received before retransmission. Some messages go through several links without any manual handling - reception and retransmission is accomplished automatically.
- d. Destination of traffic is highly variable. Many agencies use this network and other ones which are connected. So traffic flows on a world-wide scale, with some messages passing through many links, say 6, and others through only 1.

4. Strategic Air Command HF Communications

For the SAC constant-alert system and other SAC training operations, there are 4 main control stations in the United States: Westover, Massachusetts, Barksdale, Louisiana, Omaha, Nebraska, and March Air Force Base, California. These are interconnected and serve to control SAC aircraft. Aircraft flying in northern regions, or in Europe for example, receive HF signals directly from the US or from other nearby aircraft, or, if possible, from a ground station on UHF. Sometimes, subsidiary stations, such as Goose Bay, transmit HF and receive and relay back to the US. The US

TABLE IX

NORLANT HF CIRCUIT INFORMATION - 1961

System	Allocated Frequencies (Mc)	Bandwidth (kc)	Maximum Power (kw)
Andrews/Harmon	5, 8, 14, 16.	3	3
Harmon/Andrews	5, 9, 12	3	3 to 4
Andrews/Lajes	6, 8, 10, 15, 21	3 to 12	40
Lajes/Andrews	8, 10, 16, 19, 22	6 to 12	40
Thule/Sondrestrom	3, 5, 8, 9	3	3
Sondrestrom/Thule	5, 7, 8, 9	3	3
Goose/Sondrestrom	6, 8, 9, 16	3	3
Sondrestrom/Goose	5, 7, 9, 12	3	3
Harmon/Lajes	5, 8, 9, 10, 12, 16, 20	3 to 9	4 to 40
Lajes/Harmon	8, 10	9	10
Lajes/Keflavik	3, 4, 8, 12, 14, 20	3	3 to 10
Keflavik/Lajes	3, 4, 9, 12, 16, 20	3	2 to 10
Lajes/Croughton	6, 9, 16, 23	3 to 12	4 to 10
Croughton/Lajes	5, 8, 9, 10, 14, 16	6 to 12	4 to 40
Lajes/Torrejon	9, 20, 24	6 to 12	4 to 40
Torrejon/Lajes	5, 9, 10, 14, 20, 24	6 to 9	3 to 40
Lajes/Sidi Slimane	5, 11, 12, 14, 16	3	3 to 5
Slidi Slimane/Lajes	5, 7, 9, 11, 14, 16	3	3

stations have a power output of around 10 kw and up to 45 kw, if necessary. Normally, only the power actually required is used. There are 8 frequencies available in the range 2 to 30 Mc. The antennas are different types:

1. Disk cones, gain 2 db
2. Billboards, gain 20 db
3. LPS (rotating) gain 13 db

Aboard the aircraft (B52, KC135, and B47) there are Collins A 58 receivers. Their transmitter output is about 1-kw peak power. They use the same frequencies as the control. It is not necessary for control to monitor more than four frequencies at a time, because of the diurnal variation of frequency assignment. In actual operation it would be preferable to have a communication operator aboard, but the position has been abandoned. Thus, the present crews have a difficult time maintaining communication while flying the aircraft. Besides weather information and mission data, periodic reports on SAC aircraft are maintained by US control. In northern regions, use is made of DEW line facilities for UHF contact. This provides a geographical band for high-flying aircraft about 250 miles on either side of the line. Further north, HF is the only means of communication. Since July 1961, when the completely-operational 24-hour-air alert was started, there have been no serious outages. However, there have been some, and they result from propagation conditions, aircraft communications equipment failures, and nuclear testing.

V. AVAILABLE CHANNELS - MAXIMUM UTILIZATION

A. COMPUTER PROGRAM

We consider a communications network consisting of n receiving-transmitting stations, each represented by an index $i, i = 1, \dots, n$. Station i is capable of transmitting c_{ij} message-units to stations $j, j = 1, \dots, n$, during the period being considered and it is desired to transmit from i to $j, i, j = 1, \dots, n; i \neq j$, either directly or through intermediate stations, the accumulated number of l_{ij} message-units.

Two related problems are considered. First, a determination must be made of the largest number (or, more generally, the largest value) of the accumulated messages that can be transmitted through the network to the desired destinations. Next, having determined that number (or value), a way must be found of channeling the messages through intermediate points, when necessary, so as to transmit the information at a minimum cost.

In the practical cases to be considered, it is expected that many of the values c_{ij} will be 0, indicating that station i has no capability of transmitting to station j for many couples (i, j) . This fact permits us to formulate the problem in a manner that will tend to render our computations more manageable.

Assuming that an ordered couple (i, j) of stations is connected by a link, if $c_{ij} = 0$ -- There may be two distinct links, (i, j) and (j, i) with $c_{ij} \neq c_{ji}$, in general; or (i, j) may be connected by a link, but not (j, i) -- the links may be enumerated in some arbitrary fashion and represent them by an index $l, l = 1, \dots, L$, letting $c_l = c_{ij}$, for the link l which connects i to j . Furthermore, the addresses of messages shall be enumerated, each address representing an ordered couple (i, j) such that $l_{ij} \neq 0$ thus, an address represents an origin-destination combination characterizing a given message or a combination of a forwarding and a return address. Let $l_a, a = 1, \dots, \bar{a}$, where l_a is the number of message units to be sent according to the address a .

Finally, the various admissible paths which a message may take when bearing an address a must be described. A given path may be uniquely defined by indicating the links of which it is composed. The paths are enumerated by an index $p, p = 1, \dots, \bar{p}$, grouping the paths belonging to a given address next to each other and enumerating those pertaining to address $a+1$ right after those pertaining to address $a, a = 1, 2, \dots, \bar{a} - 1$.

A message transmitted through a path p may have a given value. In general, one would tend to make all values equal unless certain addresses are to be favored (i. e., for priority reasons) or even certain paths are to be favored (say, for strategic reasons). Let $v_p, p = 1, \dots, \bar{p}$ be the value of path p , which, unless otherwise indicated, is set equal to 1.

Different costs of transmitting a message through a given path p may be considered. Thus, as an example, the cost of transmitting a message from one station to another may vary, yielding different costs for different links; in that case, the cost of transmitting a message-unit through path p is the sum of the unit-costs associated with the links of which the path is made up. Unless otherwise specified, let the unit-cost for path p be equal to the number of links in it, making the cost proportional to the labor-hours required to transmit a message-unit through the path. The unit cost for path is represented by w_p , $p = 1, \dots, \bar{p}$.

Now, $x_{p, p} = 1, \dots, \bar{p}$, represent the number of message-units sent through the path p . Let $a_{l, p} = 1$ if link l belongs to path p and let otherwise $a_{l, p} = 0$. Let $a_{\bar{l}+a, p} = 1$ if the path p belongs to address a and let otherwise $a_{\bar{l}+a, p} = 0$.

The first problem is that of determining the maximum value of accumulated messages that can be transmitted through the network; the problem can be formulated as follows: find nonnegative $x_{p, p} = 1, \dots, \bar{p}$, such that the function $v = \sum_{p=1}^{\bar{p}} v_p x_p$ is maximum subject to the restrictions:

$$\sum_{p=1}^{\bar{p}} a_{l, p} x_p \leq c_l, \quad l = 1, \dots, \bar{l} \quad (64)$$

and

$$\sum_{p=1}^{\bar{p}} a_{\bar{l}+a, p} x_p \leq l_a, \quad a = 1, \dots, \bar{a} \quad (65)$$

The quantity v represents the total value (or, in a special case, the total number) of the messages transmitted through the network. Restrictions (64) specify that the total number of message units channeled through link l (which may be shared by many paths) cannot exceed c_l . Similarly, restrictions (65) specify that no more than l_a messages-units are available for useful transmission through the various paths servicing the address a .

After this first problem is solved, there is the quantity v_{\max} available which is the maximum value of v subject to the restrictions. Now solve the optimal channeling problem by minimizing the total cost $w = \sum_{p=1}^{\bar{p}} w_p x_p$ subject to x_p being nonnegative, subject to restrictions (64) and (65) and subject to the added restriction

$$\sum_{p=1}^{\bar{p}} v_p x_p = v_{\max} \quad (66)$$

This last restriction specifies that costs may not be cut by transmitting less than a total value v_{\max} of messages.

Both of these problems, as formulated, belong to the class of linear programming problems. Illustrative examples were solved at Avco RAD using a digital computer program (Math Section program 1332) based on a convex programming method described in RAD-TM-62-58.

B. EXAMPLES

To show how the mathematical program of optimized routing is carried out, some definitions will be reviewed and then three examples will be given. The network used is one with nine nodes or stations which are interconnected as shown in figure 42. Definitions are given below for terms which appear often in the test:

1. A link is a connection between two stations. The links for the example network are indicated as shown by the lines in figure 42.
2. An address is a designation of the source and destination of a message.
3. A path is the route by which a message is sent. In general, a message will be sent over one or more links.
4. The load, l_{ij} , is made up of all the messages to be sent to an address in a given interval of time.
5. The capacity, c_{ij} , is made up of all the messages which can be sent over a link.

In HF communication problems it will be l_{ij} and c_k which are used as inputs to an optimization program. l_{ij} will be determined by the users of the communication facility, and c_k will be determined by the equipment being used and by the condition of the ionosphere. In these examples, both the l_{ij} 's and the c_k 's will be assumed known. For the first example the value of c_k is taken to be 10 for all 24 links and the l_{ij} 's are listed in table X. The total is 34 messages which may be interpreted as a message rate, or as pages per hour.

TABLE X

l_{ij}

Address	Messages
i, j	l_{ij}
1, 7	4
3, 5	7
4, 1	6
4, 5	3
6, 7	5
6, 8	9
Total	34

For these examples the units are not so important as the relative values of l_{ij} and c_k . This example is a case when the capacity of the network is somewhat larger than the load placed on it. It would be expected, then, that the paths chosen would be the most direct and that they could possibly have been selected by inspection. The routing of messages from 6 to 7 and from 6 to 8 is shown in figure 43a, as a sample of the results.

The routing of 6, 7 is obvious. For 6, 8 it is evident that only five message units can pass over link 6, 7 and that the remaining four messages must pass over other links. Link 6, 7 is the only one which becomes saturated. Since the capacity is large the selection is somewhat arbitrary. All four messages could just as well have been sent over either route actually selected by the computer. If these links are open for traffic to pass, it should make little difference what is the choice. However, if it were desirable to eliminate this arbitrariness, criteria could easily be set up to pick a preferred route. The other messages to be sent in this example are straightforward and there is no saturation of any link other than 6, 7.

In the second example the link capacity has been kept at 10, but the number of addresses is increased to 12. This corresponds to a case when the capacity of the network is not large compared to the load. The first six addresses are as before. These l_{ij} and the new ones are shown in table XI.

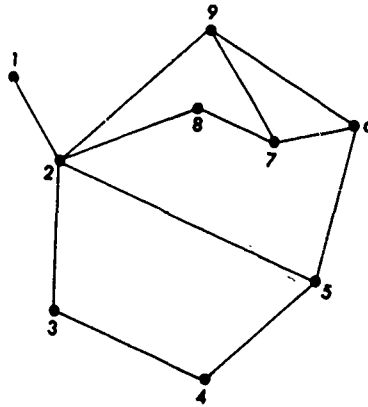


Figure 42 LINKS FOR THE EXAMPLE NETWORK

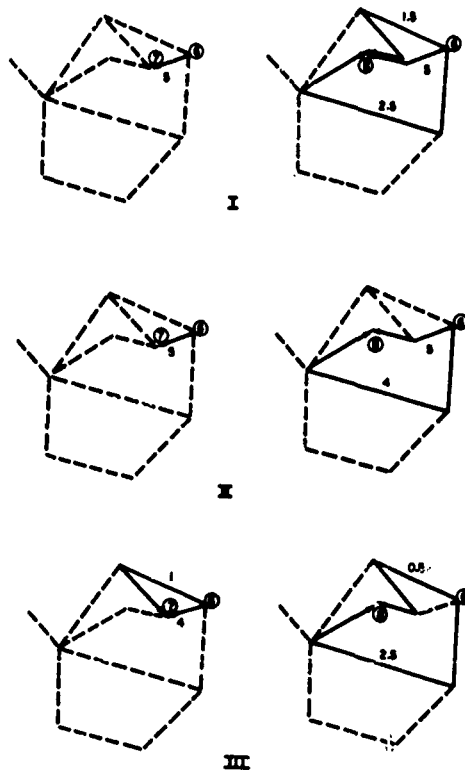


Figure 43 ROUTING OF MESSAGES - SAMPLE RESULTS

TABLE XI

i,j

Address	Messages	Address	Messages
i, j	1	i, j	1
1, 7	4	7, 1	2
3, 5	7	7, 2	4
4, 1	6	8, 1	6
4, 5	3	8, 5	1
6, 7	5	8, 9	8
6, 8	9	9, 4	2
Total i,j 57			

One important difference between the results of this example and those of the first is that four message units could not be sent out of the total of 57. If one looks at the message units going to station 1 the reason becomes obvious. Out of a total of 14, only 10 can pass over link 2, 1. Thus, four of the message units could have reached only as far as station 2.

In other respects this example is quite similar to the first one. The results for the two addresses discussed before (6, 7 and 6, 8) are shown in figure 43b.

The routing of 6, 7 is again obvious. The routing of 6, 8 is different, but this is still of an arbitrary nature. The capacity after other messages have been sent is large enough on path 6, 9, 7, 8 so that the routing could have been the same as before.

In the third example, the number of addresses and their loads has been kept the same as in the second example (see table XIV). However, the link capacity is reduced to four. This corresponds to a case when the capacity of the network is somewhat less than the load. Now the routing is rather sophisticated and could not easily be anticipated without a mathematical program such as the one used. Although the network is used in its most efficient way, 23 message units could not be sent. The reason is similar to the previous case, but is not easily seen in every instance. The routing for the two addresses, 6, 7 and 6, 8 is shown again (figure 43c) for comparison with the previous examples.

Here the routing is not arbitrary to any extent. For the address 6, 7 link 6, 7 becomes utilized fully, so one message unit is rerouted -- the shortest way. For the address 6, 8 only three of the nine message units could be sent. The ones sent are divided according to the available capacity on the paths chosen. The significant fact relating to the choice of paths is that whenever the number of messages to be sent can be increased by rerouting, the computer will indicate which ones are to be used. It is possible to spell out just what choices are arbitrary and which ones are not.

VI. COMPLETED SYSTEM

To show how the concepts and information described in this report utilized, an example of a hypothetical, but realistic communication problem will be given. First, the network and equipment parameters will be assumed. Then, the available frequencies will be found as would exist during a typical polar-cap absorption event. Finally, for a given message load, the optimum routing and selection of frequencies will be carried out.

The network used in this example is the same one used in the previous chapter, but it has been superimposed on a map, (figure 44) so that realistic communication facilities can be imagined. Assignment of equipment to these stations is expressed in terms of equipment parameters rather than their names or types. These parameters are listed in table XII. From these values it is possible to compute the radiated field strength at 1 km from the transmitter, E_0 , in the direction of the receiver. The transmitter antennas, receiver antennas, and receiver sensitivity at a station are assumed the same for all links in and out of that station, so that this information can be listed by station rather than by link. In fact, these parameters have been chosen to be the same at all stations, but there is no particular advantage in doing this. E_0 , listed in table XIII, is given by $74.8 + 10 \log P_E$ where $P_E = P_t/3$ and P_t is the power output in watts. The other parameter listed in table XIII is the minimum signal level receivable if the signal-to-noise ratio is to be 10. These also can be listed by station, but normally they would be listed by link. The allowable loss of signal strength, for any mode which is possible by consideration of the reflection layers, is then determined by the difference between the signal level indicated by E_0 at the transmitting site and the signal level indicated by the minimum signal level at the receiver. This difference must be adjusted to take into account the receiver antenna. The allowable loss is found in column three of table XIV. The adjustment F is found from $F = 30.6 - 20 \log f$, with f in Mc. The space attenuation is also given here. When that is deducted from the allowable total loss, the allowable loss due to absorption, reflection, and ground losses is found. In this example, the latter two are neglected for simplicity. It might be appropriately mentioned here that sporadic E modes are also neglected. As shown earlier, it is in relation to the presence of sporadic E that reflection losses become significant. So, for this example, the allowable loss due to absorption alone is found after space attenuation is deducted. This absorption loss is also included in table XIV.

A number of frequencies are assigned to each link. The assignment of these frequencies was guided by some general consideration, but the details were more or less arbitrary. The lowest frequency assigned is 3 Mc with the highest around 25 Mc. The spacing between frequencies for any one link was about 4 or 5 Mc. For each reciprocal link the assigned frequencies differed by 0.1 Mc in every case. It will also be noticed that for the shortest links, the low

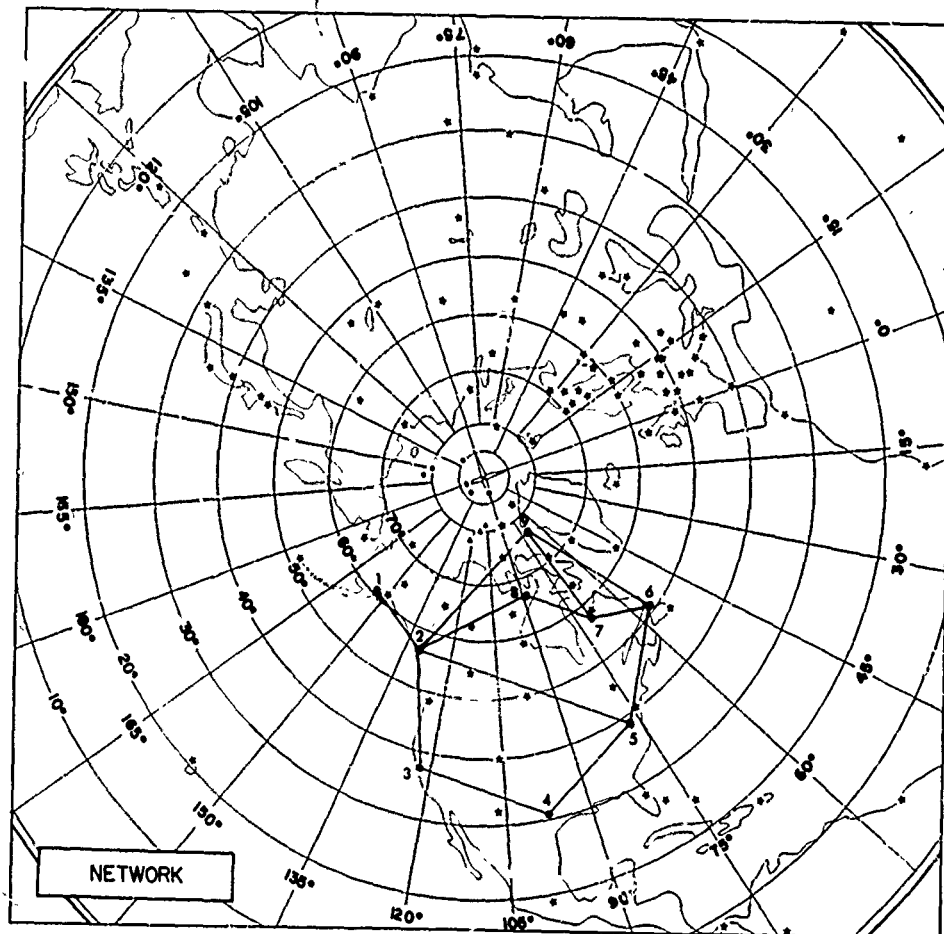


Figure 4: HYPOTHETICAL NETWORK

TABLE XII

SYSTEM PARAMETERS OF A HYPOTHETICAL
COMMUNICATION NETWORK

Station	P_t watts	G_t db	R. S. μv	G_R db	Total Noise db above $1 \mu v$
1	3×10^3	10	0.5	0	0
2	3	10	0.5	0	0
3	3	10	0.5	0	10
4	3	10	0.5	0	10
5	10	10	0.5	0	15
6	3	10	0.5	0	5
7	0.5	10	0.5	0	-10
8	0.5	10	0.5	0	-10
9	3	10	0.5	0	10

P_t Transmitter Power
 G_t Transmitter Antenna Gain
 G_R Receiver Antenna Gain over a half-wave dipole
R.S. Receiver Sensitivity

TABLE XIII

RADIATED FIELD STRENGTH AND
MINIMUM SIGNAL LEVELS

Station	E_o db above $1 \mu v/m$	Minimum Signal Level db above $1 \mu v$
1	116	10
2	116	10
3	116	20
4	116	20
5	121	25
6	116	15
7	108	4
8	108	4
9	116	20

TABLE XIV
ALLOWABLE ABSORPTION

	E _o	Minimum Signal Level	Allowable Loss	Space Attenuation	Allowable Absorption
1 to 2	116	10	106±F	55	51±F
2 to 1	116	10	106	55	51
2 to 3	116	20	96	59	37
2 to 5	116	25	91	65	26
2 to 8	116	4	112	60	52
2 to 9	116	20	96	63	33
3 to 2	116	10	106	59	47
3 to 4	116	20	96	60	36
4 to 3	116	20	96	60	36
4 to 5	116	25	91	59	32
5 to 2	121	10	111	65	46
5 to 4	121	20	101	59	42
5 to 6	121	15	106	59	47
6 to 5	116	25	91	59	32
6 to 7	116	4	112	54	58
6 to 9	116	20	96	62	34
7 to 6	108	15	93	54	39
7 to 8	108	4	104	55	49
7 to 9	108	20	88	59	29
8 to 2	108	4	98	60	38
8 to 7	108	4	104	55	49
9 to 2	116	10	106	63	43
9 to 6	116	15	101	62	39
9 to 7	116	4	112	59	53

frequencies were stressed and for the long links the high frequencies. However, for the long links, low frequencies were also assigned. A complete list of the assigned frequencies is provided in table XV. It may be noticed that there is some similarity between these frequencies and the ones assigned in the Norlant circuit information given in section IV.

The next step is to find which of these frequencies are available. A single set of ionospheric maps has been chosen for this example. These maps are for 1500 UT, 11 April 1958 when a moderate to strong PCA event was taking place. It is assumed that the conditions represented on the maps (figure 45) are valid for a certain time interval, say 1 hour (a half hour before and a half hour after the map time). The available frequencies found during this ionospheric situation will determine the network capacity for this time interval. These frequencies are found in two steps.

In the first step, analysis is made of the range of frequencies which are possible according to the reflecting properties of the ionosphere without regard to propagation losses. In this study, these ranges are solely determined by ray-path geometry and the critical frequencies of the various layers. The methods employed are described in detail in section II. Calculation of these frequency ranges yields the results shown in table XVI.

For the simple network used in this example only a few modes are available. These are the single E, F1, and F2 hops, and the double and triple E hop. As expected the lowest frequencies are possible for E hops (Modes 1, 4, and 8), a narrow frequency range for F1 hops (Mode 2), and the highest frequencies for F hops (Mode 3).

In the second step, propagation losses are calculated for the assigned frequencies that lie within the frequency range available for each mode. Calculation is carried out using the methods described in section II. The results of these calculations are shown in table XVII. The absorption is listed for all assigned frequencies which are possible according to ray-path geometry. When the absorption is greater than the amount allowable, then that frequency is considered not available. No assigned frequencies fall within the range of possible frequencies for F1 hops, so mode 2 does not appear in table XVII. The values listed under Received Field Strength are in units of db above the minimum signal level.

If this value of Received Field Strength is zero then the signal-to-noise ratio is 10, so there is no excess in field strength over the minimum required level. Whenever the calculated Received Field Strength was found to be below 10, the corresponding frequency was considered not to be available although in theory it would be. This procedure allows a margin of error in computed versus actual values. So the frequencies available are the ones listed in table XVIII which have a Received Field Strength greater than or equal to 10 db above the minimum signal level. These frequencies are listed in table XVIII without regard for the mode applicable.

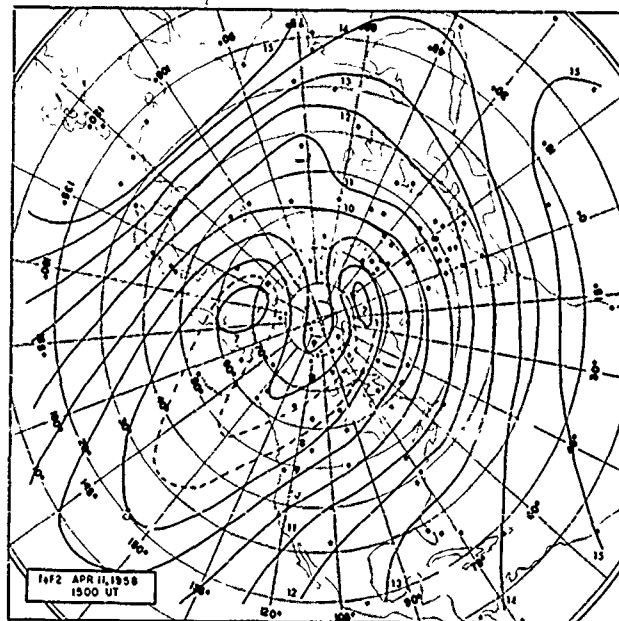
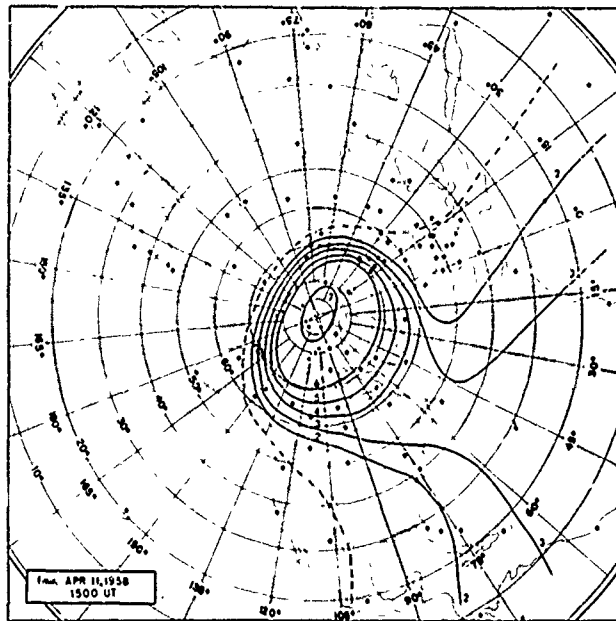


Figure 45 IONOSPHERIC MAPS FOR 1500 UT, 11 APRIL 1958

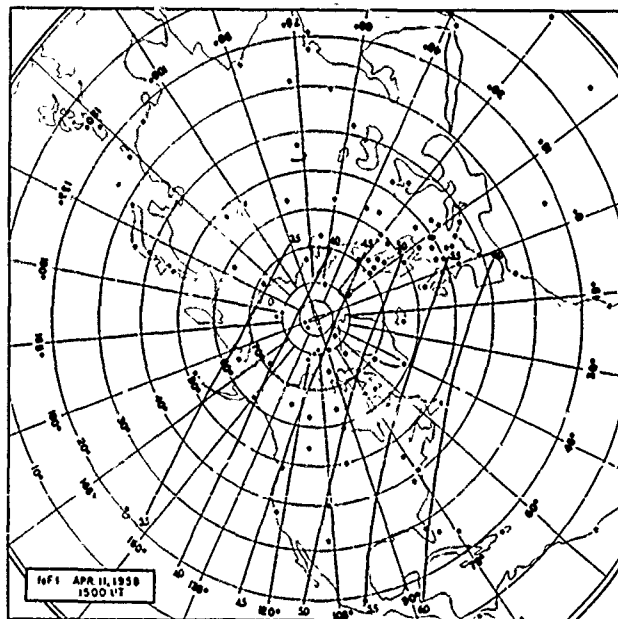
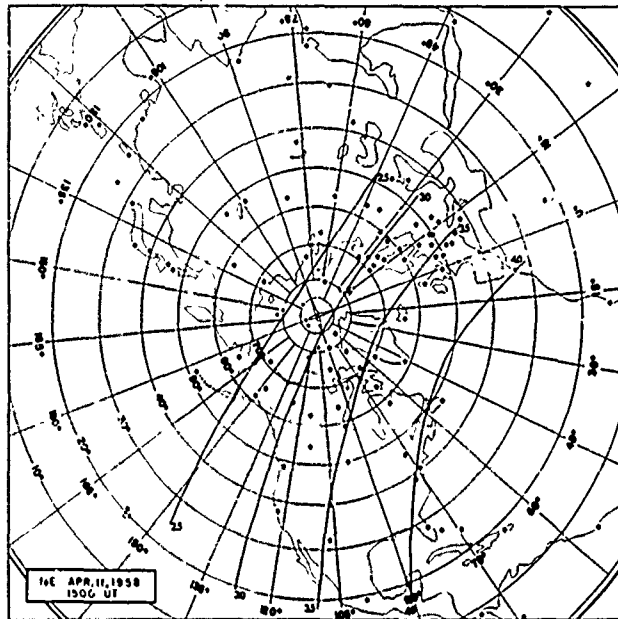


Figure 45 (Concl'd)

TABLE XV

Link	ASSIGNED FREQUENCIES					
1 to 2	3,0	7,0	12,0			
2 to 1	4,1	7,1	12,1			
2 to 3	5,0	9,0	14,0	17,0	22,0	
2 to 5	7,2	12,2	17,2	20,2		
2 to 8	6,0	9,2	13,0	18,0		
2 to 9	4,0	8,0	13,2	19,0	24,0	
3 to 2	5,1	9,1	14,1	17,1	22,1	
3 to 4	5,2	9,4	13,4	16,0	21,0	25,0
4 to 3	5,3	9,5	13,5	16,1	21,1	25,1
4 to 5	4,2	6,2	11,0	18,2	23,0	
5 to 2	7,3	12,3	17,3	20,3		
5 to 4	4,3	8,3	11,1	18,3	23,1	
5 to 6	3,2	6,2	10,0	15,0	19,2	23,2
6 to 5	3,3	6,3	10,1	15,1	19,3	23,3
6 to 7	3,4	7,4	10,2	14,2		
6 to 9	5,4	8,4	12,4	16,2	20,4	25,2
7 to 6	3,5	7,5	10,3	14,3		
7 to 8	4,4	8,6	12,6	16,4		
7 to 9	6,4	11,2	15,2	19,4	22,2	
8 to 2	6,1	9,2	13,1	18,1		
8 to 7	4,5	8,7	12,7	16,5		
9 to 2	4,1	8,1	13,3	19,1	24,1	
9 to 6	5,5	8,5	12,5	16,3	20,5	25,3
9 to 7	6,5	11,3	15,3	19,5	22,3	

TABLE XVI

FREQUENCY RANGE AVAILABLE WITHOUT PROPAGATION LOSSES

Link	Mode 1 (E)	Mode 2 (F1)	Mode 3 (F2)	Mode 4 (EE)	Mode 8 (EEE)
1 to 2	0 to 14.1	9.3 to 11.2	8.6 to 14.7		
2 to 1	0 to 14.1	9.3 to 11.2	8.6 to 14.7		
2 to 3		15.0 to 15.7	12.9 to 20.6	0 to 13.7	
2 to 5					0 to 16.5
2 to 8			11.4 to 19.2	0 to 14.7	
2 to 9			16.3 to 20.8	0 to 16.3	
3 to 2		15.0 to 15.7	12.9 to 20.6	0 to 13.7	
3 to 4			15.2 to 28.7	0 to 15.5	
4 to 3			15.2 to 28.7	0 to 15.5	
4 to 5		19.3 to 19.7	16.0 to 30.1	0 to 17.1	
5 to 2					0 to 16.5
5 to 4		19.3 to 19.7	16.0 to 30.1	0 to 17.1	
5 to 6		19.5 to 20.4	16.2 to 27.1	0 to 18.0	
6 to 5		19.5 to 20.4	16.2 to 27.1	0 to 18.0	
6 to 7	0 to 18.6	10.7 to 13.7	10.6 to 17.8	0 to 13.0	
6 to 9			18.8 to 24.7	0 to 18.5	
7 to 6	0 to 18.5	10.7 to 13.7	10.6 to 17.8		
7 to 8		11.8 to 14.2	10.6 to 16.6		
7 to 9			14.8 to 20.6	0 to 15.6	
8 to 2			14.4 to 19.2	0 to 14.7	
8 to 7	0 to 18.5	11.8 to 14.2	10.6 to 16.6		
9 to 2			16.3 to 21.8	0 to 16.3	
9 to 6			18.8 to 24.7	0 to 18.5	
9 to 7			14.8 to 20.6	0 to 15.6	

TABLE XVU
COMPUTED VALUES OF RECEIVED FIELD STRENGTH

Link	Mode 1				Mode 3				Mode 4				Mode 8						
	Allowable Absorption	Frequency	Absorption	Received Field Strength	Allowable Absorption	Frequency	Absorption	Received Field Strength	Allowable Absorption	Frequency	Absorption	Received Field Strength	Allowable Absorption	Frequency	Absorption	Received Field Strength			
1 to 2	73	3.0	83	--	60	12.0	8	32											
	65	7.0	34	31															
	60	12.0	16	44															
2 to 1	73	3.1	82	--	60	12.1	8	32											
	65	7.1	33	32															
	60	12.1	16	40															
2 to 3					45	14.0	7	30	44	9.0	74	--							
					43	17.0	5	30	48	9.0	70	8							
2 to 5													40	7.2	144	--			
													35	12.2	36	--			
2 to 8					57	18.0	14	43	67	6.0	232	--							
									63	9.2	122	--							
									60	13.0	78	--							
2 to 9					38	19.0	22	16	52	4.0	602	--							
									46	8.0	212	--							
									41	13.2	114	--							
3 to 2					54	14.1	7	47	44	5.1	92	--							
					53	17.1	5	48	50	9.1	60	18							
3 to 4					42	16.0	7	36	53	5.2	106	--							
					40	21.0	5	36	47	7.4	48	--							
					39	25.0	2	37	44	13.4	36	8							
4 to 3					42	14.1	4	36	53	5.3	104	--							
					40	21.1	4	36	47	9.3	48	--							
					39	25.1	2	37	44	13.3	36	8							
4 to 5					37	18.2	5	32	51	4.2	178	--							
					35	23.0	3	32	44	8.2	64	--							
									42	11.0	48	--							
5 to 2													59	7.3	144	--			
													55	12.2	48	7			
5 to 4					47	18.7	5	42	61	4.3	176	--							
					45	23.1	3	42	52	8.3	64	--							
									52	11.1	48	4							
5 to 6					52	19.2	8	44	48	3.2	395	--							
					40	23.2	5	45	62	6.2	132	--							
									58	10.0	57	1							
									56	15.0	29	25							
4 to 5					37	19.3	8	29	53	3.3	395	--							
					35	23.3	5	30	47	6.3	138	--							
									43	10.1	57	--							
									39	15.1	29	10							
6 to 7	78	3.4	143	--	66	14.2	10	36											
	71	7.4	57	14															
	68	10.2	36	32															
	66	14.2	22	44															
6 to 9					38	20.4	19	19	50	5.4	357	--							
									46	8.4	182	--							
									45	12.4	93	--							
									40	16.2	62	--							
7 to 6	59	3.5	139	--	46	14.3	10	34											
	52	7.5	56	--															
	49	10.3	40	9															
	46	14.3	22	24															
7 to 8	67	4.4	137	--	58	12.4	20	38											
	61	8.4	59	2															
	58	12.4	34	24															
	55	16.4	23	32															
7 to 9					34	15.2	27	9	44	6.4	280	--							
					34	19.4	17	7	40	11.2	100	--							
									4	15.2	69	--							
8 to 2					43	18.1	14	29	53	6.1	232	--							
									49	9.3	122	--							
									46	13.1	78	--							
8 to 7	67	4.5	135	--	58	12.7	20	38											
	61	8.7	58	3															
	56	12.7	34	24															
	55	16.5	23	32															
9 to 2					48	19.1	22	24	61	4.1	602	--							
									55	8.1	212	--							
									51	13.3	114	--							
9 to 6					43	20.5	19	23	55	5.5	357	--							
									51	8.5	182	--							
									48	12.5	93	--							
									45	16.5	62	--							
9 to 7					60	15.3	27	33	48	4.5	280	--							
					58	19.5	17	41	63	11.3	100	--							
									60	15.3	69	--							

TABLE XVIII

USA¹ FREQUENCIES
 (Received Signal Strength \geq 10 db Above Minimum)

Link	Usable Frequencies	Link	Usable Frequencies
1 to 2	7.0 12.0	5 to 6	15.0 19.2 23.2
2 to 1	7.1 12.1	6 to 5	15.1 19.3 23.3
2 to 3	14.0 17.0	6 to 7	7.4 10.2 14.2
2 to 5		6 to 9	20.4
2 to 8	18.0	7 to 6	14.3
2 to 9	19.0	7 to 8	12.6 16.4
3 to 2	9.1 14.1 17.1	7 to 9	19.4
3 to 4	16.0 21.0 25.0	8 to 2	18.1
4 to 3	16.1 21.1 25.1	8 to 7	12.7 16.5
4 to 5	18.2 23.0	9 to 2	19.1
5 to 2		9 to 6	20.5
5 to 4	18.3 23.1	9 to 7	15.3 19.5

To find the amount of material which can be sent over each link certain assumptions are made regarding the communication facilities. For each link a number of channels are said to exist. If each of these has a capacity of 60 words per minute, then the total capacity on a link for 1 hour is the number of channels times 3600. In table XIX the channels are listed in column one and the link capacity for these channels expressed in thousand-word units are listed in column two. In the next two columns, the channels and capacity available are listed.

The assigned load to be sent over the network is listed in table XX. Comparison can then be made on how the load should be distributed for the available capacity. This can also be done for the case when all the channels are open. The overall results can be expressed in terms of the load sent or the load remaining; the latter is shown in table XX for both maximum and available capacity.

It is seen that the message load which can be sent during the PCA is less than the amount which could be sent if the full capacity of the network were available. This condition is not surprising, as it occurs at certain times of the day and year even in undisturbed conditions. To utilize the available capacity to the best advantage, message sent of the highest priority should be sent first.

In the design of this network there were only a few links connected from any one station. In more flexible networks other links which are found to offer high capacity can be set up. For example, equipment could be installed so that direct communication can be made between stations nine and four, or between six and two. On these links, there may be other modes than the simple ones, such as M hops which occur often during the critical stages of ionospheric storms. Only by extensive testing of link capacity, or frequencies available, under a variety of storm conditions can the best links be found. Of the best ones found, those most consistent with actual requirements are chosen. Thus, as would be expected, the final design of a network depends upon the expected loads and the capacities found for quiet and disturbed ionospheric conditions.

TABLE XIX

LINK CAPACITIES

Link	Maximum Number of 16-channel Teletype Connections	Maximum Capacity	Available Number of 16-channel Teletype Connections*	Available Capacity
1 to 2	2	115	2	115
2 to 1	2	115	2	115
2 to 3	3	173	2	115
2 to 5	2	115	0	0
2 to 8	1	58	1	58
2 to 9	2	115	1	58
3 to 2	2	173	2	115
3 to 4	3	173	3	173
4 to 3	3	173	3	173
4 to 5	3	173	2	115
5 to 2	2	115	0	0
5 to 4	3	173	2	115
5 to 6	3	173	3	173
6 to 5	2	173	2	115
6 to 7	2	115	2	115
6 to 9	3	173	1	58
7 to 6	2	115	1	58
7 to 8	1	58	1	58
7 to 9	2	115	1	58
8 to 2	1	58	1	58
8 to 7	1	58	1	58
9 to 2	2	115	1	58
9 to 6	3	173	1	58
9 to 7	2	115	2	115

*This number is equal to the number of usable frequencies (see table XVIII) or to the maximum number of 16-channel teletype connections, whichever is lowest.

TABLE XX
MESSAGE LOADS

Address	Load	Load Remaining Using Maximum Capacity	Load Remaining Using Available Capacity
1 to 2	30	0	0
1 to 7	20	0	0
2 to 9	40	0	0
3 to 4	80	0	0
3 to 5	70	0	18
4 to 1	90	0	0
4 to 3	80	0	0
4 to 5	40	0	0
5 to 6	30	0	0
6 to 5	40	0	0
6 to 7	40	0	0
6 to 8	25	0	0
6 to 9	25	0	0
7 to 1	30	1	14
7 to 2	60	0	0
8 to 1	50	14	24
8 to 5	60	0	41
8 to 9	20	0	0
9 to 2	30	0	0
9 to 4	100	0	76
9 to 6	40	0	0
Total	1000	15	173

VII. REFERENCES

- Akasofu, S., Large-scale auroral motions and polar magnetic disturbances - II, *J. Atmospheric Terrest. Phys.*, 24, (1962) p. 723.
- Akasofu, S. and S. Chapman, Large-scale auroral motions and polar magnetic disturbances - III, *J. Atmospheric Terrest. Phys.*, 24, (1962), p. 785.
- Axford, W. I., Vertical transport of ionized gas due to gravity waves in the ionosphere, *URSI - IRE Joint Meeting Ottawa* (1962).
- Budden, K. G., Radio Waves in the Ionosphere, Cambridge University Press, New York (1961).
- C. C. I. R., Revision of Atmospheric Radio Noise Data, C. C. I. R. Report No. 65, International Telecommunications Union, Geneva (1957).
- Central Radio Propagation Laboratory, Ionospheric Data, U. S. Dept. of Commerce, CRPL-F, Part A (Serial).
- Central Radio Propagation Laboratory, Solar-Geophysical Data, U. S. Dept. of Commerce, CRPL-F, Part B (Serial).
- Chapman, S., The absorption and dissociative or ionizing effect of monochromatic radiation in an atmosphere on a rotating earth, Part I, Part II, Grazing incidence, *Proc. Phys. Soc.* 43 (1931) p. 26, 484.
- Chapman, S., The atmospheric height distribution of band absorbed solar radiation, *Proc. Phys. Soc.* 51, (1939) p. 93.
- Chubb, T. A., H. Friedman, R. W. Kreplin, J. E. Kupperian, Jr., Lyman alpha and X-ray emissions during a small solar flare, *J. Geophys. Res.*, 62, No. 3 (September 1957).
- Coroniti, S., et al., Research Concerning Forecasting Anomalous Propagation at High Latitudes - Final Report, Item 1, Avco-RAD-TR-63-15 (February 1963).
- Critchlow, W. Q., et al., World-wide Radio Noise Levels Expected in the Frequency Band 10 Kilocycles to 100 Megacycles, U. S. Dept. of Commerce. NBS Circular 557 (1955).
- Critchlow, W. Q., T. Disney, et al., Quarterly Radio Noise Data, U. S. Dept. of Commerce, NBS Technical Note 18 Series (1959 ff).
- Epstein, P., Reflection of plane waves in an inhomogeneous absorbing medium, *Proc. Natl. Acad. Sci. U. S.*, 16, (1930) p. 627.

Friis, H. T., Noise figure of radio receivers, Proc. Inst. Radio Engrs. 32 (1944) p. 419.

Hakura, Y., Development of ionospheric and geomagnetic storms caused by solar corpuscular emissions, Rep. Ionos. and Space Res. in Japan, XV, No. 1, (1961).

Hakura, Y., and T. Goh, Unusual solar terrestrial events in July 1959, Space Research II - Proc. of the 2nd Intern. Space Sci. Symp., Florence 10-14, (April 1961).

Handbook of Geophysics, (Revised Edition), 1960, Macmillan Co., New York (1960).

Heikkila, W., A. Adey, P. G. Burke, and S. Penstone, Rocket Electron Density Measurement at Fort Churchill, Canada, Presented at meeting of URSI, Washington, D. C. (May 1960).

Hill, G. E., Effects of corpuscular emissions on the polar ionosphere following solar flares, J. Geophys. Res., 66, No. 8, (August 1961).

Hill, G. E., Ionospheric disturbances following a solar flare, J. Geophys. Res., 65, No. 10. (October 1960).

Houston, R. E., Ionosphere Research Laboratory Internal Memo 167, quoted in An Experiment for Electron Density Determination by a Rocket Method, and Ground-based Instrumentation Design, Scientific Report 107, Ionosphere Research Laboratory, University Park, Pennsylvania (1956) p. 33.

Hultqvist, B., Studies of Ionospheric Absorption of Radio Waves by the Cosmic Noise Method, Scientific Rep. No. 3, Contract No. AF61(052)-601, Kiruna Geophys. Obs., (15 June 1962).

Institut Breisach, Ionosphären Daten - Absorptions Messungen Nr. 2 - Abs. Freiburg, (July 1957 to December 1958).

Jones, W. B., and R. M. Gallet, Methods of applying numerical maps of ionospheric characteristics, J. Research NBS 66D, (1962) p. 649.

Kahle, A., Solar Activity and Polar Cap Absorption Events, Scientific Rep. No. 2, Contract No. AF19(604)-5574, Geophysical Institute, Univ. of Alaska, (July 1962).

Kamiyama, H., Morphology of Ionospheric Storms, J. Phys. Soc. 17, Supp. A-I (1962).

Kane, J. A., Electron densities in the E region deduced from rocket observations, in Electron Density Profiles in the Ionosphere and Exosphere, ed. by B. Maehlum, Macmillan Co., New York (1962) p. 67.

Kreplin, R. W., NRL Solar Radiation I Satellite Experiment Presented to Comm. X, IAU Conf., Berkeley, California (16 August 1961).

Maehlum, B., On the Sporadic E Ionization in and Near the Auroral Zone, NDRE, Report 37 (1961).

Merriman, H. O., Radio Interference from Electrical Apparatus and Systems, Department of Transport, Ottawa (1954).

National Bureau of Standards, Ionospheric Radio Propagation, U. S. Dept. of Commerce, NBS Circular 462 (1948).

Nicolet, M., J. Atmospheric Terrest. Phys. 3, (1953) p. 200.

Northover, F. H., Reflection of electromagnetic waves from thin gaseous layers, NBS J. Research, 66D (1962) p. 73.

Obayashi, T., On the world-morphology of ionospheric disturbances, Report of Ionos. Res. in Japan, Vol. III, No. 4, (1954).

Obayashi, T., Geomagnetic Storms and the Earth's Outer Atmosphere, Rep. Ionos. and Space Res. in Japan, 13, (1959) p. 301 - 335.

Obayashi, T., and Hakura, Y., Solar Corpuscular Radiation and Polar Ionospheric Disturbances, J. Geophys. Res., 65, No. 10, (1960) p. 3131 - 3142.

Obayashi, T., and Hakura, Y., Propagation of Solar Cosmic Rays Through Interplanetary Magnetic Field, J. Geophys. Res. 65, No. 10, (1960) p. 3143 - 3148.

Obayashi, T., Propagation of Solar Corpuscles and the Interplanetary Magnetic Fields, Arctic Institute of North America, Research Paper 16 (1961).

Obayashi, T., 1962, Propagation of solar corpuscles and interplanetary magnetic fields, 67, No. 5, (May 1962).

Penndorf, R., and S. C. Coroniti, 1958, Polar Es, J. Geophys. Res. 63, (1958) p. 789.

Pfister, W., and J. C. Ulwick, Plasma Sheath Effects on Rocket Antennae, Proc. Symp. Amer. Astro. Soc., (17 March 1961).

Pierce, E. T., Atmosphericics from lightning flashes with multiple strokes, J. Geophys. Res. 65, No. 7 (July 1960) p. 1867 - 1871.

Piggott, W. R., and K. Rawer, URSI Handbook of Ionogram Interpretation and Reduction, Elsevier Publishing Co. New York (1961).

Pitts, J. J., Personal communication (1962).

Ratcliffe, J. A., The Magneto-Ionic Theory and its Applications to the Ionosphere, Cambridge University Press, London (1959).

Rawer, K., The Ionosphere, Fredrick Ungar Publishing Co., New York (1956).

Rossi, B., Radiation belt-results of the direction measurements of interplanetary plasma and magnetic field by Explorer X. J. Phys. Soc. Japan, 17, Supplement A-II, Proceedings of the International Conference on Cosmic Rays and the Earth Storm, 615 (1962).

Rydbeck, O. E. H., The reflection of electromagnetic waves from a parabolic ionized layer, Phil. Mag. 34, (1943) p. 342.

Rydbeck, O. E. H., The theory of magneto ionic triple splitting, Trans. Chalmers Univ. Tech., 101 (1951).

Schelkunoff, S. A., and H. T. Friis, Antennas, Theory and Practice, John Wiley and Sons, New York (1952) p. 341.

Seddon, J. C., and J. E. Jackson, Ionosphere electron densities and differential absorption, IGY Rocket Report Series 1, 149, Nat. Acad. Sci., Washington (1958).

Seddon, J. C., Sporadic-E as Observed with Rockets, NASA Technical Note D-1043 (1961).

Shimazaki, T., A theoretical study of the dynamical structure of the ionosphere, J. Radio Res. Lab. 6, (1959) p. 107.

Smith, E. K., World-wide Occurrence of Sporadic E, U. S. Dept. of Commerce, NBS Circular 582 (1957).

Stormer, C., The Polar Aurora, Oxford University Press, London (1955).

Utlaut, W. F., Siting Criteria for HF Communications Centers, U. S. Dept. of Commerce, NBS Technical Note 139 (1962).

Warga, J., Convergent Procedure for Convex Programming, Avco-RAD-TM-62-58 (1962).

Warwick, C., The Sudden Ionospheric Disturbance, Radio Astronomy and Satellite Studies of the Atmosphere (1963).

Watt, A. D., et al., Radio System performance in the presence of atmospheric and thermal noise, Proc. Inst. Radio Engrs. 46, (1958) p. 1914.

Whitehead, J. D., 1962, The reflection characteristics of a patchy sporadic-E layer, J. Atmosph. Terr. Phys., 24, 681.

Wright, J. W., R. W. Knecht, and K. Davies, Ionospheric Vertical Soundings, Annals IGY, III, Part I (1957) p. 1.

Wright, J. W., and J. N. Gautier, Note on a test of the equivalence theorem for sporadic E propagation, NBS J. Research 64D, (1960) p. 347.

Wright, J. W., Ionosonde Observations of Artificially Produced Electron Clouds Firefly 1960, U. S. Dept. of Commerce, NBS Technical Note 135 (1962).

Wright, J. W., L. R. Wescott, and D. J. Brown, Mean Electron Density Variations of the Quiet Ionosphere, U. S. Dept. of Commerce, NBS Technical Note 40- (serial).

DISTRIBUTION

<u>Addressee</u>	<u>No. of Copies</u>
RADC (RAUEL-3) Attn: Mr. G. Weatherup (+ 1 reproducible) Griffiss AFB NY	5
*RADC (RAAPT) Griffiss AFB NY	1
*RADC (RAALD) Griffiss AFB NY	1
*GEEIA (ROZMCAT) Griffiss AFB NY	1
*RADC (RAIS, Attn: Mr. Malloy) Griffiss AFB NY	1
*US Army Electronics R&D Labs Liaison Officer RADC Griffiss AFB NY	1
*AUL (3T) Maxwell AFB Ala	1
ASD (ASAPRD) Wright-Patterson AFB Ohio	1
Chief, Naval Research Lab Attn: Code 2027 Wash 25 DC	1
Air Force Field Representative Naval Research Lab Attn: Code 1010 Wash 25 DC	1
Commanding Officer US Army Electronics R&D Labs Attn: SELRA/SL-ADT Ft Monmouth NJ	1

*Mandatory

DISTRIBUTION (Cont'd)

<u>Addressee</u>	<u>No. of Copies</u>
National Aeronautics & Space Administration Langley Research Center Langley Station Hampton Virginia Attn: Librarian	1
RTD (RTH) Bolling AFB Wash 25 DC	1
Central Intelligence Agency Attn: OCR Mail Room 2430 E Street NW Wash 25 DC	1
US Strike Command Attn: STRJ5-OR Mac Dill AFB Fla	1
AFSC (SCSE) Andrews AFB Wash 25 DC	1
Commanding General US Army Electronics Proving Ground Attn: Technical Documents Library Ft Huachuca Ariz	1
*ASTIA (TISIA-2) Arlington Hall Station Arlington 12 Va	(If not releasable to ASTIA, IAW AFR 205-43, send the 10 copies to RADC (RAAPP-2) for secondary distribution) 10
AFSC (SCFRE) Andrews AFE Wash 25 DC	1
Hq USAF (AFCOA) Wash 25 DC	1
AFOSR (SRAS/Dr. G. R. Eber) Holloman AFB N Mex	1

DISTRIBUTION (Cont'd)

<u>Addressee</u>	<u>No. of Copies</u>
Office of Chief of Naval Operations (Op-724) Navy Dept Wash 25 DC	1
Commander US Naval Air Dev Cen. (NADC Lib) Johnsville Pa	1
Commander Naval Missile Center Tech Library (Code No 3022) Pt Mugu Calif	1
Bureau of Naval Weapons Main Navy Bldg Wash 25 DC Attn: Technical Librarian, DL1-3	1
NAFEC Library Bldg 3 Atlantic City NJ	1
Redstone Scientific Information Center US Army Missile Command Redstone Arsenal, Alabama	1
Commandant Armed Forces Staff College (Library) Norfolk 11 Va	1
ADC (ADCAC-DL) Ent AFB Colo	1
AFFTC (FTOOT) Edwards AFB Calif	1
Commander US Naval Ordnance Lab (Tech Lib) White Oak, Silver Springs Md	1

DISTRIBUTION (Concl'd)

Commanding General White Sands Missile Range N Mexico Attn: Technical Library	1
Director US Army Engineer R&D Labs Technical Documents Center Ft Belvoir Va	1
ESD (ESRL) L G Hanscom Fld Bedford Mass	1
Commanding Officer & Director US Navy Electronics Lab (LIB) San Diego 52 Calif	1
ESD (ESAT) L G Hanscom Fld Bedford Mass	1
Commandant US Army War College (Library) Carlisle Barracks Pa	1
APGC (PGAPI) Eglin AFB Fla	1
AFSWC (SWOI) Kirtland AFB N Mex	1
AFMTC (Tech Library MU-135) Patrick AFB Fla	(UNCLASSIFIED ONLY) 1
Central File	1
Document Control	5
Research Library	30